ENHANCED PRODUCTIVITY IN PASSIVE SOLAR DESALINATION USING FRESNEL LENS AND CONDUCTIVE PARTICLE-ASSISTED PHASE CHANGE MATERIAL IN TROPICAL CLIMATE

TAN JIA HUI

MASTER IN ENGINEERING SCIENCE

Lee Kong Chian Faculty of Engineering and Science
Universiti Tunku Abdul Rahman

March 2025

Copyright Statement

ENHANCED PRODUCTIVITY IN PASSIVE SOLAR DESALINATION USING FRESNEL LENS AND CONDUCTIVE PARTICLE-ASSISTED PHASE CHANGE MATERIAL IN TROPICAL CLIMATE

By

TAN JIA HUI

MASTER IN ENGINEERING SCIENCE

A dissertation submitted to the Department of Mechanical and Materials Engineering, Lee Kong Chian Faculty of Engineering and Science, University Tunku Abdul Rahman, in partial fulfilment of the requirements for the degree of Master in Engineering Science
March 2025

ABSTRACT

ENHANCED PRODUCTIVITY IN PASSIVE SOLAR DESALINATION USING FRESNEL LENS AND CONDUCTIVE PARTICLE-ASSISTED PHASE CHANGE MATERIAL IN TROPICAL CLIMATE

Solar desalination provides a sustainable solution to freshwater shortages caused by environmental issues like water pollution and global warming. However, conventional solar stills often produce insufficient water, unable to meet even a single household's needs. Ongoing research aims to improve their productivity, with promising approaches such as Thermal Energy Storage (TES) systems and sunlight concentrators. TES stores excess energy during peak sunlight hours, enabling continued water production during cloudy periods or after sunset, improving efficiency and reliability. Sunlight concentrators, like lenses, focus solar radiation onto the evaporative surface, increasing temperature and evaporation rates, thus enhancing the distillation process. This study combines concentrators and TES to enhance the performance of a simple passive single-slope solar still. The Fresnel lens was used as the concentrator, while paraffin wax, a phase change material (PCM) with added conductive particles, served as the TES. Four sizes of Fresnel lenses (FL 12.7 cm, FL 9.9 cm, FL 20 cm, and FL 33 cm) were tested, along with four types of conductive particles: Al scrap, Al_2O_3 nanoparticle, Cu nanoparticle, and Al_2O_3 + Cu nanoparticle. In indoor tests, Al_2O_3 + Cu nanoparticle showed the best performance. Outdoor tests revealed that the largest Fresnel lens resulted in over 150% higher water yield than the other smaller Fresnel lenses used in the study; regardless of the conductive particle used, with Cu and Al_2O_3 + Cu particles showing similar high performance. Interestingly, the performance of Al scrap was similar or higher in performance in some experiments. After conducting an economic analysis, it was discovered that the model implementing Al scrap PCM has the lowest cost per litre per area. Hence, the actual size prototype proceeded with the combination of FL 33 cm Fresnel lens and Al scrap Fresnel lens, which achieved a water yield of 3.3030 kg/m^2, productivity of 2.34 g/kJ.m^2, efficiency of 35.34 %, and the estimated cost per litre per unit area is 0.004 \$/(kg/m^2).

Keywords: Solar desalination, single slope passive solar still, phase change material, nanoparticles, aluminium scrap, Fresnel lens, concentration ratio

ACKNOWLEGDEMENTS

I would like to thank everyone who had contributed to the successful completion of this research. Firstly, I would like to express my utmost gratitude to my supervisors, Dr. Rubina Bahar and Dr. Jun Hieng Kiat for their insightful guidance, advice and tremendous patience throughout the journey of this research. Additionally, I would like to thank UTAR for providing the Research Scholarship Scheme and all the equipment support to proceed with the research work. Last but not least, I am deeply grateful to my parents and friends who had given me immense support and encouragement throughout my postgraduate journey.

APPROVAL SHEET

This dissertation report entitled "**ENHANCED PRODUCTIVITY IN PASSIVE SOLAR DESALINATION USING FRESNEL LENS AND CONDUCTIVE PARTICLE-ASSISTED PHASE CHANGE MATERIAL IN TROPICAL CLIMATE**" was prepared by **TAN JIA HUI** and submitted as partial fulfilment of the requirements for the degree of Master in Engineering Science at Universiti Tunku Abdul Rahaman.

Approved by:

____

(Dr. Rubina Bahar) Date: 19th March 2025
Main supervisor
Department of Mechanical and Materials Engineering
Lee Kong Chian Faculty of Engineering and Science
Universiti Tunku Abdul Rahman

____

(Dr. Jun Hieng Kiat) Date: 19th March 2025
Co-supervisor
Department of Mechanical and Materials Engineering
Lee Kong Chian Faculty of Engineering and Science
Universiti Tunku Abdul Rahman

LEE KONG CHIAN FACULTY OF ENGINEERING AND SCIENCE
UNIVERSITI TUNKU ABDUL RAHMAN

Date: 19th March 2025

SUBMISSION OF DISSERTATION

It is hereby certified that Tan Jia Hui (ID No: 22UEM00027) has completed this dissertation entitled "*Enhanced productivity in passive solar desalination using Fresnel lens and conductive particle-assisted phase change material in tropical climate*" under the supervision of Dr. Rubina Bahar (main supervisor) and Dr. Jun Hieng Kiat (co-supervisor) from the Department of Mechanical and Materials Engineering, Lee Kong Chian Faculty of Engineering and Science.

I understand that the university will upload the softcopy of my dissertation in pdf format into UTAR Institutional Repository, which may be made accessible to UTAR community and to the public.

Yours truly,

____

(TAN JIA HUI)

DECLARATION

I hereby declare that the dissertation is based on my original work except for the citations and quotations which have been duly acknowledge. I also declare that it has not been previously or concurrently submitted for any other degree at UTAR or other institutions.

(TAN JIA HUI)

Date: 19th March 2025

Table of Contents

LIST OF TABLES

LIST OF FIGURES

LIST OF ABBREVIATIONS, NOMENCLATURE AND SYMBOLS

CS	Concentrated sunlight
CR	Concentration ratio
FL	Focal length, cm
FRL	Fresnel lens
H	Height, cm
L	Length, cm
NPCM / nePCM	Nanomaterial assisted phase change material
PCM	Phase change material
PW	Paraffin wax
SDG	Sustainable development goals
TES	Thermal energy storage
W	Width, cm
Al	Aluminium (scrap), solar still model with aluminium scrap phase change material
Al_2O_3	Aluminium oxide / alumina (nanopowder), solar still model with alumina nanomaterial assisted phase change material
Cu	Copper (nanopowder), solar still model with copper nanomaterial assisted phase change material
Al_2O_3 + Cu	Solar still model with alumina and copper nanomaterial combination assisted phase change material
CO_2	Carbon dioxide
A_{b1}	Area of water basin, m^2

A_{FRL}	Area of Fresnel lens, m^2
A_R	Area of receiver of solar still, m^2
$C_{L,PCM}$	Liquid heat capacity of PCM
$C_{s,PCM}$	Specific heat capacity of PCM
d_w	Water depth, m
E	Heat energy
h_w	Latent heat of basin water, kJ/kg
$h_{conv,wg}$	Convective heat transfer coefficient from basin water to glass cover, W/m^2K
$h_{evap,wg}$	Evaporative heat transfer coefficient from basin water to glass cover, W/m^2K
$h_{rad,wg}$	Radiative heat transfer coefficient from basin water to glass cover, W/m^2K
$h_{conv,ga}$	Convective heat transfer coefficient from glass cover to atmosphere, W/m^2K
$h_{rad,gs}$	Radiative heat transfer coefficient from glass cover to sky, W/m^2K
$h_{conv,b1w}$	Convective heat transfer coefficient from water basin to basin water, W/m^2K
I(t)	Solar irradiation / solar intensity, W/m^2
$I_{eff}(t)$	Effective solar irradiation, W/m^2
k_{b1}	Thermal conductivity of water basin
k_{b2}	Thermal conductivity of PCM basin
$k_{insulation}$	Thermal conductivity of insulation, W/mK
k_{PCM}	Thermal conductivity of PCM, W/mK
L_{PCM}	Specific latent heat of PCM, J/kg

L_w	Latent heat of basin water, J/kg
m_{PCM}	Mass of PCM
m_w	Mass of basin water
m_{yield}	Mass of water yield
M_{eq}	Equivalent heat capacity of PCM
M_d	Daily water yield, kg/m^2
M_{hr}	Hourly water yield, kg/m^2
P	Productivity, $g/kJ.m^2$
P_g	Partial pressure of water vapor at temperature of glass cover, Pa
P_w	Partial pressure of water vapor at temperature of basin water, Pa
q_{wg}	Total heat transfer from basin water to glass cover, W/m^2
$q_{conv,ga}$	Convective heat transfer from glass cover to atmosphere, W/m^2
$q_{conv,b1w}$	Convective heat transfer from water basin to basin water, W/m^2
$q_{rad,gs}$	Radiative heat transfer from glass cover to sky, W/m^2
Q_w	Sensible heat stored in basin water, W/m^2
R_g	Reflectivity of glass
R_w	Reflectivity of water
R_p	Uncertainty of productivity, %
R_η	Uncertainty of efficiency, %
S	Salinity of water (ppm)
SA_{basin}	Surface area of the water basin, m^2
Δt	Time duration of the experiment, hour
T_a	Ambient temperature, °C
T_{b1}	Temperature of water basin, °C
T_g	Temperature of glass cover, °C

T_m	Melting temperature of PCM, °C
T_{sky}	Sky temperature, K
T_w	Temperature of basin water, °C
U_b	Overall bottom heat transfer coefficient from bottom to ambient, W/m^2K
u	Type B standard uncertainty
v	Wind speed, m/s
X	Measurement
x_{b1}	Thickness of water basin, m
x_{b2}	Thickness of PCM basin, m
$x_{insulation}$	Thickness of insulation, m
y	Local uncertainty
α_b	Absorptivity of basin
α_g	Absorptivity of glass cover
α'_b	Fraction of solar irradiation absorbed by water basin
α'_g	Fraction of solar irradiation absorbed by glass cover
α'_w	Fraction of solar irradiation absorbed by basin water
ε_{eff}	Effective emissivity, 0.9
η	Efficiency, %
σ	Stefan-Boltzmann constant, 5.67×10^{-8} W/m^2K^4
τ_{FRL}	Transmissivity of Fresnel lens, 0.92
μ_j	Fraction of solar flux having extinction coefficient
n_j	Extinction coefficient

CHAPTER 1

INTRODUCTION

1.1 General Introduction

Recently, some places in Malaysia have been suffering from freshwater crisis due to floods, water pollution and global warming even though the land was graced with plenty of freshwater resources. Hence, to overcome this matter, the solar desalination method was proposed to produce fresh water, which applies the natural resource, solar energy. Solar desalination is a freshwater production method that utilizes solar heat to evaporate saline or contaminated water. The method utilizes solar stills which consists of an inclined transparent lid above a feedwater basin. The following Figure 1.1 demonstrates the diagram of utilizing conventional solar stills, where the scattered solar radiation affects the low production.

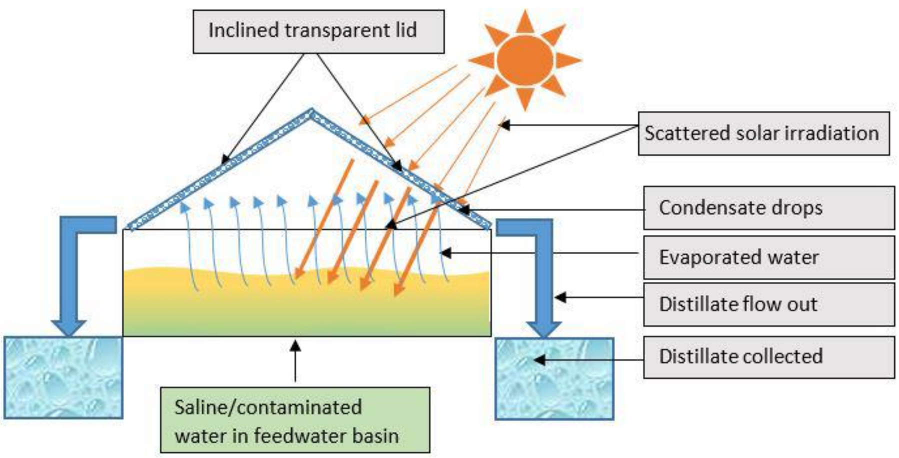

Figure 1.1: Working Principle of a double-sloped solar still (Choong, Ho and Bahar, 2020)

This study emphasizes in using a different lens design for the solar stills, which are Fresnel lens. Fresnel lenses are most commonly applied for lighthouses, where the grooves on the lens are in a series of concentric circles. The implementation of Fresnel lens increases the concentration ratio of the sunlight due to adopting the characteristic of large aperture and short focal length (Mu et al., 2019). Besides that, the phase change material (PCM) for the thermal energy storage focused on the study is nanoparticle-based. The setup for this solar desalination system is presented in Figure 1.2.

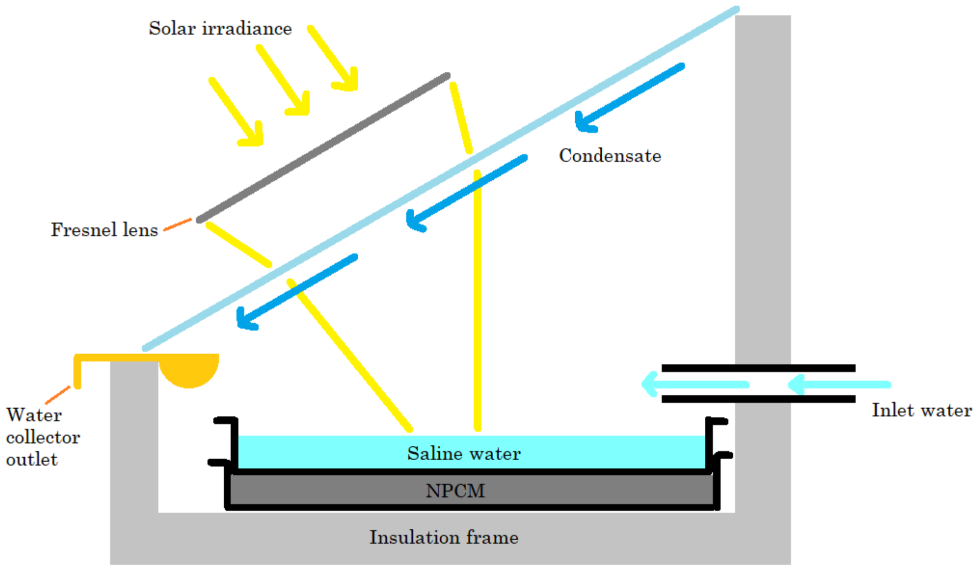

Figure 1.2: A single slope passive solar still equipped with Fresnel lens and PCM

According to the setup in Figure 1.2, the heat from the sunlight received focuses at the focal point of the Fresnel lens. The temperature at the particular focused site can reach up to 80 ~ 90 °C. Hence, formation of bubbles can only be observed at the focal point due to the elevated temperature. Besides the focal point at the water surface, the temperature of the water is much lower (about 20 to 30 °C) before heat transfer occurs at the focal point to other parts of the water in the basin. The average temperature of the feedwater in the basin is usually remained at around 50 °C; and at maximum, the temperature of feedwater can reach above 60 °C (Ho, Bahar and Koo, 2022).

The combined effect of the concentrated sunlight (CS) and nanoparticle embedded PCM (NPCM) will be investigated through indoor and outdoor experiments, which will be further discussed in Chapter 4. The success of this project will aid the country's freshwater production through utilizing the solar desalination system. Besides that, this study achieves SDG 6 (Clean Water and Sanitation) and SDG 7 (Affordable Clean Energy) by utilizing purely on solar energy to generate freshwater from saline water, which also achieves sustainability as one of the major goals in current industry trends.

1.2 Importance of the Study

Currently, there were no reports of solar desalination system integrated with Fresnel lens and nanoparticle based PCM. Furthermore, the effect of the concentration ratio on the Fresnel lenses has yet to be investigated; hence, this study provides an insight for future solar desalination systems.

The study focuses on exploring the type of Fresnel lens and PCM used which are low cost and could be easily obtained. Then, experiments are to be conducted on the test rig built based on the lenses and PCM investigated. Evaluation and analysis on the performance of the test rig is carried based on the quantity and purity of water.

1.3 Problem Statement

Based on previous research, the implementation of conventional solar stills for solar desalination has a low production rate and is unable to provide sufficient fresh water for daily usage. Despite the quality of water produced is up to standards, the quantity produced by a conventional passive solar still is too low (Sharon and Reddy, 2015). Various studies have shown comparison of conventional solar stills with the improved modified solar still integrated with thermal energy storage of optical concentrators or refractors (discussed in Chapter 2). The conventional solar stills had an average yield of below 3 L/m^2 (Al-harahsheh et al., 2018) . The primary cause is due to the unpredictable intensity of solar radiation received from the solar stills. In Malaysia, the solar irradiation received were mostly diffused; hence, resulting a lower concentration of solar energy received by the solar still.

To overcome this problem, the Fresnel lens was implemented as the concentrated sunlight (CS) device to increase the power density of solar irradiation from the diffused irradiation received. According to previous studies done, Fresnel lens was proven to have increase the production rate when it was applied as the CS device under the weather conditions such as in Malaysia; where diffused sunlight is frequently received due to the clouds (Choong, Ho and Bahar, 2020). Besides that, a phase change material (PCM) is implemented as thermal energy storage to store and provide heat when sunlight is not present. The PCM is associated with conductive nanoparticle to aid the production during cloudy weather conditions.

1.4 Aim and Objectives

The aim of this study is to investigate the suitable Fresnel lens with different concentration ratio and PCM to obtain an efficient solar desalination system. The specific objectives of this research were:

- To investigate the effect of different concentration ratio of Fresnel lens on the water production of solar still.
- To evaluate the water production of the solar still using various PCMs and conductive particle.
- To identify the optimal combination of Fresnel lens, PCM, and conductive particles for enhanced water production in the solar still.

1.5 Scope and Limitation of the Study

The scope of this study is to evaluate the suitable Fresnel lens and nanomaterials to be applied for the desalination system. The test rig for the desalination system is built to analyse the system's performance. However, limitations exist in this study and might affect the performance and efficiency of the desalination system proposed.

The limitations include fluctuated results obtained from the experiment in outdoor conditions as the diffraction of sunlight rays is different according to the location and weather. Hence, desalination system is dependent on the weather condition as it is solar driven. Moreover, there were no studies regarding the combined effect on applying Fresnel lens and nanoparticle based PCM; therefore, comparison on the performance of the system could not be done.

Furthermore, the expected efficiency in this study is about 40% to 50%, which is lower than some of the previous research. The reason is due to unexpected outdoor conditions when the experiment is carried. Meanwhile, the previous research done is based on theoretical studies, no experiment is carried by previous researchers that obtained a result of high efficiency. Moreover, there were no studies regarding the combined effect on applying Fresnel lens and nanoparticle based PCM; therefore, comparison on the performance of the system could not be done.

1.6 Contribution of the Study

The solar desalination system developed in this study is to aid underdeveloped countries for their water shortage problems. The system designed is feasible for the people to build it on their own using low-cost materials. Besides that, the utilisation of both PCM and Fresnel lens provides prospect in improving the productivity of passive solar stills. Moreover, the desalination system applies solar energy which is environmentally friendly, aids in reducing the usage of non-renewable energy which has higher CO_2 emissions.

1.7 Outline of the Report

There are a total of five chapters in this thesis report. The first chapter introduces the working principle of a desalination system using passive solar still, problems statements and the objectives of this study. Then, chapter two gives an outline of various research of the similar topic, that provides insight for this research. Furthermore, chapter three discussed about the preparation details and methodology of this study. Next, chapter four discussed and explained about the results of the experiment. Finally, chapter five concludes the pivotal findings of this research and provide insights recommendation for future works involved in solar desalination.

CHAPTER 2

LITERATURE REVIEW

2.1 Introduction

Solar desalination is a straightforward and low-cost method to produce freshwater compared to other desalination methods; for example, reverse osmosis and electrodialysis which are membrane desalination techniques; thermal desalination techniques which includes multistage flash, vapor compression, etc (Panchal et al., 2024; Mevada et al., 2023; Tan et al., 2025). However, the existing conventional passive solar stills have a low production rate despite that the freshwater produced is of high quality (Sharon and Reddy, 2015). Therefore, the current trend on the study of solar desalination system is focused on improving the efficiency and performance of the freshwater produced. There was various research based on implementing Fresnel lens and thermal energy storage to improve the performance of the system. Thus, the methods were reviewed in this chapter as a reference to this study.

2.2 Desalination Methods

Desalination is a process that removes dissolved solids (e.g. salts and minerals) to produce fresh water, that contains total dissolved solids (TDS) less than 1000 mg/L (Thimmaraju et al., 2018). There are two types of major desalination processes which were widely used in the industry, includes thermal and membrane desalination processes. Besides these two major desalination technologies, the alternative desalination technology includes freezing distillation and ion exchange methods (Saadat et al., 2018).

Thermal desalination process, also known as distillation, is the primitive method of evaporating the saline water and collect the condensate to acquire fresh water. This process is categorised into a few types which are multi-stage flash distillation (MSF), multi-effect distillation (MED) and vapour compression distillation (VC). The MSF method involves distillation in multistage chambers, where the supply water is heated under high pressure before entering the chamber with lower pressure. Hence, flashing occurs due to the pressure drop when the supply water entered the chamber, further increasing the temperature of the supply water. The process is continuous throughout the chamber as the pressure decreases in the following subsequent stages. The fresh water was collected from the condensate on the heat exchanger tubes within the chamber, due to the temperature difference between the incoming supply water (lower temperature) and the heated supply water within the heat exchanger tubes (higher temperature) (Thimmaraju et al., 2018). However, the MSF process requires high capital cost and high energy to operate (Saadat et al., 2018). Besides that, corrosion and clogging in the tubes requires maintenance, which is necessary for the plant to shut down (Thimmaraju et al., 2018; Saadat et al., 2018). The main source of thermal energy to produce steam came from fossil fuels, which produces carbon dioxide as a by-product; hence, Mohamed Tawfik, Metwally Aly and Sirag, (2025) implemented an alkaline water electrolysis unit in the MSF desalination system to reduce the carbon dioxide emissions. The electrolysis unit produces hydrogen, which will form chemical reactions with the carbon dioxide released and produces methanol.

Another widely used thermal desalination technique is multi-effect distillation (MED), which has similar working fundamentals of implementing evaporation and condensation under lower pressure. The difference is instead of directly boiling the supply water (saline water), the saline water was sprayed on the tubes carrying steam at the first effect (vessel), where the steam was transferred from a thermal compressor. The condensate in the first effect was not collected to refrain the pure distillate from mixing with impurities from the boiler (Saadat et al., 2018). Then, the vapour from the saline water at the first vessel is carried to the second (next) effect, where the pressure is lower than the previous effect, resulting the boiling temperature of the saline water to decrease. Hence, the saline water in the subsequent effects evaporates into vapour at lower temperature due to the reduced pressure. Furthermore, the process is executed at a lower temperature compared to MSF; therefore, reducing the corrosion of tubes (Thimmaraju et al., 2018). The distillate was collected from the condensation of vapour from the second effect onwards (Saadat et al., 2018). Nonetheless, the MED process is high-energy intensive and requires high capital and operational cost, and on top of that, corrosion of the materials due to contact with the brine (Saadat et al., 2018). Al-Hamzawi and Sailawi (2025) implemented a parabolic trough concentrated solar power plant and thermal energy storage with a MED system. It was reported that the analysis of the solar powered MED system has a desalination rate of 104.7 kg/s, 50 times higher than a conventional MED system study done by Askari and Ameri (2020), which has 1.91 kg/s. Meanwhile, the energy consumption required for the proposed system of Al-Hamzawi and Sailawi (2025) i is 2.5 kWh/m^3 to 3.0 kWh/m^3 and a cost rate of 0.15 \$/s, which were both lower than the RO system, that requires 3 kWh/m^3 to 4 kWh/m^3 of energy and 0.20 \$/s to 0.25 \$/s of cost rate.

Another thermal desalination method is the vapour compression distillation (VC), unlike MSF and MED where the initial heat source was produced by a boiler, it utilises a mechanical compressor or a steam ejector to compress vapour. The pressurised vapour acts as a heat source for the input saline water, and the vapour from the evaporation of saline water is collected and compressed; hence, continuing the cycle of the VC system (Thimmaraju et al., 2018). The VC method is smaller scaled compared to MSF and MED, therefore, the application is for smaller capacity usage and comparably easier to operate. However, the steam compressors in the system are high cost, and the corrosion of the evaporator components is severe due to the exposure to saline water (Saadat et al., 2018).

On the other hand, the membrane process implements membrane technology to separate the water particles from the dissolved solids when the water feed passes through. Thus, forming a low and high concentration zone, where the fresh water collected is at the low concentration section (Thimmaraju et al., 2018). The process includes reverse osmosis (RO), electrodialysis (ED) and forward osmosis (FO). The RO process utilises water pressure from the supply saline water to separate the dissolved solids when the water flows through a semi-permeable membrane. Since the water flows from a high concentration to low concentration gradient with pressure pumps applied, it was named reverse osmosis, as it defies the nature of osmosis where water flows from low concentration to high concentration solution (Thimmaraju et al., 2018). The pressure applied to the feed water ranges from 15 to 25 bar for brackish water and above 50 bars for seawater (Saadat et al., 2018). The corrosion of the system is lower compared to the thermal processes as it operates in ambient temperature. However, the membranes for the RO process are high cost and with a longevity around 5 years due to fouling (Saadat et al., 2018). Rosa, Gabrielli and Sangiorgio (2026) did an analysis on the energy, cost and carbon emissions of RO desalination globally. It was discovered that the energy consumption globally to satisfy the freshwater needed through RO requires around 805 to 1399 TWh/year of electricity, with the salinity of supply water ranging from 15 ppt (brackish water) to 40 ppt (seawater). Consequently, under the same baseline climate conditions, the energy cost is estimated to be $63 billion to $110 billion per year globally, respective to the salinity range 15 to 40 ppt of feed water applied. Meanwhile the carbon emission globally is reported that 493 to 856 million tonnes were released during the desalination process, respective to the salinity range of 15 to 40 ppt of feed water. Hence, it was advised that the energy, cost and emission can be reduced by implementing solar power into the desalination systems (Rosa, Gabrielli and Sangiorgio, 2026).

Furthermore, the electrodialysis (ED) process, a membrane separation method, dissociates the ions from the water by using electrical potential difference (Sedighi et al., 2023). Unlike the RO process, the ED process utilises ion (cation and anion) selective membranes and electromotive force to separate the dissolved solids in the supply water. Hence, the ED method is only adept in filtering the ionic components in the saline water as only ions can get attracted to the electrodes in the ED system. Even though the ED process is comparatively lower in energy demand compared to thermal processes due to the absence of phase change in the feed water (water heated to steam); nevertheless, the process is only limited to filter the ionic components in the water but not organic matter, colloids or suspended solids (Saadat et al., 2018).

Moreover, the opposite approach of RO, forward osmosis (FO), implements a semi-permeable membrane to filter the saline water from the dissolved salts through osmotic pressure gradient. The process utilises a draw solution, which is a high concentrated solution (much higher concentration than the feed water), to enable the water particles to flow through the membrane from the feed water to the draw solution, fulfilling the osmosis process. The diluted draw solution containing the water content of the supplied saline water, is processed in a separation unit, which contains a distillation column or membrane gas, to filter the draw solution from the fresh water.

Then, the draw solution is recycled back to the system, repeating the FO process (Saadat et al., 2018). However, this process is high energy consumption, which requires roughly 21 kWh/m^3, similar with the larger scale MSF process that requires 14 kWh/m^3 to 25 kWh/m^3 of energy (Sedighi et al., 2023).

Despite the abundance of fresh water produced using the above discussed desalination methods, there were several drawbacks which impacts the environment, such as the brine discharge and greenhouse gas (GHG) emission. Herrera-León et al. (2022) reported that in Chile, the main GHG emission came from water waste treatment plants, where carbon dioxide emission and nitrous oxide were released from the sludge during the biological process. Besides that, it was noteworthy to point that the GHG emissions also came from the power plants that supplies electricity to the RO desalination plants and wastewater treatment plants, which were produced by burning fossil fuels. Hence, the usage of non-renewable energy in desalination plants has higher GHG emission compared to integrating renewable energy. It was found that in 2015, there were 164 687 to 277 120 tonnes of CO_2 equivalent per year produced from the RO desalination plants and wastewater treatment plants, and it was further forecasted that it will reach 323 879 to 710 721 tonnes of CO_2 equivalent per year in 2030 (Herrera-León et al., 2022).

To reduce the GHG emissions, it was encouraged to integrate renewable energy into the desalination system, as conventional desalination plants uses fossil fuels as the main power source to operate. Ai et al. (2023) conducted a study on integrating solar energy in MED systems to investigate the impact on GHG emissions. It was calculated that the GHG emission during the construction stage for a photovoltaic-driven desalination system is 4830 tonnes of CO_2 equivalent, while the conventional thermal-driven desalination system is 12 800 tonnes of CO_2 equivalent. In the freshwater production phase, the photovoltaic-driven desalination system is 4500 tonnes of CO_2 equivalent, while the conventional thermal-driven desalination system is 93 500 tonnes of CO_2 equivalent. Therefore, the GHG emission could be reduced by 94.97 % when the energy from fossil fuels is replaced by solar energy (Ai et al., 2023). Moreover, Molinos-Senante and González (2019) assessed the economics on desalination plants when GHG emission costs were considered, as many countries are changing policies to encourage the use of renewable energy and enforcing the sustainability concept in the industry. It was found that the energy cost was 55 % to 68 % lower when the desalination plant was mainly powered by renewable energy.

2.3 Solar Desalination Technology

In Malaysia, public interest in desalination systems grew when the first plant was embarked in Sarawak. Research indicates that the urban population in Sarawak were dependent on rainwater and desalinated water due to constrained freshwater resources (Mahyan and Selaman, 2016). However, membrane-based and thermal desalination methods require significant energy and specialized infrastructure, making them considerably more expensive than using natural freshwater sources. The listed methods have also led to ecosystem and public health risk, as fuel combustion contributes to global warming, while the discharge of high salinity wastewater has negatively impacted crop growth (Alam et al., 2017) and increased infant mortality rates (Dasgupta, Huq and Wheeler, 2016). To address these challenges, renewable solar energy should be harnessed for desalination in tropical regions, offering a more sustainable and eco-friendly solution.

Solar-powered desalination operates through solar stills, where a water basin is exposed to sunlight, causing the water to heat up, evaporate, and condense into water vapor. The collected vapor, known as distillate, serves as the desired fresh water for industrial and household use. Although solar desalination is an environmentally friendly technology, conventional solar stills have relatively low efficiency and fail to meet commercial standards (Ghaffour, Reddy and Abu-Arabi, 2011). As a result, majority of the research on solar desalination aims to increase the performance through refining the design of solar stills and optimizing the key parameters.

The key parameters that have the greatest impact on the performance of solar stills include solar intensity, geographical location, ambient temperature, material and thickness of top cover, basin depth, and wind velocity (Dsilva Winfred Rufuss et al., 2016). Apart from the geometry of solar stills, the material used for fabrication and the external forces acting on the solar stills were found to have affected the efficiency of the system as well. Besides that, the concentration of solar energy also affects the efficiency of the solar still. From previous studies, most of the concentrators were built in parabolic shape, where Arun and Sreekumar (2018) and Elashmawy (2019) have reported integrating parabolic concentrators to direct sunlight to the solar still.

According to Prado, Vieira and Damasceno (2016), a solar dish concentrator built with a simplified distillation system were able to provide 4.95 kg of drinking water, which is sufficient for at least two adults per day. Moreover, (Arun and Sreekumar, 2018) applied the parabolic trough to concentrate the solar irradiation to the focal line, this heats up the receiver tube and converts the water within the tube into steam. Thus, there were various previous studies that have done the research on parabolic dish concentrators to improvise the efficiency; it has the similar concept to applying Fresnel lens, which will be conducted in this project.

2.4 Design of Solar Stills

There are various types of solar still designs that varies in shapes, and the most common designs are single-slope and double-slope stills. Dwivedi and Tiwari (2008) did an energy and exergy analysis on single and double-slope solar stills. It was reported that the overall annual yield for single-slope still is higher than double-slope still, which are 1.629 and 1.44 kg/m^2 respectively. Furthermore, the daily thermal efficiency is 21.22 to 34.2% for single-slope still, 23.14 to 36.4% for double-slope still; hence, double-slope still has a slightly higher thermal efficiency than single-slope still (Dwivedi and Tiwari, 2008).

Besides that, Altarawneh et al. (2017) conducted an experimental and numerical analysis in comparing the performance of the single-slope, double-slope and pyramidal shaped solar stills with a variation of angles tilted. It was informed that the single-slope still performs the best out of the three shapes, being double-slope still performing slightly better during summer.

Singh, Rai and Sachan (2014) conducted a study on comparing glass and acrylic as the top cover material for the single-slope solar still. It was reported that the maximum energy efficiency of the glass cover and acrylic cover is 50.37% and 29.13% respectively, whereas the maximum productivity is 3.925 L/day and 2.310 L/day for glass cover and acrylic cover respectively. The outcome was due to the result of the acrylic cover having a higher temperature than the glass cover, as the temperature difference between the condensing cover and the saline water must be larger to produce more condensate (Singh, Rai and Sachan, 2014). Hence, glass is the best material for the cover due to its high heat transmissivity.

Furthermore, the top cover thickness has to be taken into consideration when designing a solar still for desalination. Panchal (2016) conducted an experiment on using different thickness of glass cover on a solar still, which were 4 mm, 5 mm and 6 mm. It was found that the lowest thickness, 4 mm glass cover has the highest distillate collected. Moreover, according to Sarkar et al. (2017), the higher the thickness of glass cover, the higher the temperature difference between the basin water and cover surface in theoretical; but the heat transfer rate will decrease, affecting the water yield. Sarkar et al. (2017) also did a review on Ghoneyem and Ileri's work, where they found that there was 16.5 % more production when a 3 mm glass cover was used, rather than a 6 mm glass cover. Therefore, it is more suitable for the glass thickness to remain around 4 mm or less (Sarkar et al., 2017).

According to Belessiotis, Kalogirou and Delyannis (2016), the angle of inclination of the glass cover must be higher than 10º, otherwise the condensate might fall back to the saline water basin. For inclination higher than 20 º to 25 º, increases material and more likely affects the efficiency of the solar still due to more space in between the glass cover and saline water that increases convection heat losses.

2.5 Implementation of Fresnel Lens for the Desalination System

In the previous section, it was mentioned that parabolic dish concentrators were studied to increase the production rate of salination systems. Therefore, in this section, the previous findings on Fresnel lens will be discussed and reviewed. Similar to parabolic dish concentrators, Fresnel lens have been studied to improve the production rate for salination systems as well.

According to Sales (2016), Fresnel lens were applied to direct the sunlight to heat the saline water that was filled inside dark coloured glass bottles, it was observed that evaporation occurred. Furthermore, Mahmoud and Mohamed (2011) conducted an experiment using Fresnel lens for solar desalination by humidification-dehumidification process. The result shows that the yield was not achieved as there were energy losses through radiation; hence, further improvements were to be made for higher water production. Additionally, Bhambare, Kaithari and AI Hosni (2021) integrated Fresnel lens on a single slope passive solar still to improve the performance. By setting the adjustable Fresnel lens, it was reported that the temperature of the glass cover had decrease as the Fresnel lens had covered the glass cover from getting direct sunlight (except the concentrated area). Hence, it affects the increase of condensation rate due to the lower glass cover temperature. It was reported that the highest water yield collected by the solar still with Fresnel lens was 0.2 L/day, while the conventional solar still collected 0.05 L/day.

Moreover, the implementation of Fresnel lens is proven to have a lower cost compared to using other types of concentrators in terms of the material and manufacturing as mentioned by Kumar, Shrivastava and Untawale (2015) and Mu et al. (2019). According to the findings by Kumar, Shrivastava and Untawale (2015), the manufacturing process for Fresnel lens is comparably much simpler than reflectors as Fresnel lens can be mass produced using injection moulding without a high-quality surface finish and coatings. On the other hand, reflectors require a higher quality surface finish and coating at the back to maximize the reflectance. Moreover, a rigid frame is required to support the parabolic surface of a reflector while for a Fresnel lens, it was not required. Hence, Fresnel lens requires lower cost compared to parabolic dish concentrators.

Regarding the performance of the solar desalination system when it is integrated with Fresnel lens, the efficiency can achieve up to 55 % with a yield up to 30.8 litres as done by Rajesh et al. (2016). In the study of Rajesh et al. (2016), the Fresnel lens was used as a pre-heating device to pre-heat the saline water. Furthermore, an analysis was done on the exergy efficiency of a solar still utilizing Fresnel lens and energy storage material by Sathyamurthy and El-Agouz (2019); and it was reported that the maximum exergy efficiency of solar still with only Fresnel lens is 6 % during low solar intensity periods. The study found that during cloudy periods, the efficiency of the solar still is improved when Fresnel lens was implemented.

Besides that, Sansom et al. (2019) designed a desalination system that consists of Fresnel lens as the concentrator, a tracking device, control system, thermal storage with an evaporator and condenser. The study provides a good insight in this project with the detailed design of the desalination described. In addition, there is an innovative design done by Chiromawa and Ibrahim (2015) regarding bee-eyes array of Fresnel lens as the concentrator. It was found that the transmission efficiency of the lens is greater than 90 % when focal length, $f \geq 1.25$; and the transmission efficiency decreases when the number of arrays increases. To further increase the efficiency, the thermal energy storage is utilized, where it will be discussed in the next section.

2.6 Thermal Energy Storage

An alternate method to optimise the production rate of a solar desalination unit is the addition of a thermal energy storage into the system. The integration of a thermal energy storage in a solar still enables the system to continue operating during low sunlight intensity periods According to Sathyamurthy and El-Agouz (2019), the maximum exergy efficiency for the solar still with Fresnel lens and blue stones (energy material) is 11.7 % while without blue stones is 4 % during low solar intensity periods. In current trends for the material of thermal energy storage, the implementation of PCMs were more popular for solar application systems because it stores higher energy. The PCMs will only change its state when it is absorbing or releasing large amounts of (latent) heat; therefore, it results in higher energy stored compared to other materials.

The selection of the nanoparticle and PCM materials for the thermal energy storage is further explored in the next sub-section.

2.6.1 Phase Change Material (PCM)

According to Maghrabie et al. (2022), there are three types of PCMs, which are categorized into organic, inorganic and eutectic. Each type of PCMs have their pros and cons; for example, organic PCMs are nontoxic and chemically stabile but usually low in thermal conductivity. The organic PCM, paraffin compounds, were able to operate in wide ranges of temperature which is between 20 °C to 57 °C. Meanwhile, inorganic PCMs have high thermal conductivity when it comes to metallics but have low thermal conductivity when the PCM is a salt hydrate; hence, supercooling occurs and reduces the thermal efficiency of the system. Thus, the selection of PCM depends on the melting point temperature which is suitable for the application.

In the study conducted by Al-harahsheh et al. (2018), the solar desalination system utilizes a PCM can produce about 4.3 l/day.m^2 and 1.72 l/day.m^2 (takes up to 40%) during sunset. The PCM applied is sodium thiosulfate pentahydrate (STP), which were filled in all 15 plastic tubes immersed in the distilled water. STSPH is an inorganic salt which has chemical properties such as high latent heat of fusion and the change of volume is insignificant at melting point. Additionally, the material is also obtainable and low cost. The inorganic salt PCMs have a higher thermal conductivity (0.57 W/m.K) than organic salt PCMs (for example, paraffin). The properties of STP are shown in Table 2.1 below.

Table 2.1: Thermo-physical properties of sodium thiosulfate pentahydrate (Al-harahsheh et al., 2018)

Properties	**Value**
Melting point, ºC	48.5
Heat capacity (solid), J/kg.K	1460
Heat capacity (liquid), J/kg.K	2380
Density (solid), kg/m^3	1730
Density (liquid), kg/m^3	1660
Thermal conductivity, W/m.K	0.57
Latent heat of fusion, kJ/kg	208.5

Additionally, Al-Harahsheh et al. (2022) conducted a study by comparing three different PCMs in a solar still. The three PCMs involved were sodium thiosulfate pentahydrate (STP), sodium acetate trihydrate (SAT), and paraffin wax (PWAX). The PCMs were encapsulated in stainless steel tubes and submerged in brackish water inside the tank, with the total PCM mass maintained at 10 kg. The average cumulative productivity results were 6958 ml/m^2, 8045 ml/m^2, 7949 ml/m^2, and 8054 ml/m^2 for the conventional (no PCM), STP, SAT, and PWAX, respectively. The findings indicated no significant difference among the three PCM types due to their similar heat capacity and latent heat of fusion. The characteristics of the three PCMs are listed in Table 2.2.

Table 2.2: Characteristics of the different PCMs used (Al-Harahsheh et al., 2022)

Material	**Type**	**Melting point, °C**	**Specific heat, kJ/kg.K**		**Density, kg/m^3**		**Latent heat, kJ/kg**
			Solid	Liquid	Particle	Bulk	
Sodium thiosulfate pentahydrate	Salt hydrate	48.50	1.46	2.38	1730	1000	208.8
Sodium acetate trihydrate	Salt hydrate	58.00	2.79	3.00	1420	900	265.0
Paraffin wax	Organic	56.58	2.95	2.51	900	500	226

Cheng, Huo and Nian (2019) implemented shape-stabilized PCM (SSPCM), which content is 5 wt% expanded graphite composite, as the energy storage material for a pyramidal shaped solar still. It was reported that the maximum hourly yield were 0.36 L/m^2 and 0.28 L/m^2 for the modified solar still with SSPCM and conventional solar still respectively, at 3 pm. The modified solar still had 43.3 % higher daily water yield than the conventional solar still.

Besides that, Ho, Bahar and Koo (2022) is the predecessor of this project, where the implementation of Fresnel lens and PCM is available in the work. The PCM used was petroleum jelly, and it was inserted into tubes. Then, the tubes of petroleum jelly were placed in the water basin. Two models with different designs (Model A and B) were used to carry out the experiment as shown in Figure 2.1.

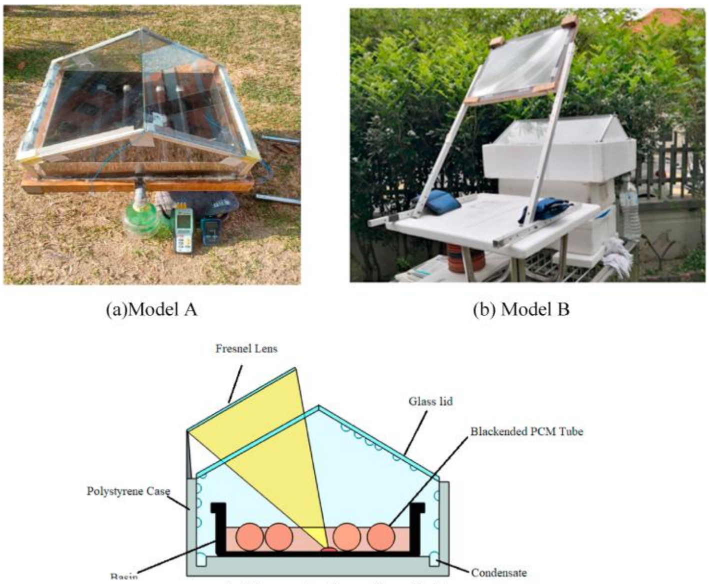

(c)Concentration of sunlight

Figure 2.1: Double slope single basin solar still prototypes Model A and B (Ho, Bahar and Koo, 2022)

The efficiency of Model A and B when both were equipped with lenses and PCM are 16 % and 32 % respectively. Meanwhile, the efficiency of Model A and B without using PCM are higher, which is 18 % and 37 % respectively. The reason was due to the leakage in the PCM tubes; hence, heat loss occurs and affects the result of the experiment when the PCM was included in the experiment (Ho, Bahar and Koo, 2022). To improvise the experiment, the PCM tubes will be placed under the water basin to avoid leakage happening.

Poonia, Singh and Jain (2022) conducted an experimental study with the combination of a parabolic dish (concentrator) and PCM (paraffin wax). The PCM was placed in an aluminium container, which acts as the receiver, that was place under the pot filled with saline water. Then, the focused sunlight gathered at the concentrator was concentrated at the receiver, where the heat received melts the PCM into liquid state (paraffin wax melting temperature is 58 °C to 60 °C). It was reported that the maximum distillate was 7.12 L/day for the setup with PCM, while it was 6.52 L/day for the setup without PCM in May. Additionally, in January, when the lowest distillate was collected, the setup with PCM collect 2.77 L/day while the setup without PCM collected 1.97 L/day. Thus, the implementation of paraffin wax as the PCM resulted in a 109 % increase in productivity.

Moreover, Thamarai Kannan et al., (2022) conducted a study in applying PCM encapsulated in waste aluminium cans for a hemispherical design solar still. Two arrangements for the placement of the PCM encapsulated aluminium cans were tested; where one solar still was placed with three cans in a triangle order, while the other was placed with four cans in a square order. The paint of the waste cans was removed and painted black to increase the heat absorbed from the sun. It was discovered that with the implementation of three PCM cans and four PCM cans had elevated the water yield by 67.12 % and 92.80 % compared to the hemispherical solar still without PCM incorporated.

In addition, Tiwari and Rathore (2022) conducted an experimental study to compare the different placement of PCM on a single slope solar still. There was a total of three experimental solar still models; the first model is a conventional solar still (CSS), second model had the involvement of PCM placed under the brackish water with a copper sheet separated (SSPC), and the third model had copper tubes filled with PCM submerged in the brackish water (SSPP). The PCM used is an inorganic material, OM 37, mixed with graphite powder (not nanopowder, as the particle size is 44 μm). It was reported that the daily distillate collected for CSS, SSPC and SSPP were 0.85 L, 1.1 L and 1.035 L respectively, where the daily distillate of SSPC and SSPP were 29.4% and 21.7 % higher than CSS.

Hence, these three types of PCMs are feasible for this study. In current study trends, further improvisation done on the PCM is to embed nanoparticles for higher conductivity. This is further discussed and studied in the next sub-section.

2.6.2 Nanoparticle Embedded PCM (NPCM)

As aforementioned, the nanoparticles embedded in the PCM provides higher conductivity; thus, the concentrated heat captured in the thermal energy storage can transfer heat uniformly throughout the whole material. Hence, providing heat to vaporize the brackish or saline water in the water basin. The PCM is usually made of low conductivity materials; therefore, it is more suitable for the embedded nanoparticles to use metal or conductive materials to enable a uniform heat transfer throughout the PCM.

According to the study done by Selimefendigil, Sirin and Oztop (2022), the preparation of the thermal energy storage unit is prepared by mixing 1 % weight concentration of copper oxide nanoparticles and the paraffin wax; both is heated up to 60 ºC for 1 hour. After the mixture is melted, it undergoes mechanical stirring for 1 hour at 500 rpm. After the mixing process, the mixture undergoes ultrasonication for 3 hours at a temperature of 60 ºC, frequency of 32 kHz, and power of 170 W. The ultrasonication process is to obtain a homogenous mixture, where then the thermal energy storage unit is completed after achieving homogenous state. The experimental results indicate that the energy efficiency of nanoparticle-embedded PCM and PCM without nanoparticles is 18.39% and 18.07%, respectively. After incorporating black paint into the nanoparticle embedded PCM, the energy efficiency increased to 19.30 %. Consequently, this study shows that adding conductive nanoparticles into the PCM increases the efficiency of the solar still.

Furthermore, a study conducted by Too (2021), had investigated the selection of nanoparticles that are suitable for solar desalination. The study was conducted on graphene and copper, it was found that implementing graphene has a higher efficiency that copper, which the respective efficiency is 45.2044 % and 45.2379 % for copper and graphene embedded PCMs. Besides that, a cost analysis is conducted for the two nanoparticle materials, the analysis shows that copper is relatively much cheaper than graphene. The cost of copper and graphene per kilogrammes is 5 dollars and 144.4 dollars respectively, which gives the cost per water yield computed is 226.08 and 46.60 ml/dollars for copper and graphene respectively. Therefore, applying copper as the nanomaterial is more feasible as it has lower cost and the difference in energy efficiency compared to implementing graphene is very insignificant.

Besides that, Lin and Al-Kayiem (2016) did a study on evaluating the performance of using copper nanoparticles (nano Cu) and paraffin wax (PW) composition for thermal energy storage (TES). The size of copper nanoparticle used is 20 nm. The experiment investigated on pure paraffin wax, 0.5%, 1.0%, 1.5%, and 2.0% weight percentage of copper nanoparticles, where the number of nanoparticles is within recommended weight ratio range, 0.2 % to 4.0 %. For the preparation of the TES, the PW was firstly heated in a beaker; secondly, nano Cu powder was disseminated in the beaker; thirdly, the mixture of nano Cu and PW undergoes ultrasonication and maintained at a temperature of 70 °C for four hours. The aim for the ultrasonication process is to disperse the nano Cu in the mixture and reduce agglomeration. After the ultrasonication process, the mixture was left to cool down for four hours under room temperature. The five samples underwent Differential Scanning Calorimetry (DSC) analysis to compare the melting and solidification points, the results were tabulated in Table 2.3.

Table 2.3: Melting and solidification temperatures of the nanocomposites compare to pure paraffin wax (Lin and Al-Kayiem, 2016a)

Material	**Melting**		**Solidification**	
	Temperature (°C)	Latent Heat (kJ/kg)	Temperature (°C)	Latent Heat (kJ/kg)
Pure PW	60.42	184.2	55.20	179.3
0.5% Nano Cu-PCM	59.57	172.2	58.62	170.6
1.0% Nano Cu-PCM	58.97	166.7	57.37	164.3
1.5% Nano Cu-PCM	58.15	160.3	56.35	159.6
2.0% Nano Cu-PCM	57.81	157.3	56.49	155.5

The results in Table 2.3 shows that the sample with higher content of copper nanoparticles provides a lower shift in the melting and solidification temperature, which are 5.22 °C, 3.95 °C, 1.60 °C, 1.80 °C, and 1.32 °C for Pure PW, 0.5% Nano Cu-PCM, 1.0% Nano Cu-PCM, 1.5% Nano Cu-PCM, and 2.0% Nano Cu-PCM respectively. Hence, the copper nanoparticles here acted as a nucleation agent in reducing the supercooling effect during the phase change process of the paraffin wax. Besides that, the latent heat of fusion and crystallization of PW is higher than the nanocomposite samples. Therefore, samples with higher PCM (PW) content absorbs and stores higher heat energy compared to samples with lower PCM content (Lin and Al-Kayiem, 2016).

The thermal conductivity and thermal diffusivity of the samples were measured using the transient hot disk thermal constant analyser, where the measurements are shown in Table 2.4. From Table 2.4 shows that the higher the amount of nanoparticle added to the sample, the higher the thermal conductivity of the sample. Besides the amount of nanoparticle added, one of the main factors that affects the thermal conductivity of the sample is the dispersion of nanoparticles. It was observed that agglomeration of the nanoparticles was found in the 1.0% Nano Cu-PCM sample; thus, the latent heat was reduced. Hence, it is advised to perform longer ultrasonication process to enable better dispersion of the nanoparticles in the PCM. Nevertheless, the overall collector efficiency increased 1.7% when the 1.0% Nano Cu-PCM was used in the site test compared to pure PW (Lin and Al-Kayiem, 2016).

Table 2.4: Enhanced thermal properties of nano Cu-PCM composite (Lin and Al-Kayiem, 2016a)

Samples	**Thermal Conductivity (W/m °C)**	**Percentage of Enhancement (%)**	**Thermal Diffusivity (mm^2/s)**	**Percentage of Enhancement (%)**
Nano Cu	401		97.1	
Pure PW	0.172	-	0.1900	-
0.5% Nano Cu-PCM	0.200	14.0	0.2086	8.9
1.0% Nano Cu-PCM	0.226	23.9	0.2589	26.6
1.5% Nano Cu-PCM	0.299	42.5	0.3124	39.2
2.0% Nano Cu-PCM	0.320	46.3	0.3446	44.9

Ouikhalfan et al. (2019) utilized myristic acid (MA) as the PCM and incorporated nanoparticles, including TiO2, CuO, Al2O3, and ZnO, at concentrations of 0.1 wt%, 0.5 wt%, 1.0 wt%, and 2.0 wt% for their study. It was discovered that the ratio of thermal conductivity for titanium oxide (TiO_2), copper oxide (CuO), aluminium oxide (Al_2O_3), and zinc oxide (ZnO) at 2.0 wt% were 1.37, 1.45, 1.49, and 1.50, respectively. The results suggested that it was more effective to incorporate Al_2O_3 and ZnO nanoparticles with the PCM, as these nanoparticles exhibited the highest thermal conductivity among the four studied (Maghrabie et al., 2022).

Furthermore, Afolabi et al. (2023) applied zinc nanoparticle and the PCM, paraffin, as the energy storage material on a double slope solar still. The zinc nanoparticle embedded PCM was microencapsulated by epoxy resin at the inner surface of the absorber basin; hence, the PCM nano-composite is between the inner surface of the absorber basin and the epoxy resin. It was reported that the solar still with the thermal energy storage (zinc nanoparticle enhanced PCM) had a 105 % increase in water yield compared to the conventional solar still. The average water yield collected were 4.5 L/m^2 and 2.8 L/m^2 for the solar still with thermal energy storage and the conventional solar still, respectively.

Moreover, Shoeibi, Kargarsharifabad and Rahbar (2021) added CuO and Al_2O_3 nanoparticles into paraffin wax to enhance the thermal properties of the PCM. 0.1 wt % and 0.3 wt % of CuO nanoparticle and Al_2O_3 nanoparticle were mixed into the paraffin wax and were filled into the copper pipes. An additional step of mixing black paint with CuO nanoparticle was carried, and the mixture was sprayed on the copper pipes to enhance the thermal conductivity. The modifications and comparison done by Shoeibi, Kargarsharifabad and Rahbar (2021) were tabulated in Table 2.5 along with the water yield collected from the solar stills. It was discovered that CSSA-NA-NP2 had the highest water yield collected, and was closely followed by CSSA-NA-NP4. Hence, the presence and higher amount of nanoparticle within the PCM had increase the performance of the solar still.

Table 2.5: The comparison of the water yield with different modifications on a double slope solar still (Shoeibi, Kargarsharifabad and Rahbar, 2021)

Abbreviation of the solar stills	**Description**	**Daily water yield, ml/m^2 per day**
CSS	Conventional double slope solar still	887.5
CSSA	Solar still filled with anthracite	1008.3
CSSA-P	Solar still with PCM tubes and anthracite	1081.2
CSSA-NA-P	Solar still with nano-coated PCM tubes and anthracite	1143.7
CSSA-NA-NP1	Solar still with nanocoated tubes filled with 0.1 wt% CuO nano-enhanced PCM and anthracite	1266.6
CSSA-NA-NP2	Solar still with nanocoated tubes filled with 0.3 wt% CuO nano-enhanced PCM and anthracite	1383.3
CSSA-NA-NP3	Solar still with nanocoated tubes filled with 0.1 wt% Al_2O_3 nano-enhanced PCM and anthracite	1220.8
CSSA-NA-NP4	Solar still with nanocoated tubes filled with 0.3 wt% Al_2O_3 nano-enhanced PCM and anthracite	1327.1

Additionally, Manoj Kumar et al. (2021) conducted a study utilizing paraffin wax (PW) as the PCM and incorporating copper oxide (CuO) and aluminum oxide

(Al2O3) as nanoparticles. The preparation of the nanoparticle embedded PCM (nePCM) was through the two-step method. Firstly, the paraffin pellets were melted and stirred at 75 °C; then, 1.0% of the nanoparticles were added to the paraffin and continue to stir for one hour. After an hour, the mixture underwent sonification for 90 minutes to ensure a uniform dispersion of the nanoparticles. Differential scanning calorimetry (DSC) was carried on the three samples at a scanning speed of 5 °C per minute at temperature 30 °C to 80 °C in a nitrogen atmosphere. The results of the DSC analysis conducted on the three samples were shown in Table 2.6.

Table 2.6: Differential scanning calorimetry (DSC) results of Sample A, B and C (Manoj Kumar et al., 2021)

Sample	**During Heating**		**During Cooling**		**Degree of Supercooling (° C)**
	Melting Point (°C)	Latent Heat (kJ/kg)	Crystallization Point (°C)	Latent Heat (kJ/kg)	
A. 100% PW	64.0	140	57.0	136	7.0
B. PW + 1% Al_2O_3	62.6	137	57.8	131	4.8
C. PW + 1% CuO	62.2	134	58.1	128	4.1

The results indicated that the CuO nanocomposite achieved the greatest reduction in supercooling, showing a 40% improvement over pure PW and an 8.58% improvement compared to Al_2O_3 nanocomposite. Furthermore, the latent heat of fusion and crystallization for Sample B had a decrement of 4.3% and 5.9% respectively, while latent heat of fusion and crystallization for Sample C had a decrement of 2.2% and 3.7% respectively. As a result, the Al_2O_3 nanocomposite demonstrates slightly superior latent heat performance compared to the CuO nanocomposite. However, the CuO nanocomposite has 21.12% higher thermal conductivity than the Al_2O_3 nanocomposite. Therefore, the CuO nano-PCM is better than Al_2O_3 nanocomposite at 1.0 wt% (Manoj Kumar et al., 2021).

Other than that, there were various studies that have reported using high-cost nanomaterials such as graphene, silver and MXene. Rajendran et al. (2026) investigated on implementing a graphene nano-coated absorber and a hybrid nanoparticle embedded PCM on a passive twin wedge solar still. The hybrid PCM which was prepared by mixing 9 g of alumina nanoparticles, 7.5 graphene oxide, and 3 g sodium oleate (a surfactant to decrease surface tension between the substances) nanoparticles into the paraffin wax. Six cases were considered for comparison; Case 1 is a conventional twin wedge solar still with black paint, Case 2 involves the graphene nano-coated absorber, Case 3 is integrated with paraffin wax (pure PCM), Case 4 is integrated with nano-PCM, Case 5 is integrated with both graphene nano-coated absorber and PCM, and lastly Case 6 is integrated with both the graphene nano-coated absorber and nano-PCM. Rajendran et al. (2026) reported that the productivity per day were 2.569 L/m^2, 3.623 L/m^2, 3.814 L/m^2, 4.414 L/m^2, 5.326 L/m^2, and 6.133 L/m^2 for Case 1, 2, 3, 4, 5, and 6 respectively. The results showed a significant increase when the nano-coated absorber and nano-PCM is involved. The cost of distillate per litre (CPL) for Case 6 is $ 0.012 per litre, lowest among the cases. The Total Dissolved Solids (TDS) measured is around 932 ppm to 935 ppm for the saline water, while the distillate is around 17 ppm to 18 ppm (Rajendran et al., 2026).

Moreover, Shaaban et al. (2025) reported using silver nanoparticle embedded PCM on a modified hybrid desalination system that uses a vertical wick solar still and spherical solar still. The nano-PCM was prepared with 25 g of silver nanoparticles and 975 g of paraffin wax. The nano-PCM is arranged with metal fins at the spherical still. There were comparisons made between the modified nano-PCM spherical still and conventional spherical still, where the water yield is 8350 ml and 4350 ml, respectively. It was reported that the productivity of the combined effect of the modified nano-PCM spherical still and vertical wick still obtained 13 litres of distillate per day, 199 % higher than the conventional spherical still. The CPL of the combined effect is $ 0.011 per litre, slightly lower than the conventional spherical still which is $ 0.02 per litre (Shaaban et al., 2025). Additionally, Guo et al. (2025) explored in implementing the PCM, polyvinyl alcohol (PVA)/cellulose nanofiber/MXene hydrogel, as an evaporator into a passive solar still. The PCM hydrogel was prepared with 10 wt% of PVA, cellulose nanofiber and 1.5 wt% of MXene (m-$Ti_3C_2T_x$), and the PCM hydrogel was moulded into an umbrella shaped evaporator. The PCM hydrogel evaporator was tested indoor and outdoor. For the indoor experiment, under one-sun of radiation received, the evaporation rate for PVA/cellulose nanofiber PCM hydrogel is 1.11 kg/m^2h while with the addition of the nanoparticle, MXene, in the PCM hydrogel, the evaporation rate is 2.09 kg/m^2h. In the outdoor experiment, the nano-PCM hydrogel was integrated in a clear acrylic single-slope solar still and achieved a yield of 16.02 kg/m^2 per day, which is 34.7 % higher than the indoor experimental results due to applying natural convection optimization (Guo et al., 2025).

In addition to that, it was reported that the use of hybrid nanoparticles PCM has enhanced the performance of solar stills due to the improved thermal properties of the mixed-nanoparticles. It was proven that the nanoparticle combination, Al_2O_3 and

Cu, TiO_2 and Ag, CuO and graphene oxide, TiO_2 and Cu, Fe_3O_4 and carbon have been proven that it elevates the performance of solar stills (Dubey and Arora, 2024). Venkatesh et al. (2024) had explore on implementing a hybrid nanofluid on a flat plate solar collector, where the nanoparticles involved are alumina (Al_2O_3), silica (SiO_2) and copper oxide (CuO). The combination of nanofluid involved were Al_2O_3/SiO_2, SiO_2/CuO, and Al_2O_3/CuO, where it was prepared with a 50:50 ratio of the hybrid nanoparticles with 0.3 wt%, mixed with water. The thermal conductivity of the nanofluids were analysed with a KD2 Pro thermal conductivity analyser, and it was measured that the thermal conductivity was 0.617 W/mK, 0.626 W/mK, and 0.631 W/mK for Al_2O_3/SiO_2, SiO_2/CuO, and Al_2O_3/CuO, respectively. The thermal conductivity for Al_2O_3/CuO is the highest among the three nanofluids, as both materials are highly thermal conductive and complimented each other well when combined together. For the experimental results of the water yield, Venkatesh et al. (2024) reported that the distillate collected were 156.2 ml/m^2, 161.5 ml/m^2, and 171.9 ml/m^2 for Al_2O_3/SiO_2, SiO_2/CuO, and Al_2O_3/CuO, respectively, showing that the Al_2O_3/CuO nanofluid combination has the highest result which could reflect to the thermal conductivity of the mixed nanomaterial being the highest (Venkatesh et al., 2024).

Other than that, Khalil et al. (2020) also reported an investigation on implementing the hybrid alumina and copper oxide nanofluid on a solar parabolic trough collector. A spectral analysis was conducted on the alumina and copper oxide nanparticles, and it was found that the alumina nanoparticle has an absorption value of 2.7 a.u. while the copper oxide nanoparticle is 1.0 a.u., which indicates that alumina has a higher solar irradiation absorption than copper oxide. Hence, with the combination of a high absorption material (alumina) and high thermal conductivity material (copper oxide), the hybrid nanofluid has better thermal properties to enhance the performance of the solar still compared to a single-material content nanofluid (Khalil et al., 2020). In addition, findings of the nano-hybrid PCM (RT50) using copper and alumina nanoparticles was implemented in a heat exchanger to store heat and maintain the water temperature (Nitsas and Koronaki, 2021). The experimental results shows that the specific heat capacity of the pure PCM was decreased, where the latent heat is 197.5 KJ/kg, and was reduced to 174.8 KJ/kg when copper nanoparticles were added. It was further reduced to 173.9 KJ/kg for the hybrid PCM, that has both copper and alumina nanoparticles added. Therefore, the energy required to phase change has decrease with the addition of nanoparticles. However, it was observed by Nitsas and Koronaki (2021), that the copper nano-PCM requires shorter time to melt compared to the hybrid nano-PCM, as copper is highly thermal conductive compared to alumina.

Furthermore, Tofani and Tiari (2021) stated that paraffin wax is a commonly chosen PCM due to its broad range of low melting points and its synergy with various types of conductive particles. Alumina and copper nanoparticles are the popular choices for nePCM in thermal applications. The case study highlights numerous reports have shown a significant enhancement in thermal system performance with the incorporation of alumina and copper nanoparticles in PCM, compared to using PCM alone. Various research on the PCM have been reported and the research for nanoparticle based PCM (NPCM) can be further improvised to increase the performance of the solar desalination system.

2.7 Summary

In this review, it shows that the combination of Fresnel lens and nano-particle embedded PCM are feasible for further study, as the Fresnel lens aids in concentrating the sunlight while the PCM stores energy and dissipates heat during low solar intensity periods. It was discovered that paraffin wax is a more common PCM due to its thermal characteristics, cost and availability in the market. Besides that, alumina and copper nanopowder is also frequently used as the thermal conductive material in the PCM to decrease the melting point, this is due to the lower cost compared to other nanomaterial such as titanium or silver. Furthermore, it was also discovered that little to none of the existing works have provided a study on mixing different nanoparticles together. Therefore, the current study will be investigating the combination of Cu and Al_2O_3 nanoparticles mixed within the PCM.

Furthermore, the design of the solar stills, such as the material, size and slope were being considered during the fabrication of the experimental solar still models. The single slope solar still design was selected as it is the simplest and lowest cost design among the other existing solar still designs. The best material for the top cover is glass, as it was concluded by Singh, Rai and Sachan (2014) that the temperature on the acrylic cover is higher than the glass cover which will affect the condensation rate.

Additionally, the study done by Thamarai Kannan et al. (2022) had provided insight on reusing waste materials to increase the thermal conductivity of the PCM. Thus, implementing waste aluminium scraps were considered as the additive to replace nanoparticles due to the low cost and recyclable material. Besides improving the performance of the desalination unit, at the same time it also reduces and recycles the metal waste. Therefore, the usage of waste materials along with the aid of a concentrator (Fresnel lens) will also be investigated in this study as there were no previous studies investigating in this field.

CHAPTER 3

METHODOLOGY AND WORK PLAN

3.1 Introduction

Firstly, the literature review will be carried on the initial phase of this study. From the literature review, the significant findings and parameters for the solar stills were narrowed. The parameters here refer to the aperture size, focal length and concentration ratio of the Fresnel lens, the conductivity of the nanoparticles for the PCM, size of the solar still, etc. By doing the literature review, it provides a better approach for the study to be conducted.

After the literature review, the findings obtained for the combined effect of Fresnel lens and nanoparticle based PCM is applied on the experiment setup of the project. There is a total of two stages for the experiment; the first stage is carried in a controlled environment with a simple setup using a solar simulator (ideal case scenario) while the second stage is carried in an outdoor environment with a test rig built (real case scenario). The first and second experiment is discussed in Section 3.3 and 3.4. After obtaining the important parameters from the experiment, the next step is to analyse the experimental results and evaluate the performance of using different Fresnel lenses and PCMs.

3.2 Fabrication Details

The material used for the external frame is polyfoam box and glass with a thickness of 2 mm (initial) is used as the top cover. The thickness of the top cover was later changed to 5 mm for outdoor experiments of Subsection 4.3.2, Subsection 4.3.3 and Subsection 4.3.4, as the glass breaks due to the high concentrated temperature focused by using the large Fresnel lens. Polyfoam box is chosen due to its waterproof and a good heat insulation characteristic. The external dimension of the polyfoam box is 19.6 cm (L) × 16.3 cm (W) × 9.6 cm (H), while the internal dimension is 16 cm (L) × 13 cm (W) × 7 cm (H). Due to the small size of the polyfoam box, the maximum inclination allowed for the top cover is 15 °.

Moreover, two different dimensions of aluminium basins were used to contain the water and the PCM, where the PCM is placed in the larger basin due to volume expansion when it receives heat. Black paint was sprayed on both basins during the preparation stage so that it receives more heat from the heat source (bulb or sun). The basin arrangement is by placing the water basin on top of the PCM basin. The dimension of the bottom basin (for PCM) is 16 cm (L) × 10.8 cm (W) × 3.8 cm (H); as for the upper basin (for saline water), the dimensions are 15.8 cm (L) × 10.2 cm (W) × 3.2 cm (H). Besides that, two water hoses were attached to the polyfoam box; the smaller diameter clear hose is used for filling the water in the basin and the larger diameter orange hose (slanted 5 °) for collecting the distillate. The solar stills were sealed using silicone sealant (Brand: Saint-Gobain Weber) at the edges of the hoses and between the glass cover and polyfoam box to reduce vapor loss.

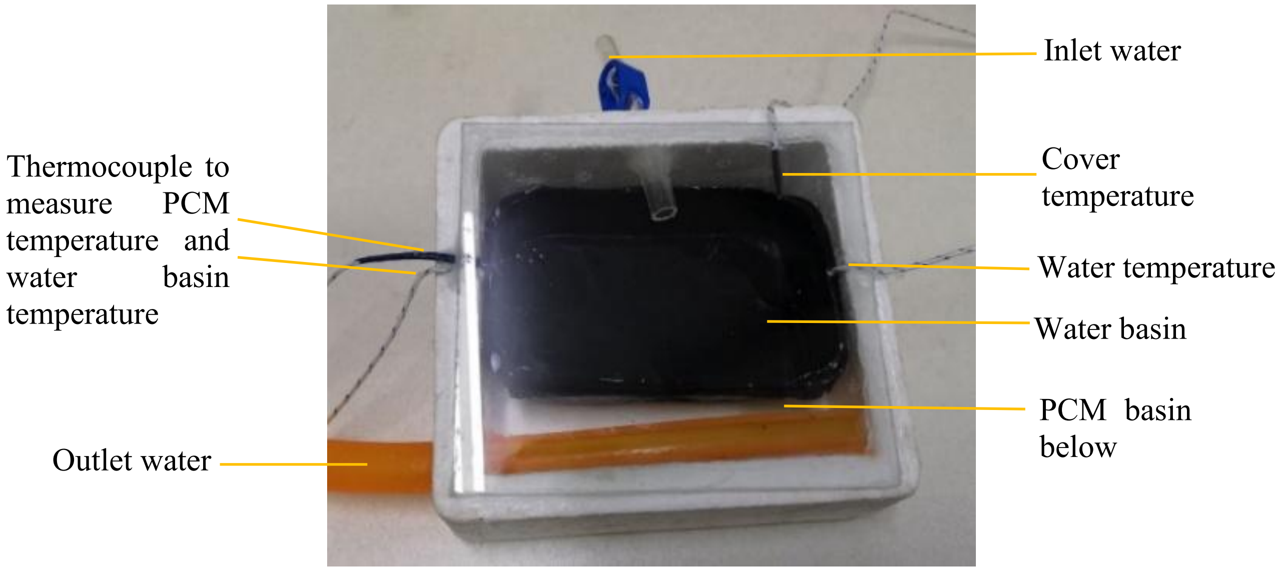

Figure 3.1: Design of the scaled-down passive solar still

Additionally, an actual scale solar still prototype was fabricated to carry out the experiment for the finalized combination of Fresnel lens and PCM. Similar with the scaled-down models, a polyfoam box was used for the outer case of the solar still while two coated steel roasting pans was used for the water basin and PCM basin. The basin was changed from aluminium to steel due to the dimensional constraint of existing aluminium trays, where the sizes of the aluminium trays are too small for the prototype. Besides that, the steel pan has a sturdy built compared to the aluminium trays, which are made of aluminium foil which are highly ductile; hence, the shape of the basin changes easily due to the weight of the water and PCM when the aluminium tray was used. The bottom PCM basin (13” roasting pan) was slightly larger than the water basin (12” roasting pan), to contain and enable the expansion of PCM when it melts. The dimensions of the prototype are 49.0 cm (L) × 37.0 cm (W) × 28.5 cm (H), with a thickness of 2.5 cm. Furthermore, the slope of the prototype was increased to 30 °, to decrease the condensate from falling back into the water basin. The overall details of the scaled-down model and prototype were listed in Table 3.1 below.

Table 3.1: Details of the scaled-down model compared with prototype

Type	Scaled-down model	Prototype
Length	19.6 cm	49.0 cm
Width	16.3 cm	37.0 cm
Height	9.6 cm	28.5 cm
Thickness	1.0 cm	2.5 cm
Slope	15 °	30 °
Glass thickness	3 mm / 5mm	5 mm
Material of water / PCM basin	Aluminium	Coated steel
Internal length of water basin	14.6 cm	30.7 cm
Internal width of water basin	9.0 cm	21.4 cm

3.3 Material Selection and Preparation Methods of the PCM

The selection of the conductive nanoparticles is proceeded with the criteria of conductivity and cost. Optimization is done on the PCM's nanoparticle density, melting point, reactivity, and other properties to decide the type and the quantity of conductive nanoparticles within the PCM. Then, the improvised formulation is established to interpret the combined thermal properties of the conductive nanoparticles and PCM.

The PCM used is usually a low conductivity material; hence the low thermal conductivity will cause the heat captured to be ununiform. Therefore, the nanoparticles chosen is a conductive material as it aids the heat transfer in the PCM to be uniform.

The PCM chosen in this study is paraffin wax (PW), where it is heated to 60 ~ 70 ºC in the preparation procedure to fabricate the thermal energy storage material. As for the conductive nanoparticle, the material chosen is Copper nanopowder (Merck, 60 - 80 nm) and Aluminium Oxide nanopowder (Merck, <50 nm), supplied from Sigma-Aldrich (also known as Merck). Besides that, aluminium scrap, which was cut in pieces (smaller than 0.25 mm^2) was also involved in this study to compare with the higher price materials as a cheaper alternative. The PCM combination weighs 50 g, where the concentration of the nanoparticle used is 1.0 wt%, which is within 0.2 % to 4.0 % recommended by Lin and Al-Kayiem (2016), while the aluminium scrap is 1.5 wt%. The contents of the four different combinations of PCMs are shown in Table 3.2 below. Besides that, the properties of the conductive particles were compiled in Table 3.3, where the thermal conductivity and specific heat capacity were referred to MatWeb (Anon., 2024).

Table 3.2: Content of conductive particles in the PCMs

Combination	**Aluminium scrap**	**Alumina nano powder**	**Copper nano powder**
1	0.75 g	-	-
2	-	0.5 g	-
3	-	-	0.5 g
4	-	0.25 g	0.25 g

Table 3.3: Properties of conductive particles

Properties	Aluminium scrap	Alumina nano powder	Copper nano powder
Thermal conductivity, W/m.K	210.0	25.0	385.0
Specific heat capacity, J/kg.K	900	880	385.0
Density, g/cm^3	2.70	3.90	8.94
Size	≤ 1 cm	< 50 nm	60-80 nm
Purity	-	-	≥ 99.5 %

The preparation of the PCMs starts by firstly heating the solid PW to liquid form using a magnetic hot plate at the temperature 85 ºC for an hour. For NPCMs, the nanopowder was added into the liquified PW with a magnetic stirrer and was stirred for 30 minutes at 500 rpm. Later, the sonication process takes place by placing the beaker filled with the NPCM solution in the ultrasonic cleaner, which supposedly the ultrasonication is prepared using an ultrasonicator probe. However, due to the limitation of the equipment in the university lab, the ultrasonic cleaner was used to replace the ultrasonicator. The temperature was set to 70 ºC and the timer at 30 minutes. Lastly, the NPCM solution is poured into an aluminium basin and cooled down at room temperature for an hour. As for aluminium scrap based PCM, the liquified PW after heated an hour was poured into the aluminium basin and the aluminium scrap was added into the basin uniformly spread. Lastly, similar to the NPCMs, it was cooled at room temperature for an hour. After the preparation of the PCMs, it is placed under the water basin in the test rig. The magnetic hot plate and ultrasonic cleaner used to prepare the PCM was shown in Figure 3.2.

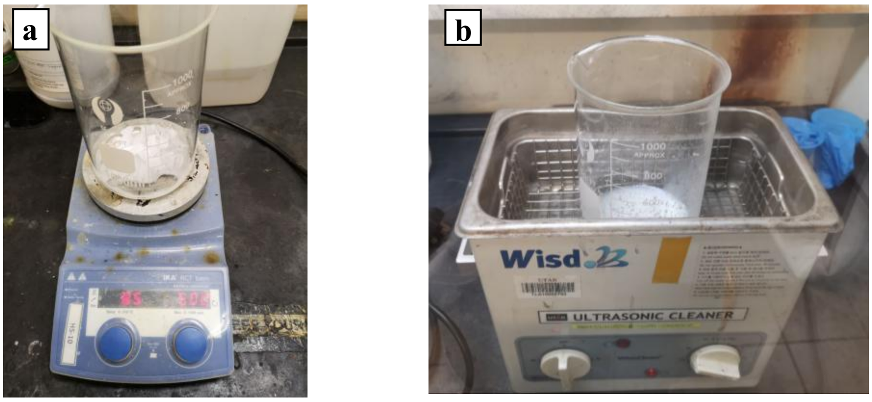

Figure 3.2: Lab equipment used to prepare the PCM (a) Magnetic hot plate (b) Ultrasonic cleaner.

Besides that, a calculation was done to determine the mass of the paraffin wax needed for the prototype. Before the calculation, water was filled in between the enclosed space of the PCM basin and water basin to determine the mass it could contained and the mass of the water measured was 313 g. Besides that, the paraffin wax is 86 % denser than water; hence the mass of the paraffin wax could be found by multiplying the mass of water with 86 %. Furthermore, important parameters to include in the calculation where the density of paraffin wax is 0.93 g/cm^3 and the volume expansion is 15 % at its melting point 75 °C. The calculation steps were proceeded as follow:

$$Mass\ of\ PW = 313\ g \times 0.86$$

$$= 269.18\ g$$

$$Volume\ of\ PW\ (solid) = \frac{269.18\ g}{0.93\ g/cm^3}$$

$$= 289.44\ cm^3$$

$$Volume\ of\ PW\ (liquid) = 289.44\ cm^3 \times 115\%$$
$$= 332.86\ cm^3$$

It was found that after volume expansion, the 269.18 g of paraffin wax occupies a volume of 332.86 cm^3. However, the enclosed space between the basins can only contained 313 cm^3 of substance. Hence, with estimation, the paraffin wax was reduced to 260 g, which is 321.5 cm^3 after expansion with a slight extra of 8.5 cm^3 more than the intended volume. The decided mass of the paraffin wax is 256 g and the Al scrap is 4g (1.5 wt%).

3.4 Experiment on Indoor Conditions

The solar simulator is applied to select the suitable Fresnel lens. A scaled down test rig is built to carry out the first experiment. The starting amount of saline water (sodium chloride solution, 9000 ppm) is 75 ml, which is lower than 1 cm water level. Due to the small size of the test rig, the work area required is small; hence, the experiment was carried out in the university laboratory. The aim of this experiment is to determine the suitable PCM; thus, it is carried out by using different types of PCM combinations to determine the best outcome.

The experiments were conducted in the university laboratory (KB730) under a solar simulator (model: Oriel LCS-100). The solar still utilised a single-slope design, making it suitable for the indoor experiment. Each solar still was equipped with four K-type thermocouple probes (sensitivity around 41 μV/°C) to monitor and measure the temperatures of the water, PCM, cover, and basin. The temperature readings were recorded using the Yowexa YET-640X thermometer. The experiment was conducted for 3 hours per model, and the temperatures were taken every 30 minutes. Besides experimenting on different PCMs, three different sizes and focal length (FL) of Fresnel lenses purchased from Edmund Optics were explored. The details of the Fresnel lenses were listed in Table 3.4.

Table 3.4: Details of the Fresnel lenses used for indoor experiment

Focal length (FL), inches	**Focal length (FL), mm**	**Dimension, mm**	**Effective diameter, inches**	**Aperture diameter, mm**
5.00	127.00	127.0 × 127.0	4.0	101.6
3.90	99.06	76.2 × 76.2	2.5	63.5
7.90	200.66	76.2 × 76.2	2.6	66.04

Figure 3.3: Setup of the indoor experiment.

3.5 Experiment on Outdoor Conditions

The outdoor experiment was conducted during June till August 2023, where the weather is occasionally cloudy and later affected by haze. The solar stills were the same as the ones used in the indoor experiments, but the duration of the experiment is different. The outdoor experiment was conducted from 9 am to 6 pm (9 hours) and the temperature readings and irradiation measurements were taken every hour. Similar to the indoor experiment, the starting amount of saline water is 75 ml, which is lower than 1 cm water level.

The initial outdoor experiments were to compare the different Fresnel lenses while using the same PCMs; hence, duplications of the same types of PCMs were prepared beforehand for the outdoor experiment. There were four different sizes of Fresnel lenses and four different types of PCMs; therefore, the similar experiment was conducted four times with different Fresnel lenses and same PCMs each time to ensure every combination of lenses and PCMs were compared. The fourth Fresnel lens, which was unable to be included in the indoor experiment due to the size limitation of the solar simulator, has the dimension 30 cm × 30 cm, effective diameter of 30 cm, and FL of 33 cm. The transmissivity of the four Fresnel lenses is the same, which is 0.9. The concentrated ratio (CR) was calculated using the aperture area divided by the estimated concentrated receiver area. The details of the Fresnel lenses used in the outdoor experiment is shown in Table 3.5.

Table 3.5: Details of the Fresnel lenses used for outdoor experiment

Focal length (FL), mm	**Dimension, mm**	**Aperture area, mm^2**	**Estimated concentrated receiver area (mm^2)**	**Concentration ratio**
127.00	127.0 × 127.0	8107.32	706.86	11.47
99.06	76.2 × 76.2	3166.92	314.16	10.08
200.66	76.2 × 76.2	3425.34	314.16	10.90
330.00	300.0 × 300.0	70685.83	2827.43	25.00

Under the Fresnel lenses, the temperature of the concentrated area was measured around noon. It was measured that the 9000 ppm saline water at the concentrated area under FL 33.0 cm Fresnel lens reached a boiling temperature of 99.40 °C after 1 to 2 minutes when the solar irradiance measured using the solar power meter is 1289 W/m^2. According to Figure 3.4, bubbles were formed aggressively at the concentrated area under the FL 33.9 cm Fresnel lens. Besides that, the water temperature at the concentrated area under Fresnel lenses FL 12.7 cm, FL 9.9 cm and FL 20.1 cm were only able to reach around 50 °C to 60 °C after 1 to 2 minutes when the solar irradiance measured is around 1000 W/m^2. The temperature at the focal point for each Fresnel lenses were listed in Table 3.6.

Figure 3.4: Aggressive bubble formation at the concentrated area under FL 33 cm Fresnel lens

Table 3.6: Temperature at concentrated area using different Fresnel lenses

FL of Fresnel lens used, cm	Solar irradiance, W/m^2	Temperature at focal point, °C
12.7	1014	56.36
9.9	1078	52.98
20.1	1037	51.41
33.0	1289	99.40

After getting the best Fresnel lens from the results, it was then used to conduct another set of experiment, which is using the same size of lenses (additional three more lenses of the same type were purchased) but different type of PCM. Lastly, the final sets of experiment were done to compare the performance of the solar still when using different salinity of saline water (10k, 20k and 30k ppm), where the experimental setup was shown in Figure 3.5. The different salinity of saline water was measured and calculated by using the equation 3.1 in Section 3.6.

Figure 3.5: Outdoor experiment setup for comparing different saline water

After comparing different combinations of Fresnel lenses, PCMs and saline water, an actual size solar still was built to validate the results. The conductive particle used for the PCM is aluminium scrap since the price of the nanomaterial is very high for such a large size. The salinity of saline water used for the prototype is 30 000 ppm, and starting amount of saline water is 300 ml, which is around 0.5 cm of water level. The prototype fabricated was shown in Figure 3.6, and the instrument used to collect the data were shown in Figure 3.7.

Figure 3.6: Actual size prototype

a) Thermometer

b) Solar power meter

c) TDS tester

d) Anemometer

Figure 3.7: Instruments used in the experiments a) Thermometer b) Solar power meter c) TDS tester d) Anemometer

3.6 Theoretical Study

This section discussed on the theoretical method on how the solar still works when applied with PCM and Fresnel lens. For a simple passive solar still, the water in the basin gains energy from the sunlight (solar energy); and when the temperature increases, the water molecules gained higher kinetic energy to phase change into vapour state. This phenomenon is called evaporation, and can be further elaborate using Antoine's correlation:

$$\log_{10} P_{sat} = A - \frac{B}{C + T}$$

Where the P_{sat} is the saturation vapour pressure of water in mmHG or bar, T is temperature in °C, and A, B, C are the constants related to the liquid (A = 8.07131, B = 1730.63, C = 233.426, for water) (Linstrom and Mallard, 2023)

Therefore, when the water temperature increases, the vapour pressure increases exponentially according to Antoine's correlation. The relationship between the evaporation rate and vapour pressure is directly proportional, where the higher the difference between the vapour pressure at water surface and the partial vapour pressure of water in the air, the higher the evaporation rate. Thus, more water condensates on lower temperature top covers of the solar still (Tiwari and Sahota, 2017; Kumar and Tiwari, 1996). In the case for saline water, the Antoine's correlation could not be directly applied as it does not act ideally like pure water. The vapour pressure of saline water is lower than pure water according to Raoult's law, where the higher the salinity of water means that the mole fraction of the solvent is lower, resulting a lower vapour pressure (Tiwari and Sahota, 2017; Dunkle, 1961)

Furthermore, the heat transfer of the solar still implemented with energy storage is more complex than the conventional solar still, as the heat transfer of the energy storage needs to be considered. There are two modes for the heat transfer of the energy storage, which is the charging mode (receives heat energy) and discharging mode (releases heat energy), and the equations for these two modes were discussed from (2) to (5) for the charging mode and (14) to (18) for the discharging mode.

Assumptions:

1. Heat capacity of glass cover, basin liner and insulation casing are negligible compared to saline water and PCM.
2. Solar still is vapor tight, heat losses from the sides and bottom are negligible.
3. Temperature of saline water is average; temperature gradient is not considered.
4. Temperature of PCM is average, no temperature gradient within the PCM due to the thin layer of PCM.
5. PCM is connected closely with the basin liner, no space is in between the basin liner and PCM.
6. Dust on the surface of Fresnel lens and glass cover are not considered.

Salinity in ppm,

$$S = \frac{m_{solute}}{m_{water}} \times 10^6 \tag{3.1}$$

Latent heat of basin saline water (Henderson-Sellers, 1984; harqawy, Lienhard V and Zubair, 2010; Tan et al., 2023; Tan et al., 2025),

$$h_w = 2500 - 2.386\, T_w \tag{3.2}$$

Power received at the surface of water basin,

$$Power = I(t) \times SA_{basin} \tag{3.3}$$

Solar energy received by the receiver (water basin) of the solar still,

$$Energy = Power \times \Delta t \tag{3.4}$$

Concentration ratio,

$$CR = \frac{A_{FRL}}{A_R} \tag{3.5}$$

The solar radiation I(t) is replace by I_{eff}(t) due to the presence of Fresnel lens (Johnson et al., 2019)

$$I_{eff}(t) = I(t) \times CR \times \tau_{FRL}$$

$$I_{eff}(t) = I(t) \times \frac{A_{FRL}}{A_R} \times \tau_{FRL} \tag{3.6}$$

The energy balance equation is shown below with the consideration of the PCM charging and discharging mode (El-Sebaii et al., 2009; Tiwari, Tiwari and Shyam, 2016; Abu-Arabi et al., 2018; Akshay et al., 2021; Agrawal, Rana and Srivastava, 2017;Sivakumar, Sundaram and Sakthivel, 2016):

During PCM charging mode

Glass cover:

Rate of energy absorbed by glass cover from effective solar radiation from FRL + Rate of energy received from water surface = Rate of energy loss to ambient through convection + Rate of energy loss to atmosphere through radiation

$$I_{eff}(t)\ \alpha'_g + q_{wg} = q_{conv,ga} + q_{rad,gs}$$

$$I_{eff}(t)\ \alpha'_g + \left(h_{rad,wg} + h_{conv,wg} + h_{evap,wg}\right)\left(T_w - T_g\right) = h_{conv,ga}\left(T_g - T_a\right) + h_{rad,gs}\left(T_g - T_{sky}\right) \quad (3.7)$$

Saline water:

Rate of energy absorbed by water surface from solar radiation through the glass cover + Rate of energy received by water from basin through convection = rate of heat energy stored in the water due to heat capacity + rate of heat transfer from water to glass cover

$$I_{eff}(t)\ \tau_g \alpha'_w + q_{conv,b1w} = Q_w + \dot{q}_{wg}$$

$$I_{eff}(t)\ \tau_g \alpha'_w + h_{conv,b1w}(T_{b1} - T_w) = \frac{m_w C_w}{A_{b1}} \times \frac{dT_w}{dt} + (h_{rad,wg} + h_{conv,wg} + h_{evap,wg})(T_w - T_g) \quad (3.8)$$

Basin liner:

Rate of energy absorbed by basin liner from solar radiation through the glass cover and water = rate of heat transfer from water through convection + Rate of heat transfer to PCM through conduction

$$I_{eff}(t)\ \tau_g \tau_w \alpha'_b = q_{conv,b1w} + \frac{1}{R_{b1}}(T_{b1} - T_{PCM})$$

$$I_{eff}(t)\,\tau_g\tau_w\alpha'_b = h_{conv,b1w}(T_{b1} - T_w) + \frac{k_{b1}}{x_{b1}}(T_{b1} - T_{PCM}) \tag{3.9}$$

PCM:

Rate of heat energy stored in the PCM due to heat capacity = rate of heat transfer from basin liner to PCM through conduction + Rate of energy loss from PCM to ambient through convection

$$Q_{PCM} = \frac{M_{eq}}{A_{b1}} \times \frac{dT_{PCM}}{dt} = \frac{1}{R_{b1}}(T_{b1} - T_{PCM}) - U_b(T_{PCM} - T_a)$$

$$\frac{M_{eq}}{A_{b1}} \times \frac{dT_{PCM}}{dt} = \frac{k_{b1}}{x_{b1}}(T_{b1} - T_{PCM}) - \left(\frac{k_{b2}}{x_{b2}} - \frac{k_{insulation}}{x_{insulation}}\right)(T_{PCM} - T_a) \tag{3.10}$$

$$M_{eq} = \begin{cases} m_{PCM}C_{s,PCM}\ for\ T_{b1} < T_m \\ m_{PCM}L_{PCM}\ for\ T_{b1} = T_m + \delta \\ m_{PCM}C_{L,PCM}\ for\ T_{b1} > T_m \end{cases}$$

Heat transfer coefficient:

$$h_{rad,wg} = \frac{\varepsilon_{eff}\,\sigma\left[(T_w + 273)^4 - \left(T_g + 273\right)^4\right]}{T_w - T_g} \tag{3.11}$$

$$\varepsilon_{eff} = \left[\frac{1}{\varepsilon_w} + \frac{1}{\varepsilon_g} - 1\right]^{-1}$$

$$h_{conv,wg} = 0.884\left[\left(T_w - T_g\right) + \left(\frac{P_w - P_g}{268900 - P_w}\right)(T_w + 273)\right]^{\frac{1}{3}} \tag{3.12}$$

$$h_{evap,wg} = (16.273 \times 10^{-3}) \times h_{conv,wg} \times \frac{P_w - P_g}{T_w - T_g} \tag{3.13}$$

$$h_{rad,gs} = \varepsilon_{eff}\,\sigma \times \frac{T_g^4 - T_{sky}^4}{T_g - T_{sky}} \tag{3.14}$$

$$T_{sky} = 0.0552\,T_a^{\frac{1}{5}}$$

$$h_{conv,ga} = \begin{cases} 2.8 + 3v\ if\ v \leq 5\ m/s \\ 5.7 + 3.8v\ if\ v > 5\ m/s \end{cases} \tag{3.15}$$

Fraction of solar radiation absorbed by glass cover, saline (basin) water and water basin, where the attenuation is taken account into the equation applied:

$$\alpha_g' = \left(1 - R_g\right)\alpha_g \tag{3.16}$$

$$\alpha_w' = \left(1 - R_g\right)\left(1 - \alpha_g\right)(1 - R_w)\left[1 - \Sigma\mu_j \exp\left(-n_j d_w\right)\right] \tag{3.17}$$

$$\alpha_b' = \alpha_b\left(1 - R_g\right)\left(1 - \alpha_g\right)(1 - R_w)(1 - \alpha_w)\Sigma\mu_j \exp\left(-n_j d_w\right) \tag{3.18}$$

According to Tiwari (2016) pg 523 Table 13.2, water depth = 0.01 m, $\Sigma\mu_j \exp\left(-n_j d_w\right) = 0.7344$

During PCM discharging mode (El-Sebaii et al., 2009)

PCM:

Rate of heat energy released from PCM at selected time interval = rate of heat transfer from PCM to basin liner through conduction + Rate of energy loss from PCM to ambient through convection

$$\frac{m_{PCM} L_{PCM}}{A_{b1}\Delta t} = h_b'(T_{PCM} - T_{b1}) + U_b(T_{PCM} - T_a)$$

$$\frac{m_{PCM}L_{PCM}}{A_{b1}\Delta t} = \frac{k_{PCM}}{x_{PCM}}(T_{PCM} - T_{b1}) + \left(\frac{k_{b2}}{x_{b2}} - \frac{k_{insulation}}{x_{insulation}}\right)(T_{PCM} - T_a)\ for\ T_{PCM} = T_m \tag{3.19}$$

Rate of heat transfer from PCM to basin liner through conduction + Rate of energy loss from PCM to ambient through convection = rate of heat stored in PCM

$$h'_b(T_{PCM} - T_{b1}) + U_b(T_{PCM} - T_a) = \frac{M_{eq}}{A_{b1}} \times \frac{dT_{PCM}}{dt}$$

$$\frac{k_{PCM}}{x_{PCM}}(T_{PCM} - T_{b1}) + \left(\frac{k_{b2}}{x_{b2}} - \frac{k_{insulation}}{x_{insulation}}\right)(T_{PCM} - T_a) = \frac{M_{eq}}{A_{b1}} \times \frac{dT_{PCM}}{dt}\ for\ T_{PCM} \neq T_m \tag{3.20}$$

$$M_{eq} = \begin{cases} m_{PCM}C_{L,PCM}\ for\ T_{PCM} > T_m \\ m_{PCM}C_{s,PCM}\ for\ T_{PCM} < T_m \end{cases}$$

Basin liner:

Rate of heat transfer from PCM to basin liner through conduction = rate of heat transfer from basin liner to water through convection

$$\frac{k_{PCM}}{x_{PCM}}(T_{PCM} - T_{b1}) = h_{conv,b1w}(T_{b1} - T_w) \tag{3.21}$$

Basin water:

Rate of heat transfer from basin to water through convection = rate of heat transfer from water to glass through convection, radiation & evaporation + rate of heat energy stored in water due to heat capacity

$$h_{conv,b1w}(T_{b1} - T_w) = h_{wg}(T_w - T_g) + \frac{m_w C_w}{A_{b1}} \times \frac{dT_w}{dt} \tag{3.22}$$

Glass cover:

Rate of heat transfer from water to glass through convection, radiation & evaporation = rate of heat loss to atmosphere through radiation + rate of heat loss to ambient through convection

$$h_{wg}\left(T_w - T_g\right) = T_{rad,gs}\left(T_g - T_{sky}\right) + h_{conv,ga}\left(T_g - T_a\right) \tag{3.23}$$

Hourly yield, (Ansari et al., 2013)

$$M_{hr} = \frac{3600 \times h_{evap,wg} \times \left(T_w - T_g\right)}{A_{b1} \times L_w} \tag{3.24}$$

Daily yield,

$$M_d = \sum_{i=1}^{8} M_{hr} \tag{3.25}$$

Productivity,

$$P = \frac{M_d}{\sum I \times \Delta t} \tag{3.26}$$

Efficiency, (Cheng, Huo and Nian, 2019)

$$\eta = \frac{M_d \times L_w}{\sum I \times \Delta t} \times 100\% \tag{3.27}$$

CHAPTER 4

RESULTS AND DISCUSSION

4.1 Introduction

This chapter discussed about the results of the indoor and outdoor experiments carried in UTAR Sungai Long Campus. The indoor experiments were carried under a solar simulator, comparing different sets of conductive particles assisted PCMs and Fresnel lenses for three hours. For the outdoor experiments, different combinations of conductive particles assisted PCMs and Fresnel lenses were compared for nine hours (from 9 am to 6 pm) with the addition of different salinity solutions. All the models started with 75 ml of basin water, except for the prototype, which started with 150 ml basin water. As mentioned in Chapter 3, the indoor experiments were conducted in the university laboratory KB730, whereas the outdoor experiments were carried out at KB building rooftop located at 3.039844 ° N, 101.794209 ° E. However, there is a slight difference for indoor and outdoor experiment where the models for indoor experiment is placed overnight in the lab, whereas the models for outdoor experiment is taken back after recording the last experiment data. Therefore, the final water yield recorded for indoor experiments have considered the condition where evaporation occurs solely from the heat of water and PCM without sunlight (outer heat source) received. Furthermore, due to ample of experiments conducted, the naming of the solar still models in each experiment were named according to the variable of the experiment. The naming system was further elaborated in each subsequent section.

4.2 Indoor Experiments

The indoor experiment was carried individually for each solar still model due to limited space. Initially, the indoor experiment was conducted without the Fresnel lenses involved to investigate the effect of different PCMs using both tap water and 9000 ppm saline water bought from the pharmacy. The thickness of the top cover (glass) is 2 mm. Later in the experiment, the three different Fresnel lenses FL 9.9 cm, FL 12.7 cm and FL 20 cm, were involved to explore the presence of FRL together with PCMs and the impact of different FRL on the performance of the solar still. The solar still model were named according to the PCMs used, since the variable for the indoor experiments in Section 4.2 are the PCMs. The four PCMs involved were listed in Table 4.1.

Table 4.1: Naming system of the solar still models for indoor experiment in Section 4.2

Naming of the solar still models	**PCM contents**
Al_2O_3 + Cu	Al_2O_3 and Cu nanomaterial with PW
Al_2O_3	Al_2O_3 nanomaterial with PW
Al	Al scrap with PW
Cu	Cu nanomaterial with PW

4.2.1 Varying PCM using Tap Water

The initial indoor experiment was started by using tap water instead of saline water and the indoor room temperature was kept around 25 °C. During the first indoor experiment, the solar irradiation was kept at approximately 1000 W/m^2 for all the setups without Fresnel lenses involved (solar irradiation is different when Fresnel lenses were involved). All the initial water temperature was heated to around 36 °C (measured during heating) to ensure the PCM melts faster. Hence, the water temperature of models with Al, Al_2O_3, Cu, and Al_2O_3 + Cu started with 35.25 °C, 36.93 °C, 36.52 °C, and 35.27 °C, respectively. From Figure 4.1, it was observed that the water temperature was around 40 °C to 41 °C for all four models in Experiment 1 after the first hour. The slowest to reach 41 °C is Cu, where it was at 40.86 °C when measured at the second half hour mark and finally reached 41.28 °C at the third hour mark. Then, it was followed by Al_2O_3, where it reached 40.34 °C at the second hour and reach 41.04 °C at the second half hour; it remained above 41 °C until the last measurement was taken at the third hour mark, which was 41.31 °C. The fastest to reached 41 °C was Al at the first and half hour mark while Al_2O_3 reached 41 °C before the second hour. Among the four setups, the fastest to reach 41 °C water temperature is Al while the slowest is Al_2O_3 + Cu.

As for the cover temperature, the initial value for models with Al, Al_2O_3, Cu, and Al_2O_3 + Cu were 30.35 °C, 33.84 °C, 32.28 °C, and 29.33 °C, respectively. The cover temperature was increased to 37 °C and above, where the maximum cover temperature for Al and Cu were 38 °C to 39 °C while the maximum cover temperature for Al_2O_3 and Al_2O_3 + Cu were around 37 °C. Besides that, the initial PCM temperature measured for models with Al, Al_2O_3, Cu, and Al_2O_3 + Cu were 28.84 °C, 31.73 °C, 28.26 °C, and 27.89 °C, respectively. Later, the PCM temperature increases to 40 °C with Al_2O_3 being the fastest to reach at the 2-hour mark, followed by Cu and Al_2O_3 + Cu at the 2-hour 30-minute mark; and lastly, Al being the slowest to reach 40 °C at the 3-hour mark. This result shows that the Al scrap mixed PCM has the lowest heat transfer rate among the four types of PCMs. Moreover, the water yield collected during the experiment (within the three hours) were recorded to be 0.1522 kg/m^2, 0.1674 kg/m^2, 0.2207 kg/m^2, and 0.1826 kg/m^2 for models with Al, Al_2O_3, Cu, and Al_2O_3 + Cu, respectively. Showing that Cu has the highest water yield at the 3-hour mark of the experiment.

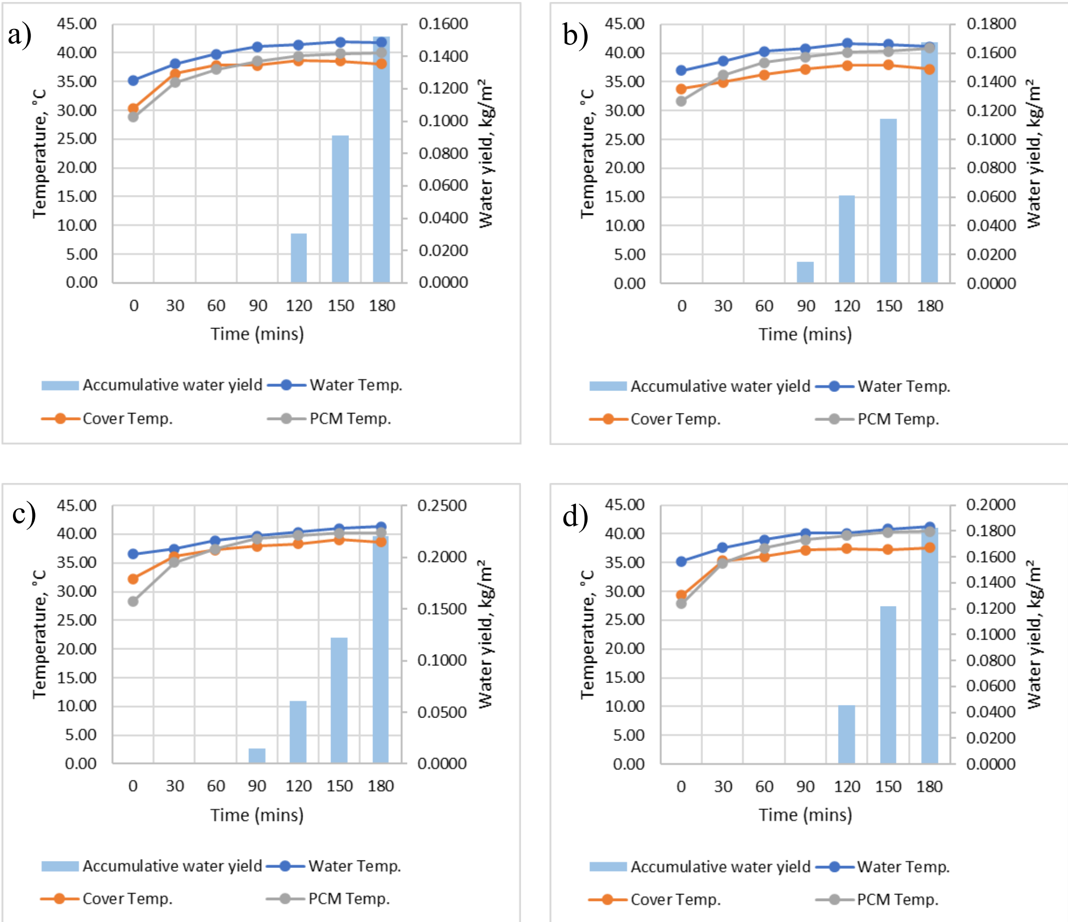

Figure 4.1: Temperature and water yield results for different PCMs using tap water (a) Al scrap PCM (b) Al_2O_3 NPCM (c) Cu NPCM (d) Al_2O_3 and Cu NPCM

The daily water yield showed in Table 4.2 is the final water collected after leaving the solar stills overnight. It was observed that among the four types of PCM combinations, the Al_2O_3 and Cu NPCM has the best result with the highest water yield, productivity, and efficiency of 0.3120 kg/m^2, 2.20 g/kJ.m^2 and 6.95 %, respectively. Al_2O_3 + Cu has the highest performance despite having the lowest water temperature was due to its low cover temperature considering higher temperature difference between the top cover and water increases the evaporation rate of water in the basin (Al-Harahsheh et al., 2022). Comparing Al_2O_3 + Cu to Al_2O_3, both have similar high performances due to high temperature difference between the cover and water. As for Al and Cu, both have the same daily water yield, productivity and efficiency, which are 0.2740 kg/m^2, 1.93 g/kJ.m^2 and 6.10 %, respectively.

Table 4.2: Daily water yield, productivity, and efficiency of varying PCM using tap water

Variation in PCM	**Daily water yield, kg/m^2**	**Productivity, g/kJ.m^2**	**Efficiency, %**
Al scrap PCM	0.2740	1.93	6.10
Al_2O_3 NPCM	0.3044	2.15	6.78
Cu NPCM	0.2740	1.93	6.10
Al_2O_3 and Cu NPCM	0.3120	2.20	6.95

4.2.2 Varying PCM using 9000 ppm Saline Water

For the second indoor experiment conducted, saline water with the salinity of 9000 ppm was used as basin water instead of tap water while all other conditions remained the same. The saline water was preheated to around 40 °C before the experiment started, it was increased from 35 °C (from experiment in Subsection 4.2.1) to 40 °C due to saline water having higher energy demand compared to tap water, which has lower salinity. It was observed that the water temperature of the solar stills was maintained around 37 °C to 39 °C under the solar simulator. Among the four models, Cu has the highest water temperature, 39.01 °C, which was reached at the third hour. Next is Al_2O_3 + Cu, where the water temperature is maintained around 38 °C and followed by Al_2O_3, where its water temperature is 37 °C to 38 °C. Meanwhile, Al had the lowest water temperature, and it maintained around 37 °C to 38 °C throughout the experiment.

On the other hand, Cu has the highest PCM temperature, maintaining above 37 °C after the second hour of the experiment. Followed by Al_2O_3 + Cu, where the PCM temperature was maintained at 35 °C; whereas the PCM temperature for Model 2A and 2B are at 34 °C and 33 °C, respectively. After the experiment (three hours), the water collected was observed and recorded. According to Figure 4.2, it was observed that the water collected for models with Al, Al_2O_3, Cu, and Al_2O_3 + Cu were 0.1522 kg/m^2, 0.1979 kg/m^2, 0.1522 kg/m^2, and 0.1826 kg/m^2, respectively. It was found that Al_2O_3 has the highest water yield after three hours under the solar simulator.

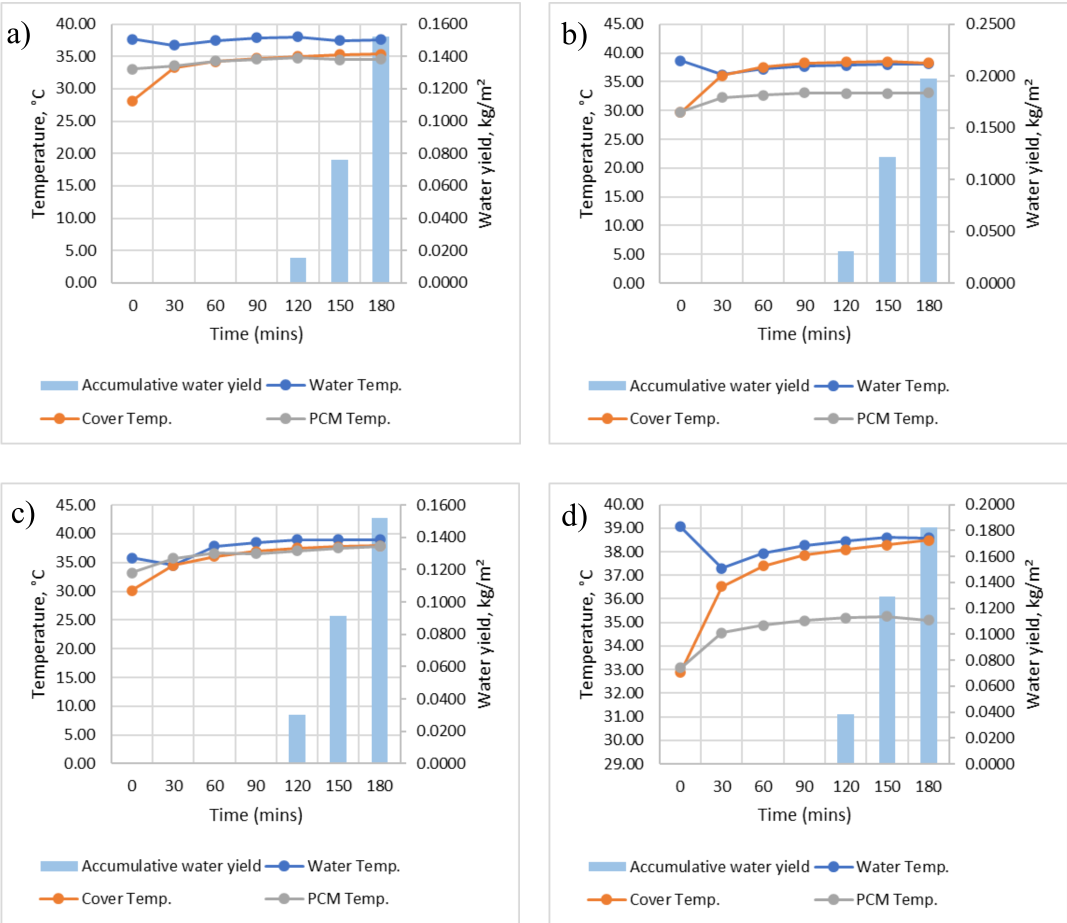

Figure 4.2: Temperature and water yield results for different PCMs using 9k ppm saline water (a) Al scrap PCM (b) Al_2O_3 NPCM (c) Cu NPCM (d) Al_2O_3 and Cu NPCM

According to Table 4.3 shows the final water yield collected, productivity and efficiency of models with Al, Al_2O_3, Cu, and Al_2O_3 + Cu. The daily water yield collected after a night were 0.2435 kg/m^2, 0.2588 kg/m^2, 0.2359 kg/m^2, and 0.2968 kg/m^2 for Al, Al_2O_3, Cu, and Al_2O_3 + Cu, respectively. Moreover, the productivity of Al, Al_2O_3, Cu, and Al_2O_3 + Cu were 1.72 g/kJ.m^2, 1.82 g/kJ.m^2, 1.66 g/kJ.m^2, and 2.09 g/kJ.m^2, respectively. As for the efficiency, it was 5.44 %, 5.77 %, 5.26 %, and 6.62 % for Al, Al_2O_3, Cu, and Al_2O_3 + Cu, respectively. These results emphasized that Al_2O_3 + Cu has the highest water yield (0.2968 kg/m^2), productivity (2.09 g/kJ.m^2) and efficiency (6.62 %) among the four models, which was similar to the results of the first indoor experiment conducted with tap water. Later, followed closely by Al_2O_3 with the second highest performance and with Al and Cu being the third and last. From the first and second experiment, it shows that the model applied with Al_2O_3 and Cu NPCM has the best performance, following by Al_2O_3 NPCM, Al scrap PCM, and lastly Cu NPCM. To further investigate on improving the passive solar desalination system due to the low productivity, the next indoor experiment conducted involves Fresnel lenses.

Table 4.3: Daily water yield, productivity, and efficiency of varying PCM using 9000 ppm saline water

Variation in PCM	Daily water yield, kg/m^2	Productivity, g/kJ.m^2	Efficiency, %
Al scrap PCM	0.2435	1.72	5.44
Al_2O_3 NPCM	0.2588	1.82	5.77
Cu NPCM	0.2359	1.66	5.26
Al_2O_3 and Cu NPCM	0.2968	2.09	6.62

4.2.3 Varying PCM using FL 12.7 cm Fresnel Lens

The third indoor experiment involved a 12.7 cm (sizes stated are focal length) Fresnel lens, where all the contents of the solar still samples remained the same. The solar irradiance was adjusted to 500 W/m^2 input instead of 1000 W/m^2 due to limited height of the solar simulator after placing a Fresnel lens under. The basin water used is 9000 ppm saline water and it was preheated to approximately 40 °C. From Figure 4.3, the water temperature for Al, Al_2O_3 and Cu were maintained around 38 °C to 39 °C after the first hour of the experiment while Al_2O_3 + Cu remains around 37 °C until the end of the experiment. Meanwhile, the cover temperature is around 37 °C to

38 °C for Al_2O_3, Cu, and Al_2O_3 + Cu; apart from Al, which around 35 °C to 36 °C after the first hour of the experiment. The PCM temperature measured is around 34 °C to 35 °C for Al, Al_2O_3, and Al_2O_3 + Cu; except Cu, which is the highest around 36 °C. Furthermore, Model 3D has the highest initial water yield, which was 0.2131 kg/m^2; followed by both Al_2O_3 and Al_2O_3 + Cu, which have the same water yield at 0.1826 kg/m^2; lastly being Al at the yield of 0.1674 kg/m^2 after three hours.

The results shows that even though Al_2O_3 + Cu had the lowest water and PCM temperature throughout the experiment. The amount of water yield collected during the three-hour experiment was the same as Al_2O_3 and higher than Al despite having a lower water and PCM temperature than the two models. Besides that, another highlight in this experiment is that the water yield of model using Cu NPCM is the highest during the 3-hour experiment with the application of a 12.7 cm FL Fresnel lens. It was observed that the water temperature of Cu had remained above 39 °C after the first hour and had the highest water temperature among the four models. Meanwhile the PCM temperature was around 36 °C, which was the highest among the four models, had provided more heat to the saline water compared to others. Hence, the Cu NPCM was able to store more heat from the focused artificial sunlight with the aid of a 12.7 cm FL Fresnel lens. The water yield of the model using Cu NPCM has greatly increased when a 12.7 cm FL Fresnel lens was applied due to receiving a focused sunlight (artificial).

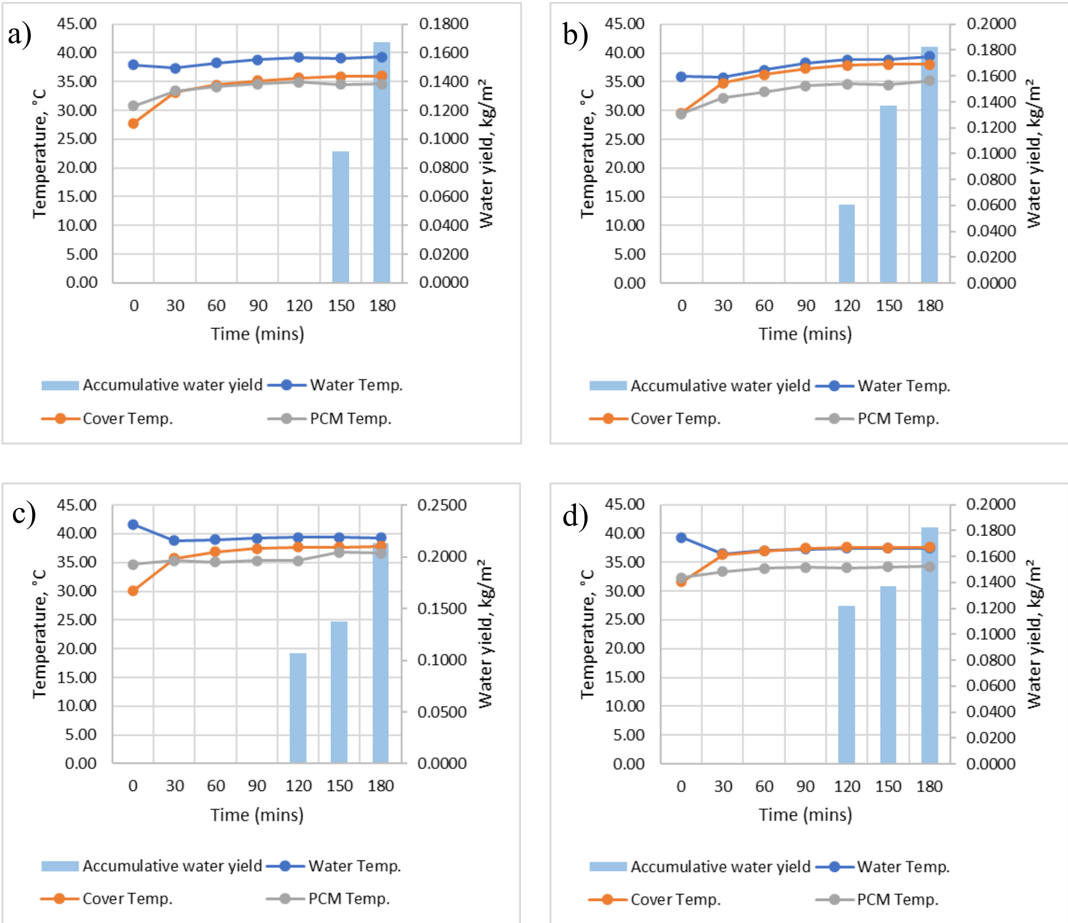

Figure 4.3: Temperature and water yield results for different PCMs using 9k ppm saline water and 12.7 cm FL Fresnel lens (a) Al scrap PCM (b) Al_2O_3 NPCM (c) Cu NPCM (d) Al_2O_3 and Cu NPCM

In the final water yield collected it was found that Al_2O_3 + Cu is the highest among the four models, as shown in Table 4.4 with the final water yield of 0.3425 kg/m^2. On the other hand, Cu with the highest initial water yield is the second highest with a final water yield of 0.3196 kg/m^2. Then, it was followed by Al_2O_3 with a yield of 0.2664 kg/m^2 and lastly, Al with a yield of 0.2435 kg/m^2. From Table 4.4, it was shown that the productivity and efficiency from highest to lowest is Al_2O_3 + Cu, Cu, Al_2O_3, and Al. The results shows that the performance of Al_2O_3 + Cu is close with Cu while Al is close with Al_2O_3. Overall, the best performance for Experiment 3 is model with Al_2O_3 + Cu with the highest water yield, productivity and efficiency which are 0.3425 kg/m^2, 4.83 g/kJ.m^2, and 15.29 %, respectively.

Table 4.4: Daily water yield, productivity, and efficiency of varying PCM using FL 12.7 cm Fresnel lens

Variation in PCM	Daily water yield, kg/m^2	Productivity, g/kJ.m^2	Efficiency, %
Al scrap PCM	0.2435	3.43	10.86
Al_2O_3 NPCM	0.2664	3.75	11.89
Cu NPCM	0.3196	4.50	14.24
Al_2O_3 and Cu NPCM	0.3425	4.83	15.29

4.2.4 Varying PCM using FL 9.9 cm Fresnel Lens

In Experiment 4, a 9.9 cm FL Fresnel lens was applied with an input of 500 W/m^2 solar irradiance. The basin water consists of 75 ml 9000 ppm saline water and was preheated to around 40 °C. From Figure 4.4, Cu had the highest water temperature, which was around 39 °C after the first hour. Meanwhile the water temperature for Al_2O_3 + Cu was slightly lower, which maintained around 38.5 °C after the first hour; closely followed by Al_2O_3 at around 38 °C then Al at 37.5 °C. Besides that, the cover temperature recorded was around 38 °C for Al_2O_3, Cu, and Al_2O_3 + Cu, while it was around 35 °C for Al after the first hour. Additionally, the PCM temperature was the highest for Cu, which was above 36 °C after the first hour and rose above 37 °C in the second half of the experiment. Al_2O_3 + Cu had the second highest PCM temperature, where it was maintained around 35 °C while Al was around 34.5 °C and Al_2O_3 around 33 °C after the first hour. The accumulative water yield collected after the 3-hour experiment were 0.1522 kg/m^2, 0.1979 kg/m^2, 0.1522 kg/m^2, and 0.1826 kg/m^2 for Al, Al_2O_3, Cu, and Al_2O_3 + Cu, respectively. Despite having the highest water and PCM temperature, Cu did not have the best performance among the four models. In fact, it had the lowest performance together with Al, with the same water yield collected within the three hours. On the other hand, Al_2O_3 had the highest initial water yield followed closely by Al_2O_3 + Cu.

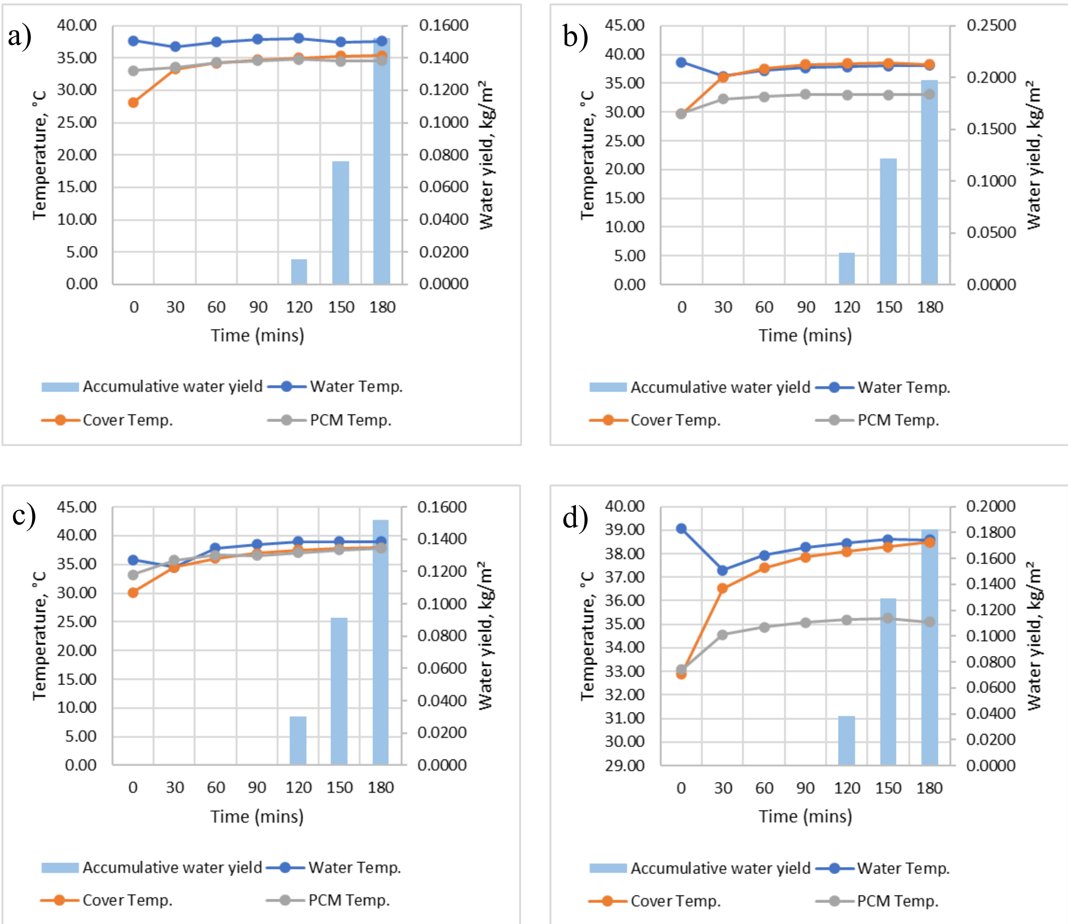

Figure 4.4: Temperature and water yield results for different PCMs using 9k ppm saline water and 9.9 cm FL Fresnel lens (a) Al scrap PCM (b) Al_2O_3 NPCM (c) Cu NPCM (d) Al_2O_3 and Cu NPCM

After measuring the final water yield, which was recorded and shown in Table 4.5, it was observed that Al_2O_3 + Cu has the highest water yield at 0.2968 kg/m^2.

Moreover, the final water yield for Al, Al_2O_3, and Cu were 0.2435 kg/m^2, 0.2588 kg/m^2, and 0.2359 kg/m^2, respectively. In addition, according to Table 4.5, Al_2O_3 + Cu had the highest productivity and efficiency, which were 4.18 g/kJ.m^2 and 13.24 %, respectively. In contrast, Cu had the lowest performance where the productivity and efficiency were 3.32 g/kJ.m^2 and 10.53 %, respectively. The result of Al is closely similar to Cu, where the productivity and efficiency were 3.43 g/kJ.m^2, and 10.87 %. The outcome of Experiment 4 (Subsection 4.2.4) for model with Cu NPCM had diverged from what had been discovered in Experiment 3 (Subsection 4.2.3), even though both had high water and PCM temperature under the implement of Fresnel lenses. However, the Fresnel lenses used in Experiment 3 and 4 were different in sizes and optical characteristics, where the 12.7 cm FL Fresnel lens used in Experiment 3 is larger than the 9.9 cm FL Fresnel lens in Experiment 4. Therefore, the larger Fresnel lens has a higher concentration ratio which increases the performance of the solar still model.

Table 4.5: Daily water yield, productivity, and efficiency of varying PCM using FL 9.9 cm Fresnel lens

Variation in PCM	**Daily water yield, kg/m^2**	**Productivity, g/kJ.m^2**	**Efficiency, %**
Al scrap PCM	0.2435	3.43	10.87
Al_2O_3 NPCM	0.2588	3.65	11.55
Cu NPCM	0.2359	3.32	10.53
Al_2O_3 and Cu NPCM	0.2968	4.18	13.24

4.2.5 Varying PCM using FL 20 cm Fresnel Lens

The last indoor experiment, Experiment 5 was conducted using a 20 cm FL Fresnel lens. The input irradiance was 315.5 W/m^2, lower than the irradiance in Experiment 3 (Subsection 4.2.3) and Experiment 4 (Subsection 4.2.4) due to the focal length of the Fresnel lens at 20 cm. The 9000 ppm basin water was preheated to approximately 40 °C before the experiment starts. From Figure 4.5, the highest water temperature (without considering the initial temperature after preheated) was above 36 °C, achieved by Al at the third hour. Then, it was followed by Cu and Al_2O_3 + Cu, where both maintained above 35 °C after the first hour. Al_2O_3 + Cu had the lowest water temperature where it gradually decreases to 34 °C after the first hour and eventually decreased to 33.75 °C at the end of the experiment. Besides that, the PCM temperature of the four models ranges around 29 °C to 34 °C, with Cu having the highest PCM temperature throughout the experiment where it was maintained around 33 °C to 34 °C. It was then followed by Al_2O_3 + Cu, where the PCM temperature started at around 33.50 °C and gradually decrease to 32.34 °C at the end of the experiment. Meanwhile, Al was maintained around 32 °C during the experiment with a sudden temperature increase at the end of the experiment, which was measured at 33.50 °C. Al_2O_3 had the lowest PCM temperature, where it was maintained around 30 °C throughout the experiment and was decreased to 29 °C at the end of the experiment.

Furthermore, it was observed that Al_2O_3 + Cu had the highest cover temperature at 36 °C, which was maintained throughout the three-hour experiment. It was followed closely by Cu, where the cover temperature was 36.21 °C at the first hour and it gradually decreases to 35.85 °C at the end of the experiment. Al and Al_2O_3 had similar cover temperature, which were around 35 °C. Hence, four solar still models have similar cover temperature which ranges from 34 to 36 °C. From Figure 4.5, it can be observed that unlike previous indoor experiments, there was no fresh water collected at the second hour and most of the water yield recorded was in the last hour. In the initial freshwater collection, Al_2O_3 + Cu had the most initial water yield, which was 0.1065 kg/m^2; whereas Al_2O_3 and Cu both had 0.0913 kg/m^2; lastly, Al with the least initial water yield at 0.0609 kg/m^2. The final water yield was recorded in the following day.

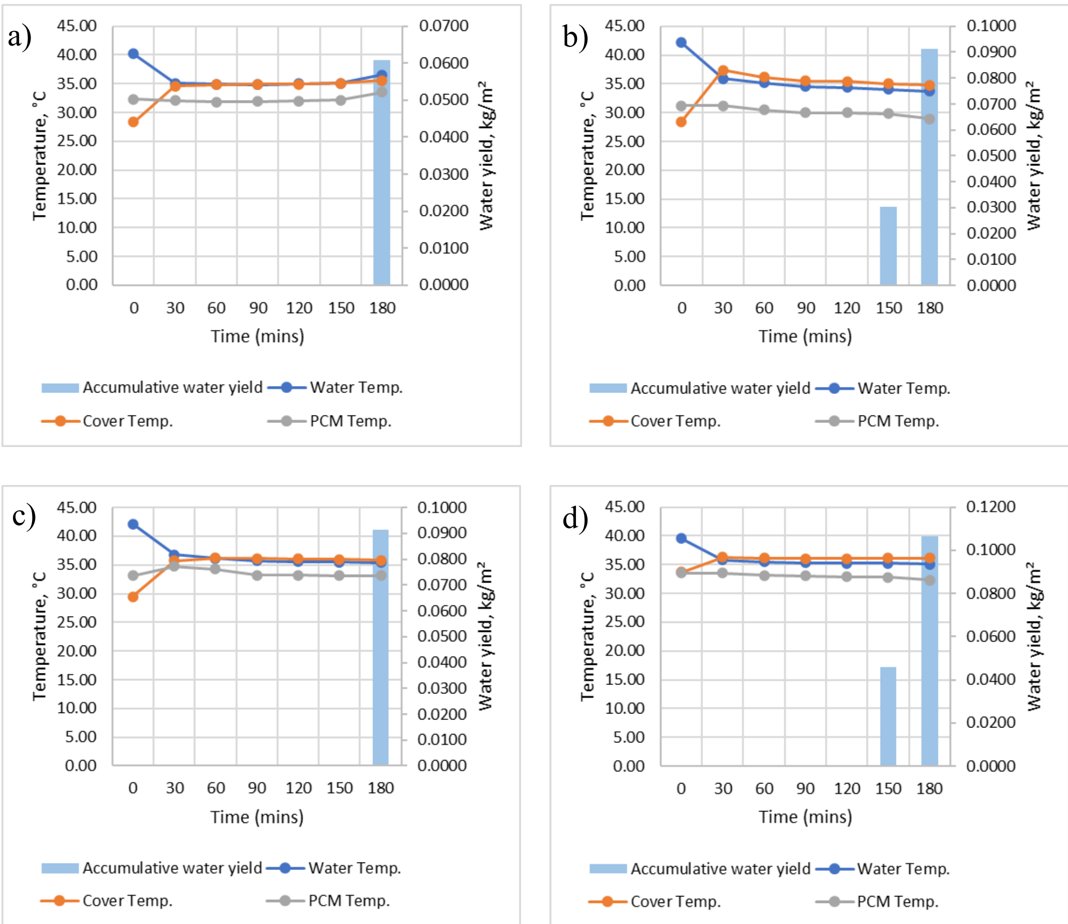

Figure 4.5: Temperature and water yield results for different PCMs using 9k ppm saline water and 20 cm FL Fresnel lens (a) Al scrap PCM (b) Al_2O_3 NPCM (c) Cu NPCM (d) Al_2O_3 and Cu NPCM

From Table 4.6, it was observed that Al_2O_3 had the highest final water yield at 0.1903 kg/m^2 while Al and Al_2O_3 + Cu had the same final water yield at 0.1826 kg/m^2;

lastly, Cu with the least final water yield at 0.1598 kg/m^2. The productivity and efficiency of the solar still models in Experiment 5 were shown in Table 4.6, where Al_2O_3 had the highest productivity and efficiency which were 4.25 g/kJ.m^2 and 13.48 %, respectively. Even though Al_2O_3 had the lowest water and PCM temperature, it had the highest performance. Besides that, unlike the previous experiments, the model with Al_2O_3 + Cu in Experiment 5 did not have the best performance among the four models. However, one of the interesting findings was Al had the same result as Al_2O_3 + Cu, with a productivity and efficiency of 4.08 g/kJ.m^2 and 12.94 %, despite being one of the lower performance solar still models in previous experiments.

Table 4.6: Daily water yield, productivity, and efficiency of varying PCM using FL 20 cm Fresnel lens

Variation in PCM	Daily water yield, kg/m^2	Productivity, g/kJ.m^2	Efficiency, %
Al scrap PCM	0.1826	4.08	12.94
Al_2O_3 NPCM	0.1903	4.25	13.48
Cu NPCM	0.1598	3.57	11.31
Al_2O_3 and Cu NPCM	0.1826	4.08	12.94

From all the indoor experiments, it was observed that the overall best PCM was Al_2O_3 and Cu NPCM, as it had the best performance in all the indoor experiments conducted, excluding Experiment 5 (Subsection 4.25). Moreover, it was observed that using different Fresnel lens provide a different outcome, where using a larger dimension Fresnel lens increases the concentration ratio and therefore allowing a better performance. The best Fresnel lenses among the three were unable to be decided as the input irradiation was different for the 20 cm Fresnel lens; hence, the Fresnel lenses were further investigated by carrying the experiment outdoors. Besides that, the water collected were tested using a TDS tester and it was found that most of the value measured were below 20 ppm. It was recommended by the WHO (Herschy, 2012), that the TDS value of a palatable water is less than 600 mg/l, which is roughly 600 ppm. Hence, the freshwater collected is too pure and is required for additional essential minerals to be added before used for drinking.

4.3 Outdoor Experiments

The outdoor experiments consist of comparing the different Fresnel lenses and different PCMs. This was divided into two sets of experiments where one of the variables remained constant. In Subsection 4.3.1, compares the four solar still models with the same PCM content but with different sizes of Fresnel lenses. Whereas in Subsection 4.3.2 compares the four solar still models with different PCM content but same Fresnel lenses (best out of the four). For Subsection 4.3.3, comparison of different salinity of basin water under the same condition of PCMs and Fresnel lenses was done to investigate the impact on the performance of solar still. Lastly, the experiment is conducted using a solar still prototype, fabricated in actual size instead of the previous scaled down models, using a lower cost PCM and the best Fresnel lens. The thickness of the top cover was 2 mm in Subsection 4.3.1; however, it was changed to 5 mm for Subsection 4.3.2, Subsection 4.3.3 and Subsection 4.3.4, after trial and error with recurring glass breaking due to the concentrated heat focused by the FL 33 cm Fresnel lenses.

4.3.1 Comparing different Fresnel lenses with the same PCMs (9k ppm saline water)

The first sets of outdoor experiments were conducted in late June to early July 2024, with several failures and redos. Therefore, the experiment order follows the type of PCM used (start with Al scrap PCM, Al_2O_3 NPCM, Cu NPCM, and ends with Al_2O_3 and Cu NPCM) and do not align with the experiment date. Besides that, four different Fresnel lenses were used in each experiment carried with the condition of same PCM. The experiment was repeated four times to ensured that all four of the PCMs were involved. To ease the explanation, the solar still model were named according to the focal length of different Fresnel lenses used. The four Fresnel lenses involved were listed in Table 4.7.

Table 4.7: Type of Fresnel lenses used for the models in indoor experiment

Fresnel lens (FRL)	Focal length (FL) of Fresnel lenses	Naming of the solar still models
I	12.7 cm	FL 12.7
II	9.9 cm	FL 9.9
III	20.0 cm	FL 20
IV	33.0 cm	FL 33

4.3.1.1 Varying Fresnel lenses with same Al scrap PCM

Experiment 6 was carried on 24^{th} July 2023 using four solar still models that contain the same PCM, which was Al scrap PCM. The four Fresnel lenses used were different in sizes and optical characteristics which were specified in Chapter 3 Methodology, Section 3.4 and 3.5. According to Figure 4.6 shows the solar irradiance, water temperature, PCM temperature and cover temperature of the four solar still models in Experiment 6. The experiment started at 9 am, where the solar irradiance received were 279 W/m^2, 268 W/m^2, 310 W/m^2, and 263 W/m^2 for Model 6A, 6B, 6C, and 6D respectively due to the cloudy morning weather. The day was relatively sunny as after 10 am, the clouds no longer block the sunlight, and the solar irradiance received increases and remained above 900 W/m^2 until 4 pm. According to Figure 4.6, the maximum solar irradiance received for all four models was at 1 pm, which were 1161 W/m^2, 1192 W/m^2, 1158 W/m^2, and 1099 W/m^2 for Model 6A, 6B, 6C, and 6D respectively, measured using the Solar Power Meter.

Furthermore, the water temperature was the highest around 2 pm to 3 pm, where it was 65.15 °C, 62.36 °C, 65.47 °C, and 84.93 °C for FL 12.7, FL 9.9, FL 20, and FL 33 respectively. The PCM temperature reached the peak around the period of 1 pm to 3 pm, where the highest recorded temperature measured was 60.12 °C, 60.35 °C, 60.10 °C, and 71.39 °C for FL 12.7, FL 9.9, FL 20, and FL 33 respectively. As for the cover temperature, it was measured to be around 45 °C to 58 °C for Model 6A, 6B, and 6C. However, for FL 33, the cover temperature was much higher than the other solar still models, where it ranges between 60 °C to 74 °C with an outlier of 80.94 °C at 11 am due to direct sunlight contact with the temperature sensor. Besides that, Figure 4.7 shows the cumulative water yield for the four models using different Fresnel lenses. It was observed that FL 33 had the highest water yield where the line graph significantly increased 2.435 kg/m^2 after 10 am, while the other three increased gradually and was followed by FL 12.7 (0.457 kg/m^2), FL 9.9 (0.221 kg/m^2) and lastly, FL 20 (0.167 kg/m^2). Moreover, FL 33 had a significant increase of water yield after 3 pm, which was measured to be 3.006 kg/m^2. The saline water was refilled for FL 12.7 and FL 33, where FL 12.7 was refilled once at 4 pm for 25 ml while FL 33 was refilled three times at 11 am for 25 ml, 1 pm for 50 ml and 4 pm for 25 ml.

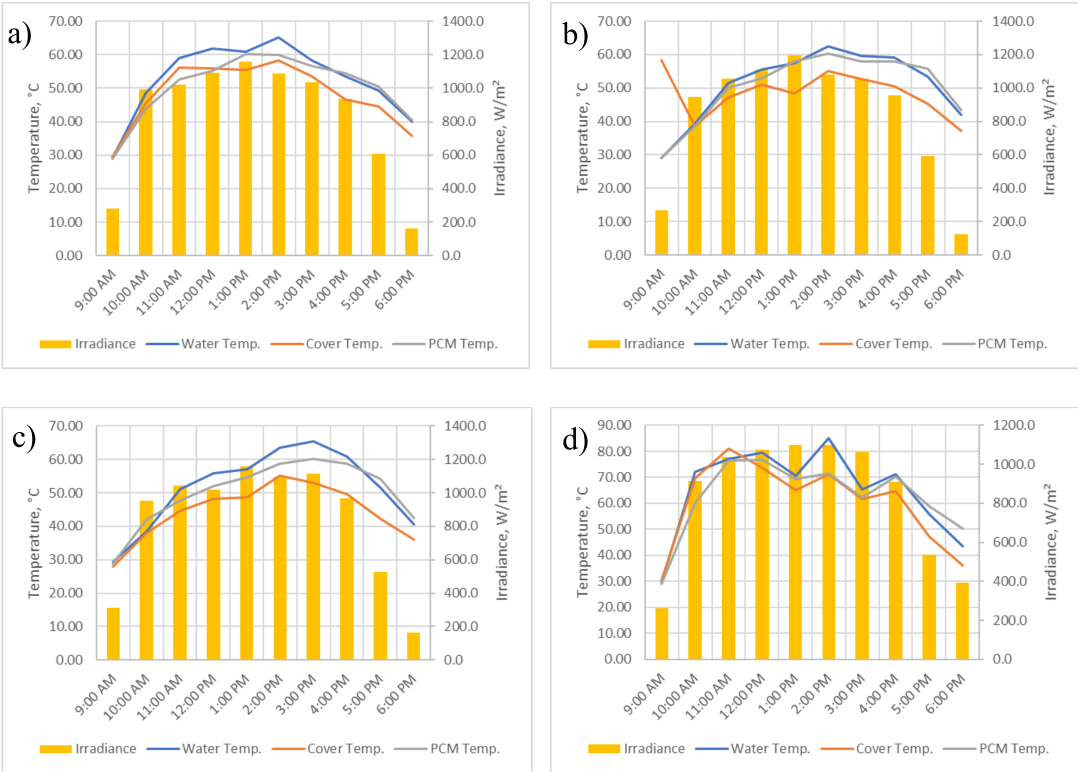

Figure 4.6: Temperature and irradiance results for different Fresnel lenses using 9k ppm saline water and Al scrap PCM (a) FL 12.7 cm (b) FL 9.9 cm (c) FL 20 cm (d) FL 33 cm

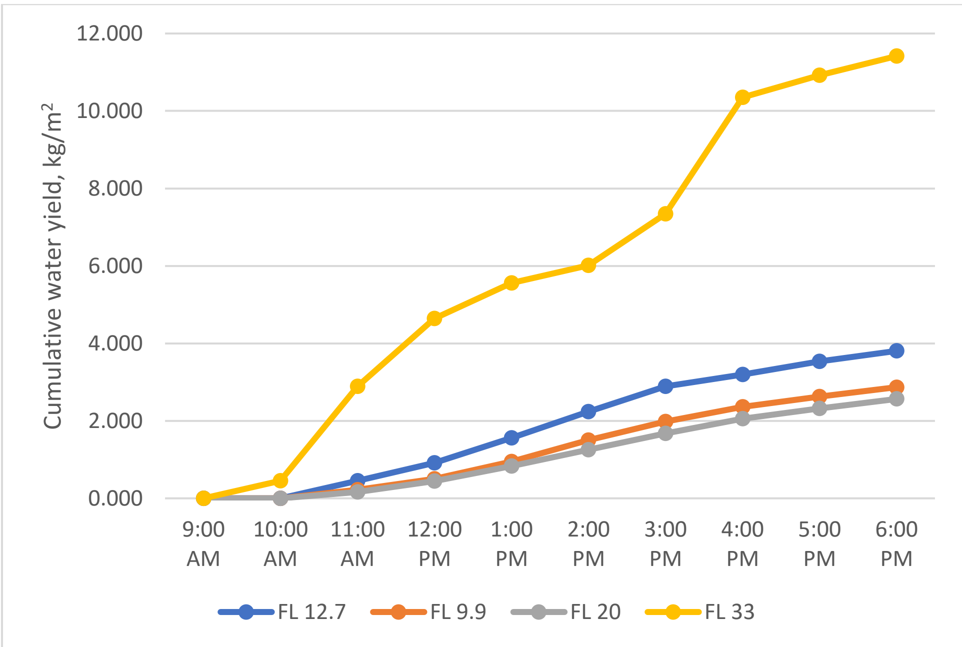

Figure 4.7: Cumulative water yield results for different Fresnel lenses using 9k ppm saline water and Al scrap PCM

The experiment ended at 6 pm, where the final recordings of the temperatures, irradiance and distillate collected were done. The data was recorded and calculated into the results shown in Table 4.8. FL 33 had the best performance with the highest water yield, productivity and efficiency, which were 11.4155 kg/m^2, 31.98 g/kJ and 96.99 % respectively. It was then followed by FL 12.7, with a water yield, productivity and efficiency of 3.8052 kg/m^2, 10.67 g/kJ.m^2 and 32.82 %. Meanwhile FL 9.9 had a water yield, productivity and efficiency of 2.8691 kg/m^2, 8.04 g/kJ.m^2 and 24.76 % respectively; and lastly, FL 20 had a water yield, productivity and efficiency of 2.5647 kg/m^2, 7.21 g/kJ.m^2 and 22.19 % respectively. It was shown that both FL 9.9 and FL 20 have similar low performances. The measured TDS in the collected water were 5 ppm, 6 ppm, 8 ppm, and 12 ppm for FL 12.7, FL 9.9, FL 20, and FL 33 respectively.

Table 4.8: Daily water yield, productivity, and efficiency of varying FRL using Al scrap PCM

Variation in FRL	**Daily water yield, kg/m^2**	**Input energy, kJ**	**Productivity, g/kJ.m^2**	**Efficiency, %**
FL 12.7 cm	3.8052	356.60	10.67	32.82
FL 9.9 cm	2.8691	356.81	8.04	24.76
FL 20.0 cm	2.5647	355.62	7.21	22.19
FL 33.0 cm	11.4155	356.98	31.98	96.99

4.3.1.2 Varying Fresnel lenses with same Al_2O_3 NPCM

Experiment 7 was conducted using Al_2O_3 NPCM for all four solar still models on the 17th July 2023, where the weather is fairly sunny till 3 pm and starts to rain around 4 pm. The starting solar irradiance received at 9 am was 177 W/m^2, 151 W/m^2, 172 W/m^2, and 182 W/m^2 for FL 12.7, FL 9.9, FL 20, and FL 33. According to Figure 4.8, the solar irradiance increased to above 800 W/m^2 at 10 am and lasted till around 3 pm before it rains. The maximum solar irradiance was recorded at 2 pm for FL 12.7, FL 9.9, FL 20, and FL 33, which were 1027 W/m^2, 1047 W/m^2, 1031 W/m^2, and 1034 W/m^2 respectively. Besides that, the water temperature for all four solar still models were above 50 °C when there was sufficient sunlight around the period of 10 am to 3 pm. The highest water temperature achieved was 57.35 °C, 60.33 °C, 56.23 °C, and 74.74 °C for FL 12.7, FL 9.9, FL 20, and FL 33 respectively.

Moreover, the PCM temperature had maintained above 40 °C during the period with presence of sunlight and was able to reached at the maximum temperature of 58.79 °C, 57.13 °C, 54.40 °C, and 73.15 °C for FL 12.7, FL 9.9, FL 20, and FL 33 respectively. The cover temperature measured during the sunshine hours was around 40 to 50 °C for FL 12.7, FL 9.9 and FL 20; except for FL 33, which had a higher cover temperature above 50 °C. This was due to the larger focus area of sunlight being focused on the top cover compared to other models using smaller Fresnel lenses. In addition, the graph presented in Figure 4.9 shows that FL 33 had a significant increase in water yield, which is 1.560 kg/m^2, between 10 am to 11 am compared to FL 12.9 (0.304 kg/m^2), FL 9.9 (0.274 kg/m^2) and FL 20 (0.221 kg/m^2), which were increasing gradually. Furthermore, the cumulative water yield of FL 12.9 was leading FL 9.9 from the start but was soon overtaken at 4pm, giving the result where FL 9.9 had the second highest water yield; then, followed by FL 12.9 and lastly, FL 20. In this experiment, only FL 33 had been added saline water with the amount of 25 ml at 12 pm.

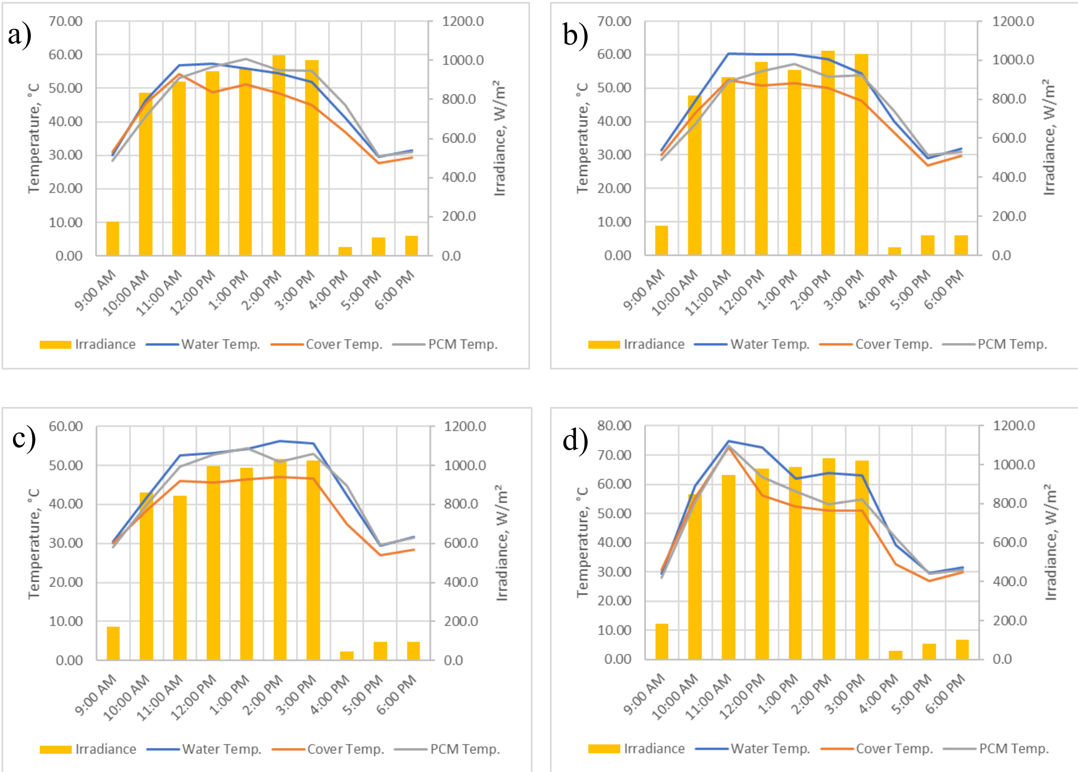

Figure 4.8: Temperature and irradiance results for different Fresnel lenses using 9k ppm saline water and Al_2O_3 NPCM (a) FL 12.7 cm (b) FL 9.9 cm (c) FL 20 cm (d) FL 33 cm

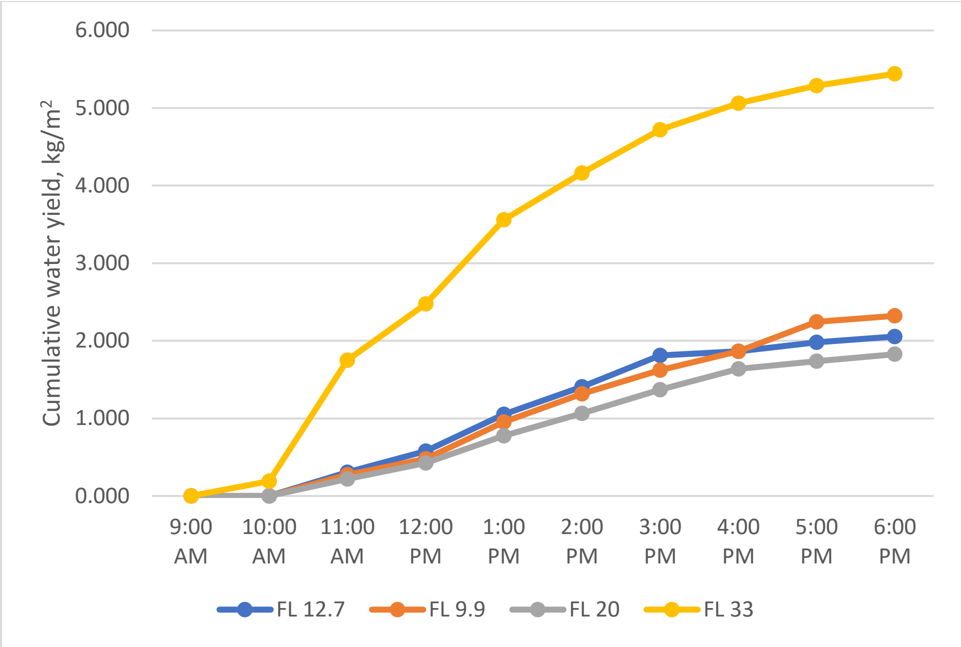

Figure 4.9: Cumulative water yield results for different Fresnel lenses using 9k ppm saline water and Al_2O_3 NPCM

There was distillate collected in the last three hours even though it was raining, and the amount of freshwater collected from 9 am to 6 pm in Experiment 7 was shown in Table 4.9 along with the productivity and efficiency of each solar still models. Among the models, FL 33 had the highest performance with a water yield, productivity and efficiency of 5.4414 kg/m^2, 20.51 g/kJ.m^2 and 62.77 % respectively. On the other hand, the lowest performing solar still model is FL 9.9 with a water yield, productivity and efficiency of 1.8265 kg/m^2, 6.97 g/kJ.m^2 and 21.59 % respectively. Meanwhile, FL 12.7 and FL 9.9 have similar water yield collected, where it was 2.0548 kg/m^2 and 2.3212 kg/m^2 respectively; but due to slightly different amount of energy received from the sun, the productivity and efficiency was different. The TDS of the water collected is 14 ppm, 10 ppm, 11 ppm, and 12 ppm for FL 12.7, FL 9.9, FL 20, and FL 33 respectively.

Table 4.9: Daily water yield, productivity, and efficiency of varying FRL using Al_2O_3 NPCM

Variation in FRL	Daily water yield, kg/m^2	Input energy, kJ	Productivity, g/kJ.m^2	Efficiency, %
FL 12.7 cm	2.0548	258.69	7.94	24.56
FL 9.9 cm	2.3212	261.77	8.87	27.46
FL 20.0 cm	1.8265	262.22	6.97	21.59
FL 33.0 cm	5.4414	265.27	20.51	62.72

4.3.1.3 Varying Fresnel lenses with same Cu NPCM

Next, Experiment 8 was conducted on 6th July 2023, a cloudy day and rained at 3 pm, using Cu NPCM as the TES for all four solar still models. The starting solar irradiance received was 188 W/m^2, 184 W/m^2, 198 W/m^2, and 179 W/m^2 for FL 12.7, FL 9.9, FL 20, and FL 33 respectively, at 9 am. Due to the cloudy weather, the average solar irradiance received for all four models were slightly above 300 W/m^2 for the day, where the solar irradiation trend is shown in Figure 4.10. The solar irradiance remained above around 500 W/m^2 but lower than 700 W/m^2 from 11 am to 2 pm before it rains at 3 pm and remains cloudy for the rest of the day. The maximum solar irradiance was recorded at 11 am, which were 687 W/m^2, 625 W/m^2, 653 W/m^2, and 643 W/m^2 for FL 12.7, FL 9.9, FL 20, and FL 33 respectively.

In addition, the water temperature was above 50 °C during the higher solar intensity hours from 11 am to 1 pm, where the maximum water temperature measured for FL 12.7, FL 9.9, FL 20, and FL 33 were 56.85 °C, 55.74 °C, 53.58 °C, and 70.80 °C respectively. The PCM temperature were above 50 °C from 11 am to 3 pm for all the models, where the highest PCM temperature was 71.64 °C, achieved by FL 33.

Furthermore, the cover temperature for all four models was measured to be above 40 °C during the presence of sunlight (11 am to 3 pm) and dropped below 30 °C when it rains after 3 pm. The cumulative water yield of the four models were recorded as shown in Figure 4.11. FL 33 had a steep increase compared to FL 12.7, FL 9.9 and FL 20, with a higher gradient in the interval of 10 am to 1 pm in Figure 4.11. It was recorded that FL 33 had a cumulative water yield of 1.979 kg/m^2 at 1 pm, while the cumulative water yield for FL 12.7, FL 9.9 and FL 20 were 1.050 kg/m^2, 0.951 kg/m^2 and 0.776 kg/m^2, respectively at 1 pm. Then, the water yield collected in FL33 increases gradually after 1 pm, where the gradient is similar with the other three experiment models. No saline water was refilled for any of the experiment models in this Subsubsection 4.3.1.3.

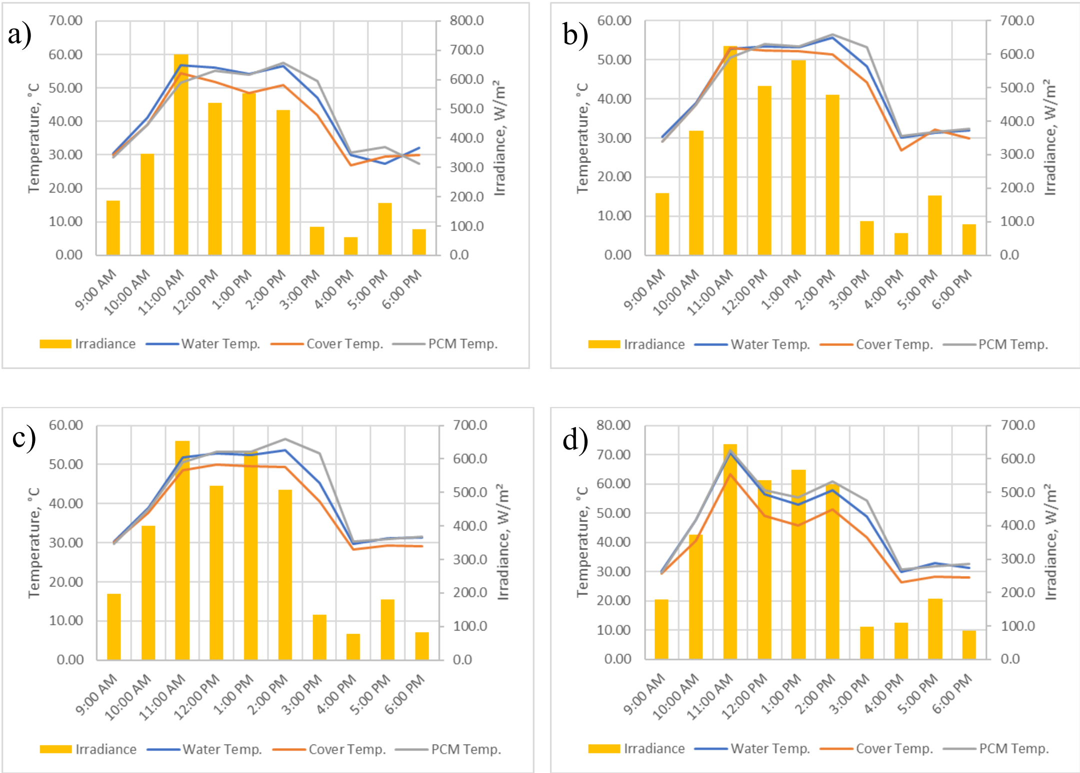

Figure 4.10: Temperature and irradiance results for different Fresnel lenses using 9k ppm saline water and Cu NPCM (a) FL 12.7 cm (b) FL 9.9 cm (c) FL 20 cm (d) FL 33 cm

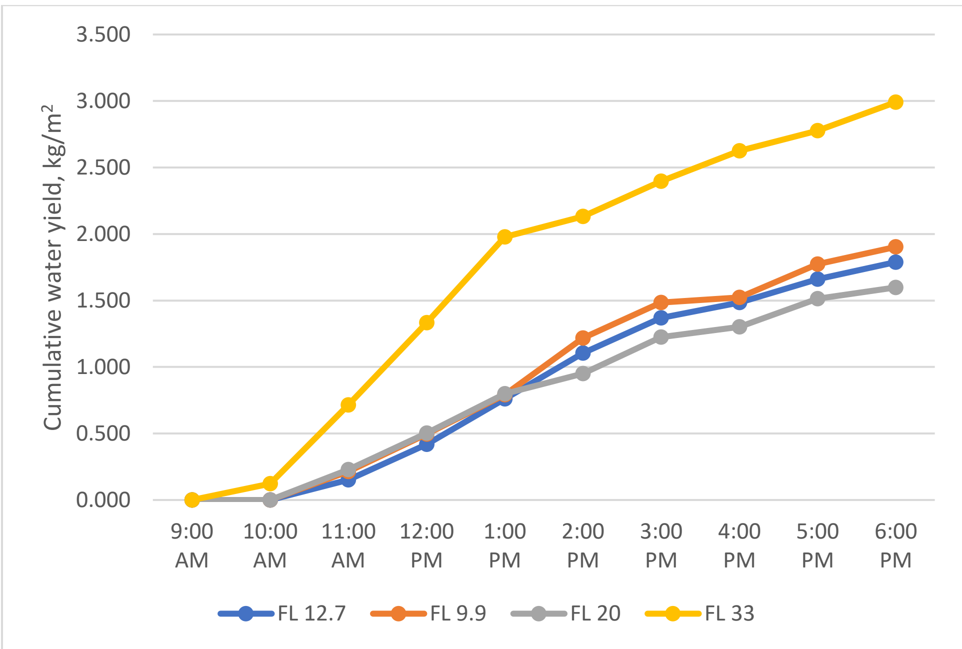

Figure 4.11: Cumulative water yield results for different Fresnel lenses using 9k ppm saline water and Cu NPCM

After 6 pm where the experiment ends, the total water yield measured for FL 12.7, FL 9.9, FL 20, and FL 33 were 1.7884 kg/m^2, 1.9026 kg/m^2, 1.5982 kg/m^2, and 2.9909 kg/m^2 respectively. Among the four models, FL 33 had the best performance with the highest water yield, productivity and efficiency as shown in Table 4.10. However, the lowest performing solar still was FL 20, with the productivity of 11.11 g/kJ.m^2; followed by FL 12.7 and FL 9.9, where both have similar performance with a productivity of 13.04 g/kJ.m^2 and 13.04 g/kJ.m^2 respectively. The TDS for FL 12.7, FL 9.9, FL 20, and FL 33 measured were 13 ppm, 14 ppm, 11 ppm, and 10 ppm respectively.

Table 4.10: Daily water yield, productivity, and efficiency of varying FRL using Cu NPCM

Variation in FRL	**Daily water yield, kg/m^2**	**Input energy, kJ**	**Productivity, g/kJ.m^2**	**Efficiency, %**
FL 12.7 cm	1.7884	137.12	13.04	40.50
FL 9.9 cm	1.9026	135.47	14.04	43.61
FL 20.0 cm	1.5982	143.84	11.11	34.57
FL 33.0 cm	2.9909	140.39	21.30	65.87

4.3.1.4 Varying Fresnel lenses with same Al_2O_3 and Cu NPCM

Experiment 9 was conducted on a fairly cloudy day with 2 hours of sunshine during noon on 12th July 2023. The PCM used for all four solar still models were the Al_2O_3 and Cu combination NPCM. According to Figure 4.12, the maximum solar irradiation for FL 12.7, FL 9.9, FL 20, and FL 33 occurred at 1 pm, where it was measured to be 1140 W/m^2, 1161 W/m^2, 1181 W/m^2, and 1217 W/m^2 respectively. Due to the cloudy weather, the solar irradiation measured for the experimental models were mostly below 500 W/m^2 after 1 pm. Besides that, the water temperature maintains around 45 °C to 60 °C for FL 12.7, FL 9.9 and FL 20, while FL 33's water temperature is much higher and ranges around 50 °C to 80 °C during the sunlight peak hours (11 am to 3 pm). Meanwhile the PCM temperature for FL 12.7, FL 9.9 and FL 20 was kept around 40 °C to 60 °C from 11 am to 4 pm, while FL 33 was around 50 °C to 70 °C. The PCM temperature was able to maintained around 37 °C to 40 °C near the end of the experiment even though the weather had turned cloudy and started rain showers. On the other hand, the cumulative freshwater collected was shown in Figure 4.13, where FL 33 had a significantly greater increase during noon compared to FL 12.7, FL 9.9 and FL 20. The average freshwater collected per hour during 11 am to 1 pm (peak solar irradiance hours) was 0.9 kg/m^2 for FL 33, while it was around 0.4 kg/m^2 for FL 12.7, FL 9.9 and FL 20. Moreover, it was observed that the water collected decreases gradually due to the low solar irradiation received after 2 pm. Furthermore, due to the cloudy weather, no additional saline water was added to the experimental models.

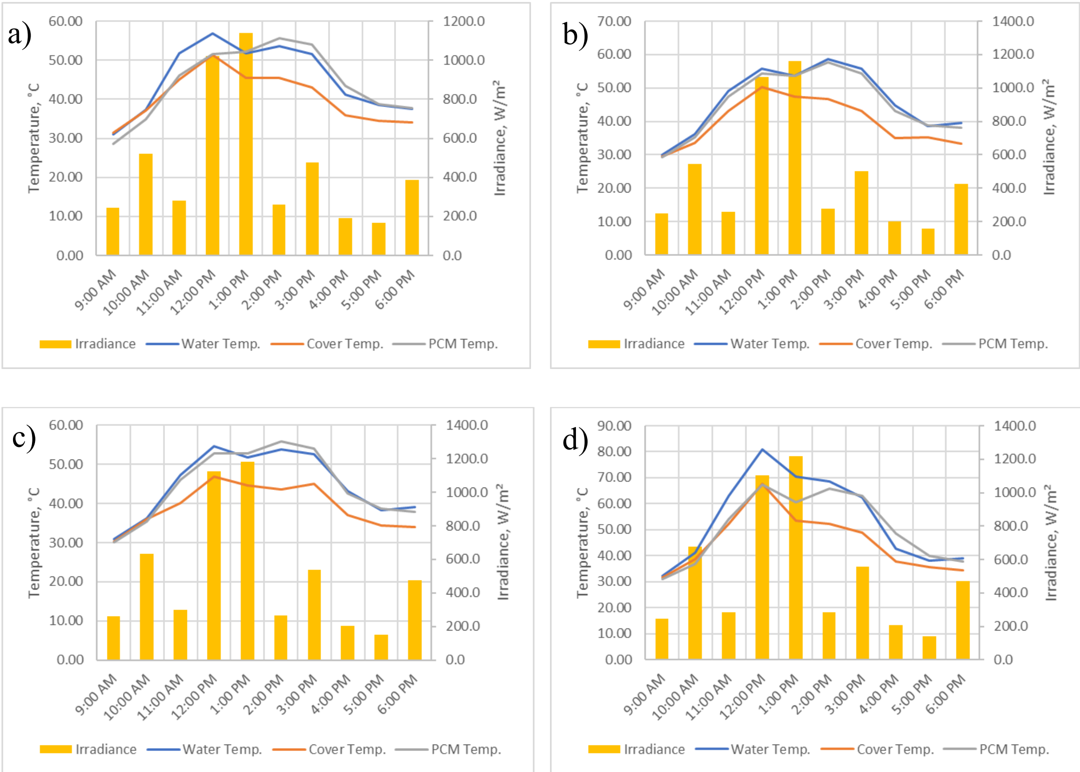

Figure 4.12: Temperature and irradiance results for different Fresnel lenses using 9k ppm saline water and Al_2O_3 and Cu NPCM (a) FL 12.7 cm (b) FL 9.9 cm (c) FL 20 cm (d) FL 33 cm

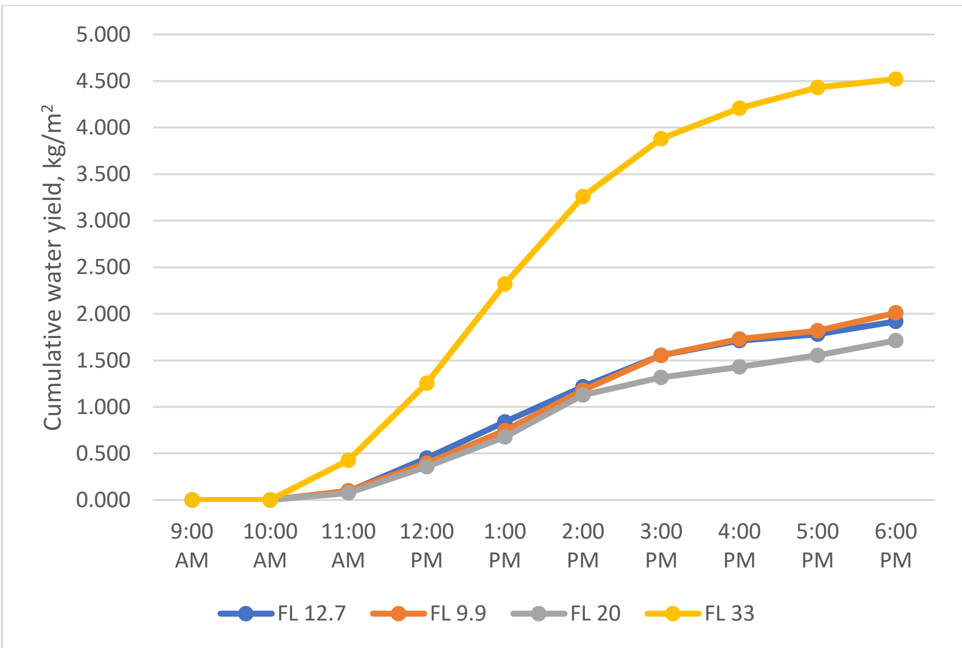

Figure 4.13: Cumulative water yield results for different Fresnel lenses using 9k ppm saline water and Al_2O_3 + Cu NPCM

At the end of the experiment, the distillate collected for FL 12.7, FL 9.9, FL 20, and FL 33 were 1.9178 kg/m^2, 2.0091 kg/m^2, 1.7123 kg/m^2, and 4.5205 kg/m^2 respectively. Similar to previous outdoor experiments, FL 33 had the best performance with the highest water yield, productivity (20.48 g/kJ.m^2) and efficiency (62.49 %) as shown in Table 4.11. Nevertheless, FL 20 had the lowest performance, with a productivity and efficiency of 7.84 g/kJ.m^2 and 24.30 % respectively. The TDS level for FL 12.7, FL 9.9, FL 20, and FL 33 were 16 ppm, 43 ppm, 15 ppm, and 19 ppm respectively. The TDS level for FL 9.9 was slightly higher due to small amount of saline water mixed with the condensate, as it was observed that tiny drops of saline water residue was left on the top cover.

Table 4.11: Daily water yield, productivity, and efficiency of varying FRL using Al_2O_3 + Cu NPCM

Variation in FRL	Daily water yield, kg/m^2	Input energy, kJ	Productivity, g/kJ.m^2	Efficiency, %
FL 12.7 cm	1.9178	199.81	9.60	29.73
FL 9.9 cm	2.0091	206.35	9.74	30.11
FL 20.0 cm	1.7123	218.47	7.84	24.30
FL 33.0 cm	4.5205	220.68	20.48	62.49

In Subsection 4.3.1, it was concluded that the solar still models that utilized 33 cm FL Fresnel lens, has the best performance out of the four models. It was followed by FL 9.9 and FL 12.7, where both were similar in results; and lastly, FL 20 which had the lowest performance for the four outdoor experiments in this section. The best Fresnel lens chosen was affected by its affective aperture area, concentration ratio and focal length (FL). The larger the affective aperture area of the Fresnel lens, the larger the concentration ratio, as the concentration ratio was calculated using the ratio of aperture area over the receiver area. Moreover, for the focal length, it was observed that the higher the focal length of the lens, the more difficult it is to focus the sunlight on the receiver during the experiment. Therefore, even though 20 cm FL Fresnel lens have a slightly higher concentration ratio than the 9.9 cm FL Fresnel lens, it had the lower performance. Similar for the comparison between the 12.7 cm FL Fresnel lens and 9.9 cm FL Fresnel lens, even though FL 12.7 had a higher concentration ratio, the performance is still slightly lower than FL 9.9 in Experiment 7, 8 and 9 (Subsubsection 4.3.1.2, 4.3.1.3 and 4.3.1.4). Regardless of which type of PCM was used, the results were similar in this section as the Fresnel lenses played a vital role in focusing the solar irradiation which was received by the solar still. Therefore, to further investigate the PCMs in outdoor conditions, the type of Fresnel lens will remain constant while four types of PCMs will be used for the experiments in the next section.

4.3.2 Comparing different PCMs with same Fresnel lenses and saline water

There are a total of three experiments conducted in this subsection by comparing the different types of PCMs. The Fresnel lenses applied were the 33 cm FL Fresnel lenses and different salinity of saline water (10k ppm, 20k ppm and 30k ppm) were tested in each experiment. The solar still models were named according to the PCMs used, since the variable for the outdoor experiments in Subsection 4.3.2 are the PCMs. The four PCMs involved were listed in Table 4.12.

Table 4.12: Naming system of the solar still models for outdoor experiment in Subsection 4.3.2

Naming of the solar still models	PCM contents
Al_2O_3 + Cu	Al_2O_3 and Cu nanomaterial with PW
Al_2O_3	Al_2O_3 nanomaterial with PW
Al	Al scrap with PW
Cu	Cu nanomaterial with PW

4.3.2.1 Varying PCM with same Fresnel lens and 10 000 ppm saline water

Experiment 10 was conducted on 25th July 2023, where the water basins of the four solar stills were filled with 10 000 ppm of saline water. The day was fairly sunny as the average solar irradiation for all four models were above 700 W/m^2 in the 9-hour experiment. According to Figure 4.14, the maximum irradiation occurs at 11 am for Al_2O_3 + Cu, Al_2O_3 and Al while it is at 2 pm for Cu. The maximum irradiation measured for Al_2O_3 + Cu, Al_2O_3, Al, and Cu were 1173 W/m^2, 1138 W/m^2, 1116 W/m^2, and 1132 W/m^2 respectively. Moreover, the water temperature and PCM temperature for all the models were above 50 °C from 10 am to 6 pm. The highest water temperature for Al_2O_3 + Cu, Al_2O_3, Al, and Cu were 69.05 °C, 81.28 °C, 74.10 °C, and 96.68 °C respectively, while for the maximum PCM temperature measured were 75.67 °C, 72.07 °C, 79.03 °C, and 72.63 °C respectively. Besides that, the cover temperature was measured to be around 50 °C to 75 °C most of the time during the experiment, except for Al_2O_3 + Cu and Al_2O_3 not going over 65 °C.

In addition, the cumulative water yield in Figure 4.15 shows that Al_2O_3 + Cu and Cu's lines were slightly steeper than Al_2O_3 and Al. The highest freshwater collected per hour occurred at 12 pm, where it was measured 1.804 kg/m^2, 1.575 kg/m^2, 1.697 kg/m^2, and 1.826 kg/m^2 for Al_2O_3 + Cu, Al_2O_3, Al, and Cu respectively. The high amount of freshwater collected was due to the temperature difference between the water and the cover and outside temperature, as the solar radiation reduced to around 330 W/m^2 at 12 pm compared to the high solar irradiation, 1100 W/m^2 at 11 pm. Therefore, the heat energy stored in the saline water has a much higher temperature (around 60.00 °C) compared to the lower outside temperature (30.30 °C) when the presence of sunlight is low. Apart from that, additional saline water was added into the experimental models as the sunny weather escalates the evaporation rate. All the experimental models were refilled three times, where each time is 25 ml; hence a total of 75 ml was added. Al_2O_3 + Cu and Cu with the steeper cumulative freshwater lines, the saline water was added at 12 pm, 1 pm and 3pm; meanwhile, Al_2O_3 and Al were added at 12 pm, 2 pm and 3 pm.

Figure 4.14: Temperature and irradiance results for different PCMs using 10k ppm saline water and FL 33 cm Fresnel lens (a) Al_2O_3 and Cu NPCM (b) Al_2O_3 NPCM (c) Al scrap PCM (d) Cu NPCM

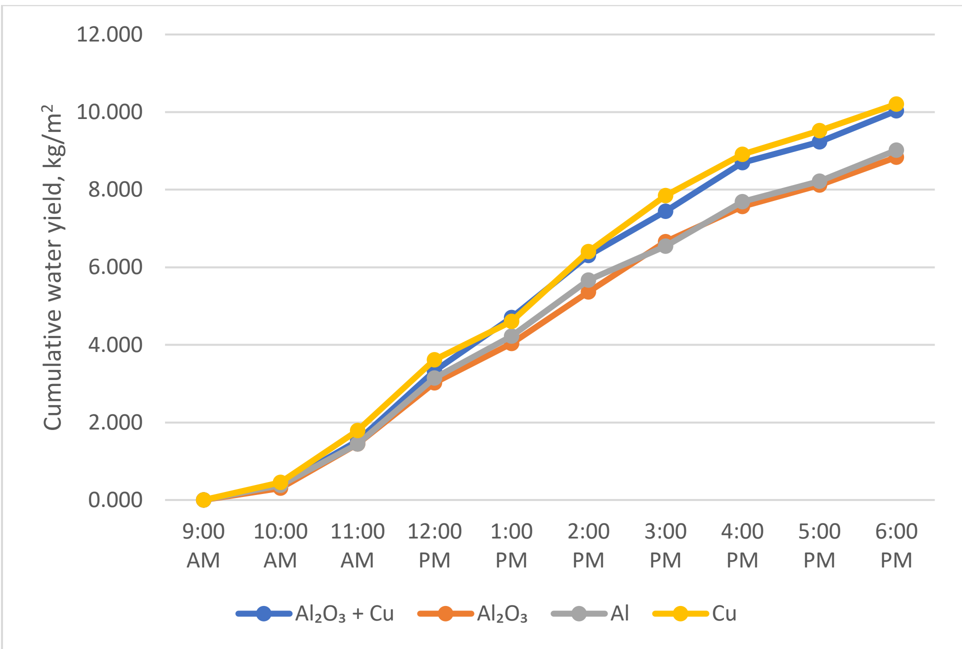

Figure 4.15: Cumulative water yield results for different PCMs using FL 33 cm Fresnel lenses and 10k ppm saline water

The distillate collected at the end of Experiment 10 for Al_2O_3 + Cu, Al_2O_3, Al, and Cu were 10.0304 kg/m^2, 8.8356 kg/m^2, 9.0183 kg/m^2, and 10.2055 kg/m^2 respectively. According to Table 4.13, Cu had the most water yield but Al_2O_3 + Cu had the best productivity and efficiency. This was due to the different amount of energy received by both Al_2O_3 + Cu and Cu, where it was calculated from the solar irradiance that Al_2O_3 + Cu had an input energy of 319.56 kJ while Cu received 329.76 kJ of energy. Therefore, Al_2O_3 + Cu that had a slightly lower energy input than Cu, had a better performance because both solar still models produced similar amount of distillate at the end of the experiment. Besides that, it was noteworthy that the efficiency of the four models have an efficiency higher than 80 % due to its small compact design. On top of that, Al had a similar performance to Al_2O_3, was an interesting outcome as the low-cost aluminium scrap was able to get a better performance than the high-cost alumina nanopowder. The TDS level of Al_2O_3 + Cu, Al_2O_3, Al, and Cu were 14 ppm, 14 ppm, 20 ppm, and 10 ppm respectively.

Table 4.13: Daily water yield, productivity, and efficiency of varying PCM using FL 33 and 10k ppm saline water

Variation in PCM	**Daily water yield, kg/m^2**	**Input energy, kJ**	**Productivity, g/kJ.m^2**	**Efficiency, %**
Al_2O_3 and Cu NPCM	10.0304	319.56	31.39	95.82
Al_2O_3 NPCM	8.8356	319.73	27.63	84.25
Al scrap PCM	9.0183	323.05	27.92	85.40
Cu NPCM	10.2055	329.78	30.95	93.79

4.3.2.2 Varying PCM with same Fresnel lens and 20 000 ppm saline water

In Experiment 11, the saline water used had a salinity of 20 000 ppm and was conducted on a cloudy day on the 27th July 2023, where it also rained at 1 pm for less than an hour. According to Figure 4.16, it was observed that the solar irradiance was relatively low compared to Experiment 10, where it had an average of 450 W/m^2 during the 9-hour experiment. The highest solar irradiance measured for Al_2O_3 + Cu, Al_2O_3, Al, and Cu were 999 W/m^2, 985 W/m^2, 1006 W/m^2, and 971 W/m^2 respectively, at 4 pm. In addition, the water temperature for the Al_2O_3 + Cu, Al_2O_3, Al, and Cu were in an average of 45.8 °C, 44.6 °C, 46.9 °C, and 48.5 °C respectively; meanwhile the highest water temperature measured were 54.36 °C, 53.43 °C, 59.30 °C, and 63.05 °C respectively. The average PCM temperature for Al_2O_3 + Cu, Al_2O_3, Al, and Cu were 45.4 °C, 44.3 °C, 46.1 °C, and 47.5 °C respectively, which were similar with the average water temperature. Moreover, the cover temperature was in an average of around 40 °C for Al_2O_3 + Cu, Al_2O_3 and Al, while Cu had a higher average cover temperature around 45 °C.

Additionally, the cumulative water yield for Al_2O_3 + Cu, Al, and Cu have similar lines while Al_2O_3 line is slightly gradual in comparison, as shown in Figure 4.17. The freshwater collected increases moderately and further slows down at 1pm when it rains; then, it increased after 3 pm where the solar irradiation (around 1000 W/m^2 measured at 4 pm) had increased. The highest freshwater collected per hour were scattered around, where Al_2O_3 + Cu collected 0.571 kg/m^2 at 4 pm, both Al_2O_3 and Al at 5 pm collected 0.419 kg/m^2 and 0.525 kg/m^2 respectively, while Cu collected 0.571 kg/m^2 at 12 pm. Even though the highest freshwater collected per hour for the four models were at different hours, the freshwater collected per hour were higher at 12 pm and 4pm to 6pm, compared to other time intervals. No additional saline water was added to the experimental models due to the low solar radiation, which affected the low evaporation rate of the saline water.

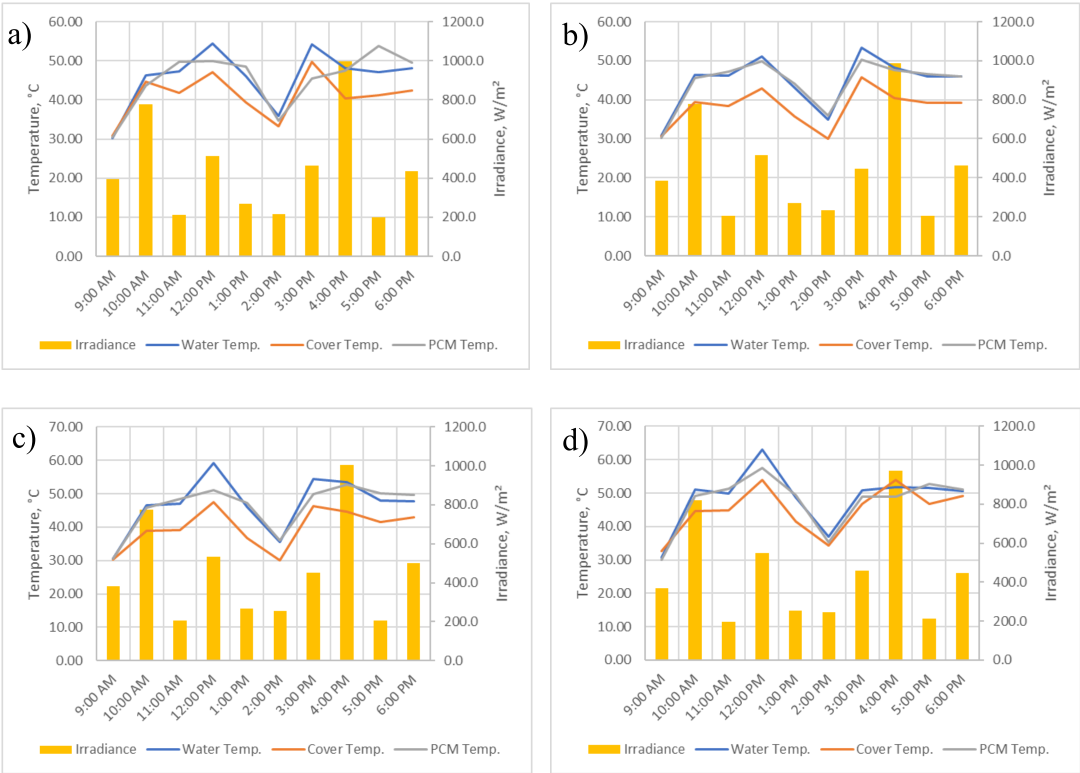

Figure 4.16: Temperature and irradiance results for different PCMs using 20k ppm saline water and FL 33 cm Fresnel lens (a) Al_2O_3 and Cu NPCM (b) Al_2O_3 NPCM (c) Al scrap PCM (d) Cu NPCM

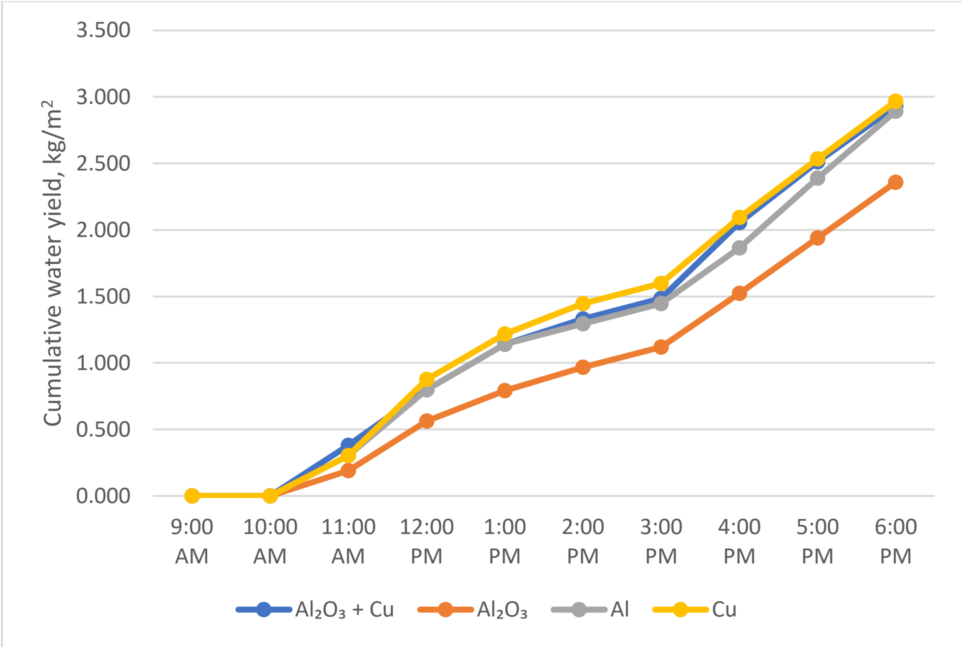

Figure 4.17: Cumulative water yield results for different PCMs using FL 33 cm Fresnel lenses and 20k ppm saline water

The water yield collected in Experiment 11 (Subsubsection 4.3.2.2) is much less than in experiment 10 (Subsubsection 4.3.2.1), which were 2.9300 kg/m^2, 2.3592 kg/m^2, .2.8919 kg/m^2, and 2.9680 kg/m^2 for Al_2O_3 + Cu, Al_2O_3, Al, and Cu respectively. According to Table 4.14, Al_2O_3 + Cu and Cu have a very similar result, both having a productivity and efficiency of around 15g/kJ.m^2 and 47 % respectively. Interestingly, Al had a higher performance than Al_2O_3 in this experiment compared to the previous Subsubsection 4.3.2.1, where the difference is lower. The TDS level of Al_2O_3 + Cu, Al_2O_3, Al, and Cu were 34 ppm, 12 ppm, 12 ppm, and 6 ppm respectively.

Table 4.14: Daily water yield, productivity, and efficiency of varying PCM using FL 33 and 20k ppm saline water

Variation in PCM	Daily water yield, kg/m^2	Input energy, kJ	Productivity, g/kJ.m^2	Efficiency, %
Al_2O_3 and Cu NPCM	2.9300	190.94	15.34	47.13
Al_2O_3 NPCM	2.3592	190.73	12.37	38.05
Al scrap PCM	2.8919	195.50	14.79	45.35
Cu NPCM	2.9680	192.35	15.43	47.21

4.3.2.3 Varying PCM with same Fresnel lens and 30 000 ppm saline water

Experiment 12 was conducted on 30th August 2023 using 30 000 ppm saline water for all solar still models with different PCMs. According to Figure 4.18, strong solar irradiance which were above 800 W/m^2 were recorded at 11 am, 1 pm, 3 pm, and 4 pm, while the rest of the times were below 500 W/m^2. The highest solar irradiance recorded was at 11 am, which were 1246 W/m^2, 1240 W/m^2, 1258 W/m^2, and 1258 W/m^2 for Al_2O_3 + Cu, Al_2O_3, Al, and Cu respectively. Moreover, the water temperature was high as it was able to maintained above 60 °C from 11 am to 4 pm for four of the experimental models. The highest water temperature recorded were 82.87 °C, 84.93 °C, 88.11 °C, and 86.11 °C for Al_2O_3 + Cu, Al_2O_3, Al, and Cu respectively. Meanwhile for the PCM temperature, it was usually lower than its water temperature for Al_2O_3 + Cu and Al_2O_3; however, the PCM temperature was usually higher than its water temperature for Al and Cu, which aided the rise in water temperature during the absence of strong sunlight. The highest PCM temperature reached were 75.99 °C, 79.20 °C, 80.28 °C, and 90.00 °C for Al_2O_3 + Cu, Al_2O_3, Al, and Cu respectively, which occurred at 11 am or 1 pm. Furthermore, the cover temperature measured for the solar still models was an average of 54 °C, where the highest temperature reached 70 °C to 80 °C at noon. It was observed from Figure 4.18. that Al_2O_3 + Cu (Figure 4.18a) has the highest difference in water temperature and cover temperature, which resulted a high evaporation rate even though the water temperature is much lower than the others.

In addition, the cumulative water yield for four of the experimental models were similar in this experiment as shown in Figure 4,19. By close observation, the Cu line is slightly leading while the Al_2O_3 line is slightly lagging in comparison. The highest water yield collected per hour scattered around 1 pm to 3 pm, where Al_2O_3 + Cu collected 1.941 kg/m^2 at 3 pm, Al_2O_3 collected 1.826 kg/m^2 at 2 pm, Al collected 1.826 kg/m^2 at both 1 pm and 2 pm, and finally, Cu collected 1.903 kg/m^2 at 3 pm. Due to the good weather, the freshwater collected per hour were above 1 kg/m^2 from 11 am to 4 pm for all the experimental models as high solar radiation (around or above 1000 W/m^2) were recorded at 11 am, 1 pm and 3 pm. On the other hand, saline water was added twice at 12 pm and 2 pm for all the experimental models, where each was 50 ml. Hence, a total of 100 ml of saline water was added to all four of the experimental models.

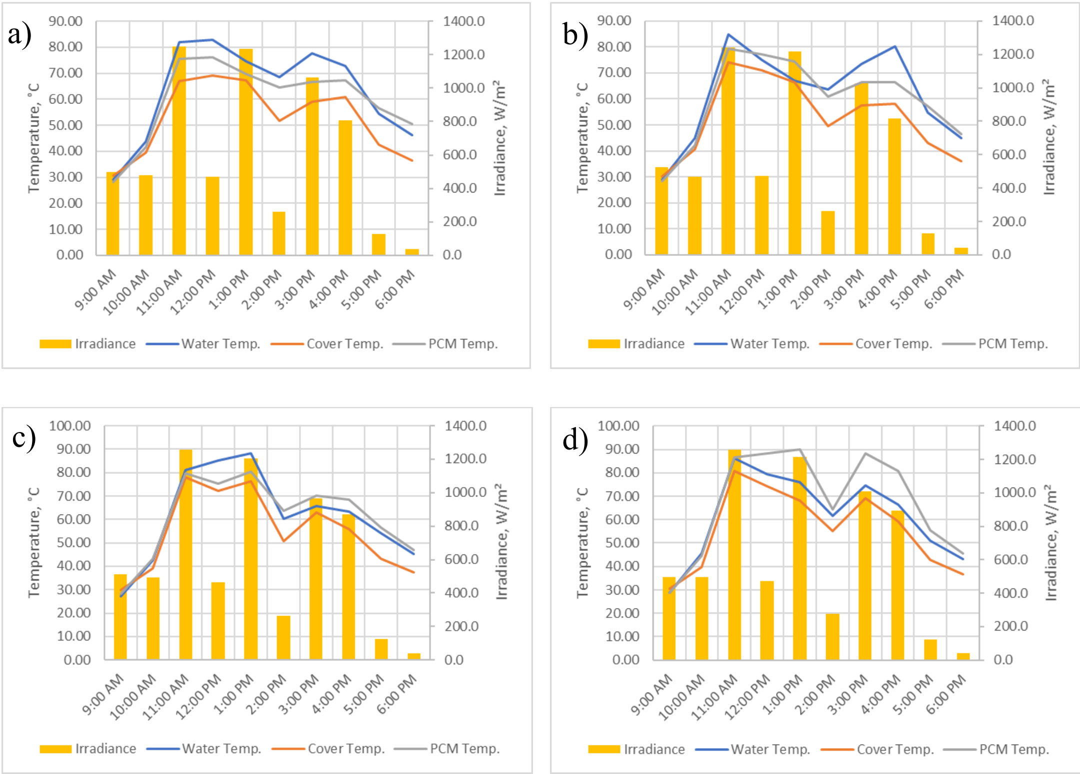

Figure 4.18: Temperature and irradiance results for different PCMs using 30k ppm saline water and FL 33 cm Fresnel lens (a) Al_2O_3 and Cu NPCM (b) Al_2O_3 NPCM (c) Al scrap PCM (d) Cu NPCM

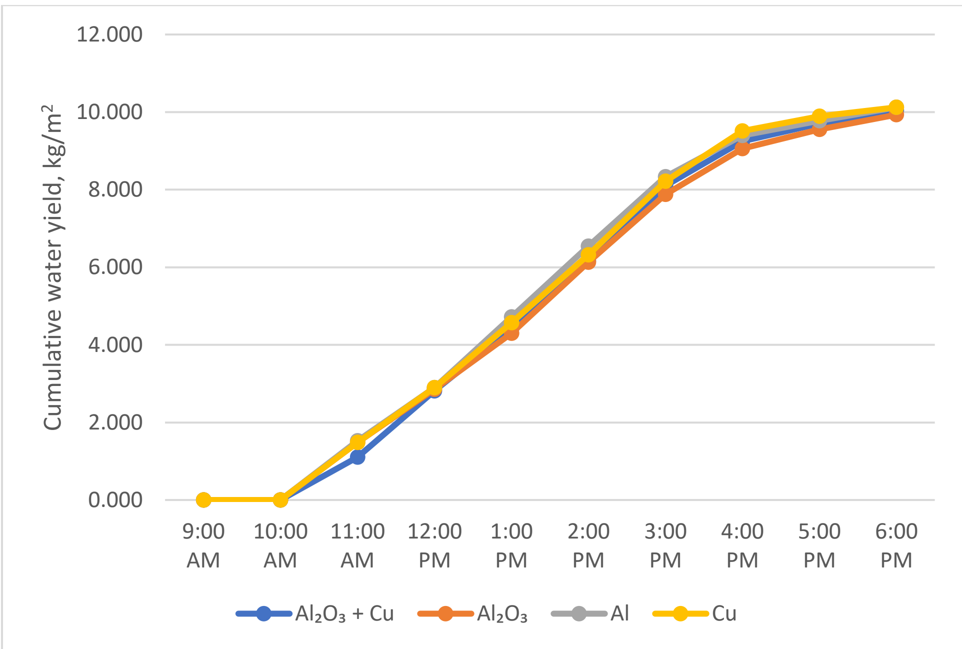

Figure 4.19: Cumulative water yield results for different PCMs using FL 33 cm Fresnel lenses and 30k ppm saline water

The water yield collected in Experiment 12 for Al_2O_3 + Cu, Al_2O_3, Al, and Cu were 10.0457 kg/m^2, 9.9315 kg/m^2, 10.1218 kg/m^2, and 10.1218 kg/m^2 respectively, where Al and Cu have the same water yield. However, according to Table 4.15, the productivity of Al is slightly higher than Cu. This is because the energy received by Al is calculated to be 264.01 kJ, while the energy received by Cu is 267.46 kJ, which was around 3 kJ higher than Al. Furthermore, it was observed that the efficiency was higher than 100 %, where it was 112.16 %, 111.86 %, 113.72 %, and 112.27 % for Al_2O_3 + Cu, Al_2O_3, Al, and Cu respectively. This was due to the aid of Fresnel lenses, where it concentrated the solar irradiance received on a day with long periods of high solar radiation. Hence, the energy flux per unit area becomes denser on the concentrated area on the receiver, which is the water basin. The concentrated solar energy beneath the Fresnel lens could not be measured, as the irradiance value was much higher than the safety range of the solar power meter. Thus, the concentrated area could not be considered the same like other cases and normal efficiency calculation is not applicable here. Besides that, the solar irradiance recorded may be slightly inaccurate due to the weather conditions, as the clouds may be present during the time when the measurement were taken but absent during the intervals. The TDS level measured for Al_2O_3 + Cu, Al_2O_3, Al, and Cu were 23 ppm, 16 ppm, 10 ppm, and 12 ppm respectively.

Table 4.15: Daily water yield and productivity of varying PCM using FL 33 and 30k ppm saline water

Variation in PCM	Daily water yield, kg/m^2	Input energy, kJ	Productivity, g/kJ.m^2
Al_2O_3 and Cu NPCM	10.0457	265.1569	37.89
Al_2O_3 NPCM	9.9315	263.6285	37.67
Al scrap PCM	10.1218	264.0117	38.34
Cu NPCM	10.1218	267.4601	37.84

This subsection provides information about the PCMs used, where in Experiment 10 (Subsubsection 4.3.2.1) and Experiment 11 (Subsubsection 4.3.2.2) shows that Al_2O_3 and Cu NPCM is the best while in Experiment 12 (Subsubsection 4.3.2.3) shows that Al scrap PCM is the best. Furthermore, the performance of the solar stills using Al_2O_3 and Cu NPCM and only Cu NPCM is very similar, while for Al scrap PCM is mostly higher in performance than Al_2O_3 NPCM. This establishes that Al scrap is a better conductive particle compared to Al_2O_3 nanoparticle in terms of performance, the cost was further discussed and compared in Section 4.5. In the next Subsection 4.3.3, further discussion on comparing the saline water while the type of PCM remained constant was considered to determine how the salinity of the basin water affects the performance of the desalination system.

4.3.3 Comparing different salinity of saline water with the same PCMs and Fresnel lenses

In this subsection, a total of four experiments were conducted comparing different saline water (10k ppm, 20k ppm and 30k ppm) while using the same size of Fresnel lenses (FL 33) and same type of PCMs in each experiment. The solar still models were named after the variable, salinity of the basin water, for each experiment conducted as listed in Table 4.16.

Table 4.16: Naming system of the solar still models for outdoor experiment in Subsection 4.3.3

Naming of the solar still models	Salinity of basin water
10k	10 000 ppm
20k	20 000 ppm
30k	30 000 ppm

4.3.3.1 Varying saline water with same Fresnel lens and Al scrap PCM

Experiment 13 was conducted on 9th August 2023, where all the experimental models were using FL 33 cm Fresnel lenses and Al scrap PCMs. The weather was sunny till 1 pm and started to get cloudy around 2 pm till the sun sets, where the bar chart of the solar irradiance was shown in Figure 4.20. The average solar irradiance for the three experiment models were around 580 W/m^2; while the highest solar irradiation measured was at 1pm, which were 1189 W/m^2, 1190 W/m^2 and 1184 W/m^2 for 10k, 20k and 30k respectively. After 2 pm, the weather got cloudy and the solar irradiance decreases to approximately 250 W/m^2; eventually, it was measured to be lowest at 4 pm, which was around 77 W/m^2. Furthermore, the water temperature for

10k and 30k have less fluctuations from 10 am to 1 pm, where the water temperature maintained around 70 °C to 80 °C; meanwhile the water temperature of 20k reaches the highest peak at 11 am, then decreases gradually till the end of the experiment. The highest water temperature recorded for 10k, 20k and 30k were 81.04 °C, 93.52 °C and 79.57 °C respectively, where it occurred at 11 am for 10k and 20k while it occurred at 12 pm for 30k.

Moreover, the PCM temperature has a similar trend with the water temperature, where both 10k and 30k were more stable between 10 am to 1 pm and 20k having to reach peak at 11 am and eventually decreases. The PCM temperature for 20k was higher than its water temperature after 11 am while the PCM temperature of the other two experimental models were usually lower than its water temperature before 3 pm. Besides that, the average cover temperature was 53.5 °C, 53.9 °C and 50.7 °C for 10k, 20k and 30k respectively. Additionally, according to Figure 4.21, the cumulative water yield of 10k, 20 and 30k started similar until 11 am. After 11 am, 10k began to lead the other two with the increase of 2.892 kg/m^2 at 12 pm, while 20k and 30k only increased 2.093 kg/m^2 and 2.283 kg/m^2 respectively. The cumulative water yield for 20k and 30k was similar before 1 pm; then, 20k began leading 30k at 1 pm by collecting a 0.342 kg/m^2 extra of water yield than 30k. The collection of freshwater began to slow down after 3 pm, leaving 10k having the highest water yield, followed by 20k and lastly, 30k. Besides that, additional saline water was added to the three experimental models in this experiment due to the high evaporation rate affected by high solar radiation received. A total of 100 ml saline water was added, where it was separated into three times at 11 am (25 ml), 12 pm (25 ml) and 1 pm (50 ml).

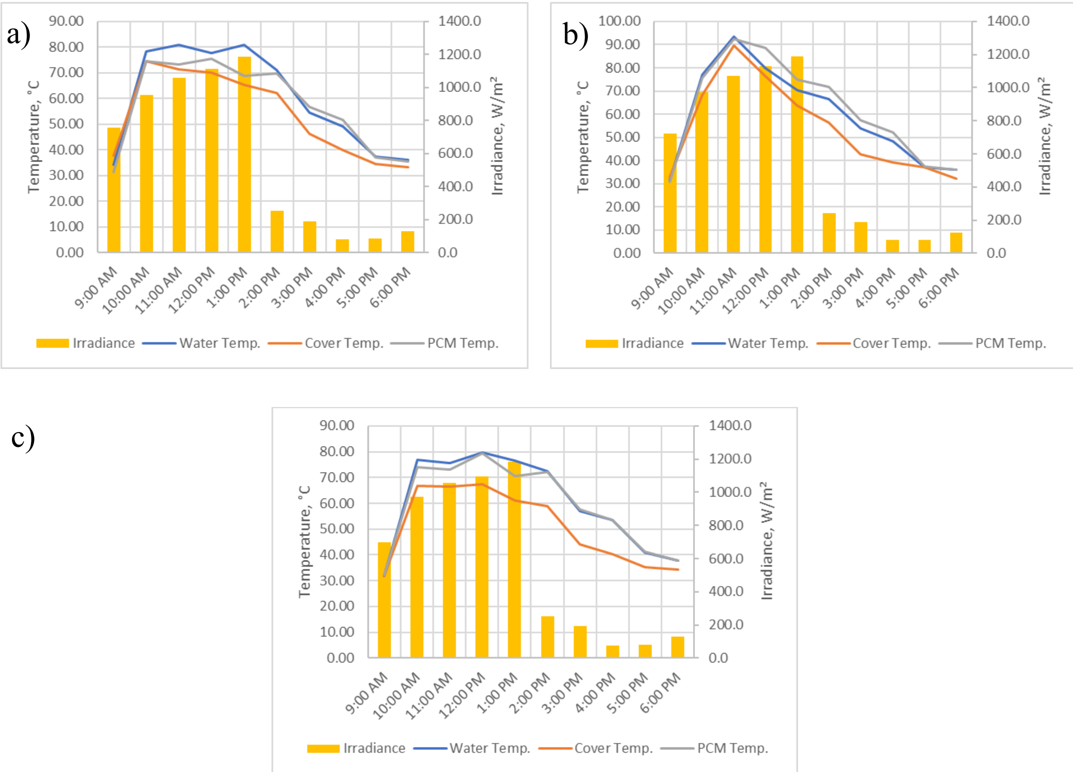

Figure 4.20: Temperature and irradiance results for different saline water using FL 33 cm Fresnel lens and Al scrap PCM (a) 10k ppm (b) 20k ppm (c) 30k ppm

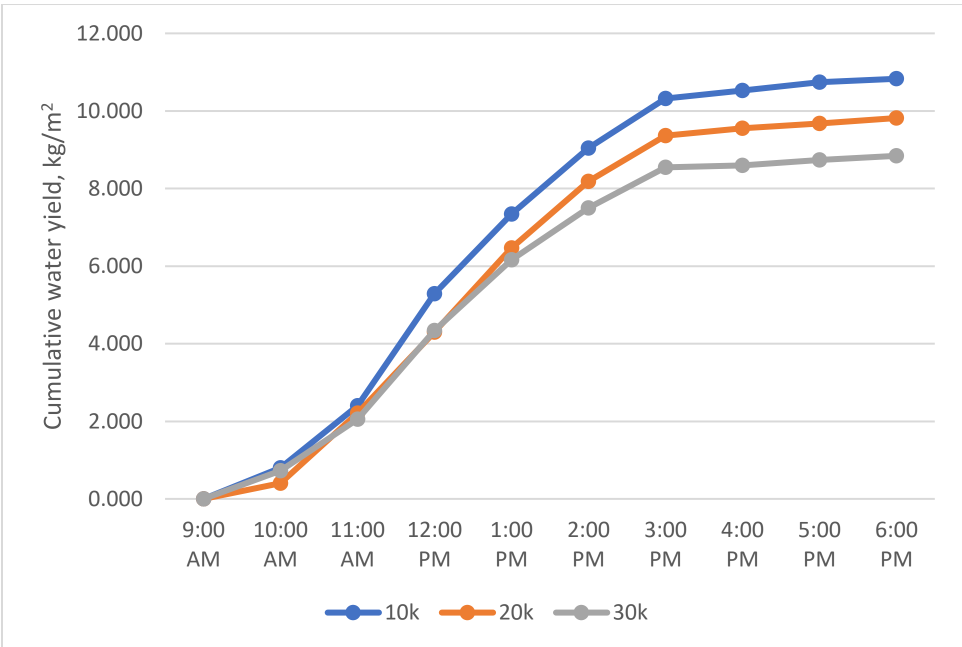

Figure 4.21: Cumulative water yield results for different saline water using FL 33 cm Fresnel lenses and Al scrap PCM

As mentioned, 10k had the highest water yield, which was 10.8295 kg/m^2; and was followed by 20k and 30k, which were 9.8174 kg/m^2 and 8.8432 kg/m^2 respectively, according to Table 4.17. With similar input energy, around an average of 246 kJ, 10k had the highest productivity of 43.86 g/kJ.m^2 given that it had the highest water yield among the three experimental models. Then, it was followed by 20k with a productivity of 39.72 g/kJ.m^2 and lastly, 30k with a productivity of 36.21 g/kJ.m^2. The result was according to what was predicted as the higher the salinity of basin water, the higher the energy required to vaporize the saline water in the basin. Furthermore, the efficiency was 132.66 %, 118.98 % and 107.34 % for 10k, 20k and 30k respectively. Similar to Subsubsection 4.3.2.3, the efficiency exceeded 100 % due to receiving concentrated solar energy, which was focused by the Fresnel lenses on a day with long periods of exposure to strong solar radiation. The saline water on the concentrated area was constantly boiling under the long exposure of strong solar radiation received. However, on the days with lower solar radiation, the saline water at the concentrated area does not boil frequently. Therefore, the normal efficiency calculation is not applicable as the concentrated area could not be considered same like other cases on days with strong solar radiation. The TDS level of the water yield collected by 10k, 20k and 30k were 14 ppm, 27 ppm and 61 ppm respectively.

Table 4.17: Daily water yield, productivity, and efficiency of varying saline water using FL 33 and Al scrap PCM

Variation in saline water	Daily water yield, kg/m^2	Input energy, kJ	Productivity, g/kJ.m^2
10k ppm	10.8295	246.9013	43.86
20k ppm	9.8174	247.1568	39.72
30k ppm	8.8432	244.2107	36.21

4.3.3.2 Varying saline water with same Fresnel lens and Al_2O_3 NPCM

Experiment 14 was conducted on 12th August 2023, using the FL 33 cm Fresnel lenses and Al_2O_3 NPCMs for the three experimental models, 10k, 20k and 30k. It was a cloudy day with only two hours of sunlight around noon. The average irradiance was 411.4 W/m^2, 425.5 W/m^2 and 431.9 W/m^2 for 10k, 20k and 30k. According to Figure 4.22, the highest irradiance recorded occurred at 12 pm, which were 1090 W/m^2, 1138 W/m^2 and 1144 W/m^2 for 10k, 20k, and 30k respectively. There were rain showers happened at 2 pm, causing the sudden drop in the solar irradiance received, which were recorded to be 368 W/m^2, 364 W/m^2 and 391 W/m^2 for 10k, 20k and 30k. The weather remained cloudy for the rest of the day after the slight rain at 2 pm. Furthermore, the temperature lines for water, PCM and cover were similar, where the temperature increased until 1 pm (peak) and decreased after 1 pm till the end of the experiment. The highest water temperature for 10k, 20k and 30k were 74.85 °C, 76.67 °C and 68.90 °C respectively. Besides that, it was observed that the PCM temperature for 10k is usually lower than the water temperature while the PCM temperature for 20k and 30k is usually higher than its water temperature after 1 pm, which was during the low solar radiation period. The highest PCM temperature recorded were 73.39 °C, 80.21 °C and 69.58 °C for 10k, 20k and 30k respectively. As for the cover temperature, it was an average of 40 °C for the three experimental models, where the highest cover temperature reached was 62.30°C, 65.44 °C and 61.37 °C for 10k, 20k and 30k respectively at 1 pm.

Other than that, the cumulative water yield of 10k, 20k and 30k was shown in Figure 4.23. It was observed that the freshwater collected were similar during the start, from 9 am to 11 am. However, at 12 pm, 30k was slightly leading 10k and 20k, where the cumulative water yield at 12 pm was 0.875 kg/m^2, 0.723 kg/m^2 and 0.989 kg/m^2 for 10k, 20k and 30k respectively. Due to the high solar radiation at 12 pm, high amount of freshwater was collected at 1 pm, which were 1.712 kg/m^2, 1.636 kg/m^2 and 1.522 kg/m^2 for 10k, 20k and 30k within the time span of an hour. The freshwater collected decreased at 2 pm due to rain showers, which caused low solar radiation received. In this situation, the PCM plays an important role during the low sunlight intensity period, as the heat energy stored in the PCM during the high solar intensity period (around 12 pm to 1 pm) was able to provide to the basin water. Hence, the freshwater collected was able to gradually increase after 2 pm due to the aid of the PCM. Additionally, 25 ml of saline water was added during the experiment for the three experimental models at 2 pm, as the saline water decreases drastically after 1 pm (high solar intensity hours).

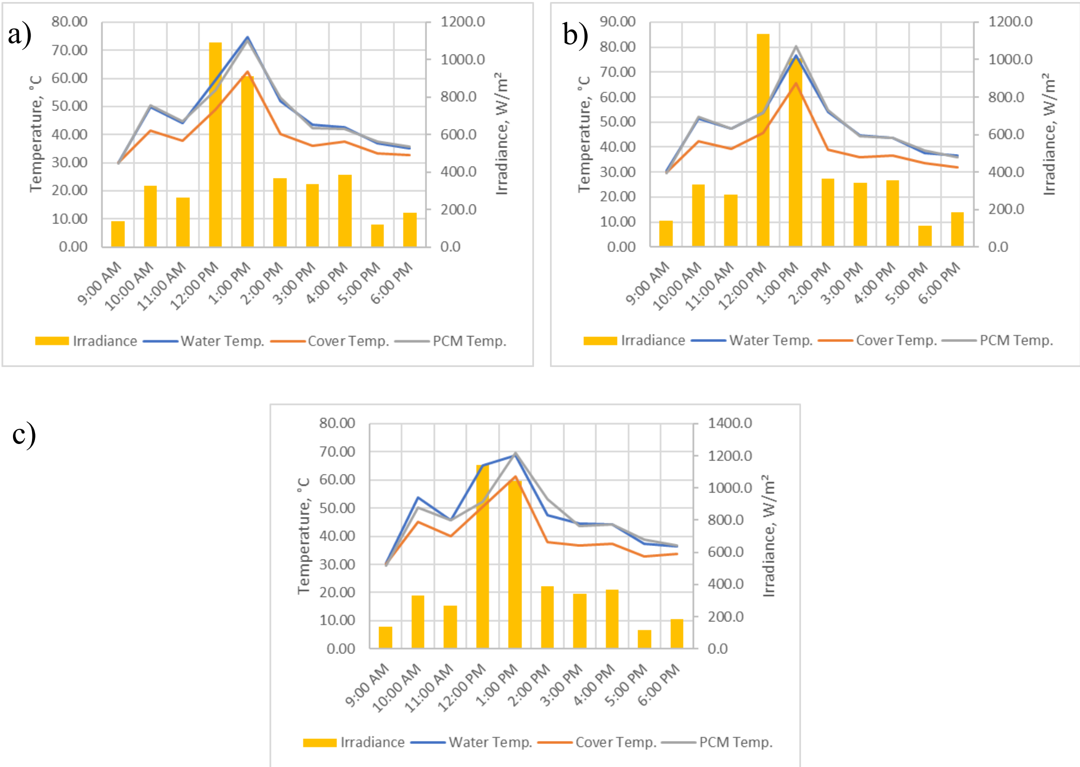

Figure 4.22: Temperature and irradiance results for different saline water using FL 33 cm Fresnel lens and Al_2O_3 NPCM (a) 10k ppm (b) 20k ppm (c) 30k ppm

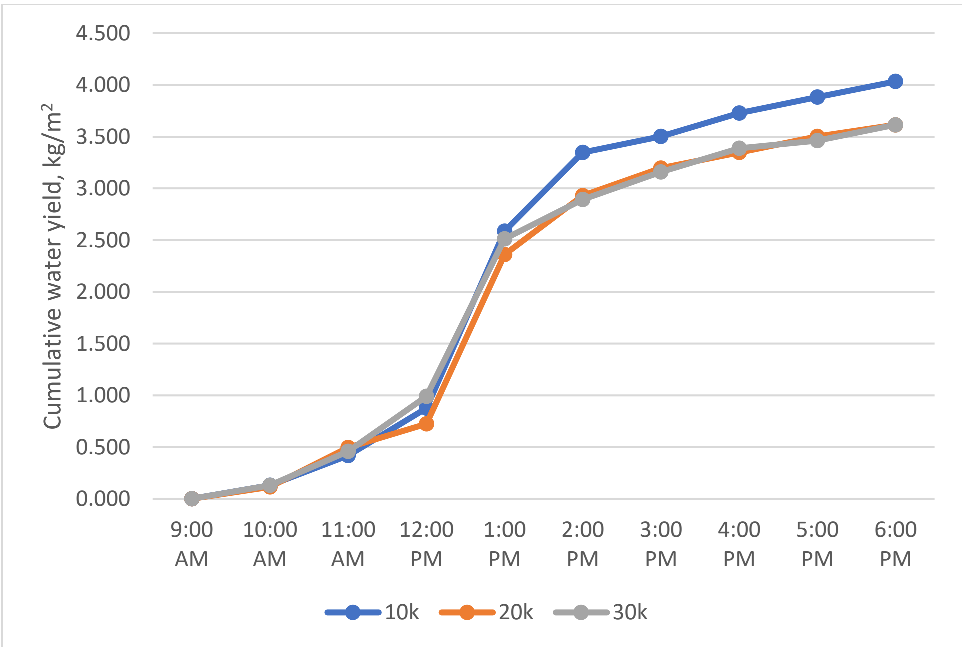

Figure 4.23: Cumulative water yield results for different saline water using FL 33 cm Fresnel lenses and Al_2O_3 NPCM

The water yield, productivity and efficiency of Experiment 14 were tabulated in Table 4.18. Even though with a slightly lower input energy than the others, 10k was able to achieve the highest water yield, productivity and efficiency among the three experimental models. Next, according to performance, it was followed by 20k and lastly 30k, where 30k had highly similar performance with 20k. This was the result of both 20k and 30k collected the same amount of water yield, but due to the difference of the input energy (solar irradiance), 30k has a slight lower performance than 20k. Unlike Experiment 13 (Subsubsection 4.3.3.1), under the circumstances of lower solar radiation, the difference in performance between 20k and 30k had decreased. The TDS level of 10k, 20k and 30k were 11 ppm, 16 ppm and 9 ppm respectively.

Table 4.18: Daily water yield, productivity, and efficiency of varying saline water using FL 33 and Al_2O_3 NPCM

Variation in saline water	Daily water yield, kg/m^2	Input energy, kJ	Productivity, g/kJ.m^2	Efficiency, %
10k ppm	4.0335	175.1308	23.03	70.62
20k ppm	3.6149	181.1549	19.95	60.49
30k ppm	3.6149	183.8839	19.66	59.17

4.3.3.3 Varying saline water with same Fresnel lens and Cu NPCM

Experiment 15 was conducted on a partly cloudy day with approximately two hours of strong sunlight around noon on 15th August 2023, using FL 33 cm Fresnel lenses and Cu NPCMs. The average solar irradiation received were 543.9 W/m^2, 539.7 W/m^2 and 545.7 W/m^2 for 10k, 20k and 30k respectively. According to Figure 4.24, the highest solar irradiation recorded was at 1 pm, which were 1216 W/m^2, 1159 W/m^2 and 1182 W/m^2 for 10k, 20k an 30k respectively. Moreover, the line plot of the water temperature for 10k, 20k and 30k were similar, except at 4 pm, where there was a peak for 20k while 10k and 20k only had a slight increase. The water temperature measured for 20k was around 9.00 °C higher than 10k and 30k at 4 pm. The average water temperature for 10k, 20k and 30k were 55.0 °C, 56.8 °C and 53.7 °C respectively. Additionally, the water temperature was the highest at 11 am (solar irradiance measured exceeds 1000 W/m^2), which were 80.90 °C, 82.71 °C and 77.19 °C for 10k, 20k and 30k respectively.

Furthermore, the PCM and cover temperature plot lines of 10k, 20k and 30k were similar. The average PCM temperature for 10k, 20k and 30k were 55.4 °C, 53.9 °C and 52.3 °C respectively, while the average cover temperatures were 48.7 °C, 47.5 °C and 49.7 °C respectively. The difference between the average water temperature and average cover temperature was the highest for 20k, with a difference of 9.3 °C. Meanwhile, the average temperature difference between the water and cover for 10k and 30k were 6.4 °C and 4.0 °C respectively. Besides that, the cumulative water yield of 10k, 20k and 30k were plotted and compared in Figure 4.25, where the plots were similar with 10k slightly lower. Despite having the lowest salinity, the water yield collected in 10k was lower than 20k and 30k, which was an unusual result obtained. Other than that, an additional 25 ml of saline water was added at 1 pm. The extra saline water added was made sure to follow according to the experimental model's basin water salinity. The saline water was added to the model one by one where there were labels attached on the prepared saline water and experimental models; hence, the unusual result was not caused by human error.

Figure 4.24: Temperature and irradiance results for different saline water using FL 33 cm Fresnel lens and Cu NPCM (a) 10k ppm (b) 20k ppm (c) 30k ppm

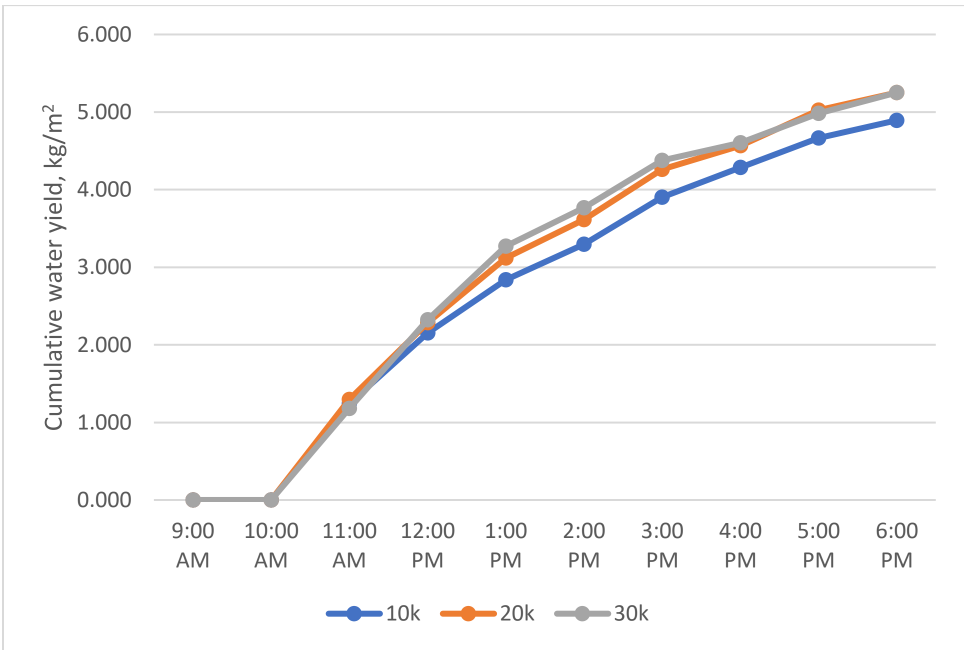

Figure 4.25: Cumulative water yield results for different saline water using FL 33 cm Fresnel lenses and Cu NPCM

The water yield, productivity and efficiency for 10k, 20k and 30k in Experiment 15 were tabulated in Table 4.19. It was found that 30k had the highest performance, and was closely followed by 30k, while 10k had the lowest performance. This phenomenon was especially strange for 10k, since the results for comparing just 20k and 30k were valid and similar with the 20k and 30k in Experiment 14 (Subsubsection 4.3.3.2), where the water yield collected were the same and the productivity and efficiency for 20k was just slightly higher than 30k. Therefore, the reason might be due to the condensate falling back to the water basin instead of sliding down to the water collector outlet, as the inclination of the cover is only 15°, where the slope is lower than most existing solar stills for desalination. Furthermore, the evaporation rate is very high, which is one of the reasons the condensate falls back into the saline water basin. The TDS level for 10k, 20k and 30k were 10 ppm, 14 ppm and 13 ppm respectively.

Table 4.19: Daily water yield, productivity, and efficiency of varying saline water using FL 33 and Cu NPCM

Variation in saline water	**Daily water yield, kg/m^2**	**Input energy, kJ**	**Productivity, g/kJ.m^2**	**Efficiency, %**
10k ppm	4.8935	231.5578	21.13	64.59
20k ppm	5.2511	229.7697	22.85	68.98
30k ppm	5.2511	232.3241	22.60	67.78

4.3.3.4 Varying saline water with same Fresnel lens and Al_2O_3 + Cu NPCM

Experiment 16 was conducted on 22nd August 2023, a cloudy day with rain showers from 10 am to 1 pm, where the solar irradiance measured is usually below 300 W/m^2. The average solar radiation received by 10k, 20k and 30 k were 322.5 W/m^2, 325.5 W/m^2 and 322.3 W/m^2 respectively. According to Figure 4.26, the highest solar radiation received was at 3 pm, which were 1184 W/m^2, 1180 W/m^2 and 1171 W/m^2 for 10k, 20k and 30k respectively. Moreover, the water, PCM and cover temperature line plots were similar, where it was observed that the temperatures gradually increased to its peak at 4 pm and decreased drastically at 5 pm. The average water temperature for 10k, 20k and 30k were 41.5 °C, 40.8 °C and 40.4 °C respectively, while the highest temperature measured at 4 pm were 73.13 °C, 69.74 °C and 64.43 °C respectively. As for the PCM temperature, the data were similar with the water temperature, which the average PCM temperature were 40.5 °C, 41.4 °C and 42.0 °C for 10k, 20k an 30k respectively; while the highest PCM temperature measured at 4 pm were 71.56 °C, 69.89 °C and 66.95 °C respectively. On the other hand, the cover temperatures were lower than the water and PCM temperatures, where the average cover temperature were 36.5 °C, 36.3 °C and 36.5 °C for 10k, 20k and 30k respectively.

In addition, it was observed that no freshwater was collected from 9 am to 12 pm, which was shown in Figure 4.27, due to the low solar radiation received, which was lower than 300 W/m^2 within that duration. It was observed that little amount of freshwater was finally collected at 1 pm, which were 0.282 kg/m^2, 0.259 kg/m^2 and 0.251 kg/m^2 for 10k, 20k and 30k respectively. The cumulative water yield remained stagnant until 4 pm, where the hourly freshwater collected was the highest in Experiment 16 (Subsubsection 4.3.3.4), which were 1.332 kg/m^2, 1.020 kg/m^2 and 0.989 kg/m^2 for 10k, 20k and 30k respectively. This was due to the high solar radiation received at 3 pm, the saline water and PCM were able to receive and store sufficient heat energy to increase the evaporation rate of the saline water in the basin. Furthermore, the cumulative water yield continued to increase gradually after 4 pm even though the solar radiation received was below 200 W/m^2. This could be explained by the usage of PCM where the stored heat was released during the low solar intensity period to the basin water. Therefore, despite the low solar radiation received, the water temperature was able to remained above 40 °C, which was also similar with the PCM temperature measured as shown in Figure 4.26. Due to the cloudy weather, no additional saline water was added in this experiment.

Figure 4.26: Temperature and irradiance results for different saline water using FL 33 cm Fresnel lens and Al_2O_3 + Cu NPCM (a) 10k ppm (b) 20k ppm (c) 30k ppm

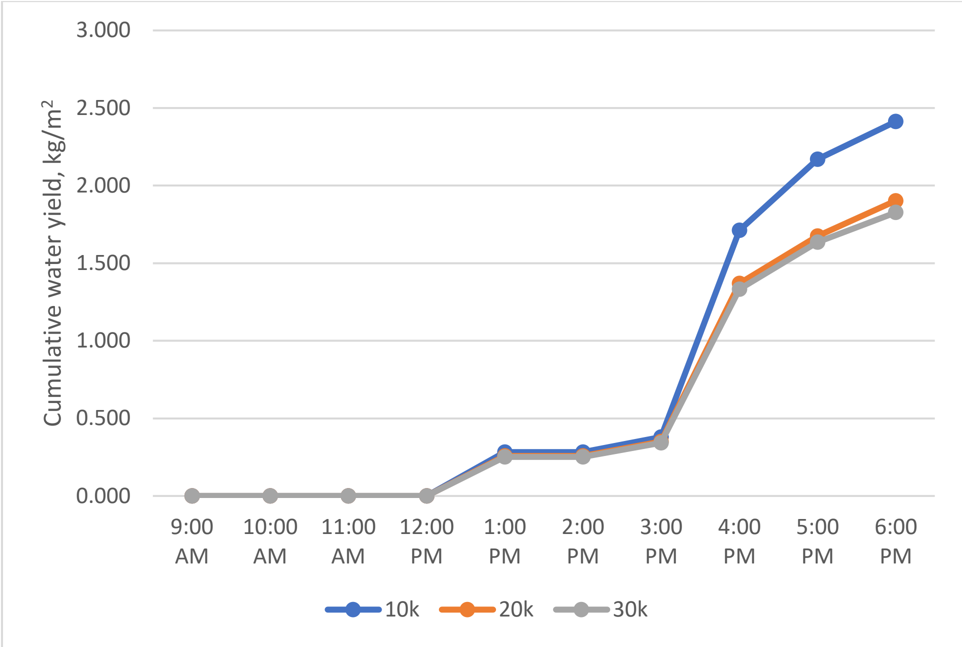

Figure 4.27: Cumulative water yield results for different saline water using FL 33 cm Fresnel lenses and Al_2O_3 + Cu NPCM

The water yield, productivity and efficiency of 10k, 20k and 30k in Experiment 16 were tabulated in Table 4.20. The results were similar with Experiment 13 (Subsubsection 4.3.3.1) and Experiment 14 (Subsubsection 4.3.3.2), where the performance of 10k is the highest among the three experiment models, while the performance of 20k is slightly higher than 30k. The TDS level of 10k, 20k and 30k were 11 ppm, 13 ppm and 14 ppm respectively.

Table 4.20: Daily water yield, productivity, and efficiency of varying saline water using FL 33 and Al_2O_3 + Cu NPCM

Variation in saline water	**Daily water yield, kg/m²**	**Input energy, kJ**	**Productivity, g/kJ.m²**	**Efficiency, %**
10k ppm	2.4125	137.2999	17.57	53.94
20k ppm	1.9026	138.5771	13.73	41.81
30k ppm	1.8265	137.2147	13.31	40.24

In this Subsection 4.3.3, it was found that in majority of the experiments conducted, the relationship between the salinity and performance (productivity and efficiency) of the experimental solar still models were inverse. From the results of Subsubsection 4.3.3.1, Subsubsection 4.3.3.2 and Subsubsection 4.3.3.4, the higher the salinity of the basin water, the lower the water yield collected; hence, the lower the productivity and efficiency. The inverse relationship result obtained was validated to the study done by Ahmed et al. (2024), which was a study based on different salinity of brine to the altered desalination system.

4.3.4 Prototype

After conducting various experiments on the scaled-down solar still, the best combination was selected to conduct on the actual scale prototype of a solar still for desalination. The FL 33 cm Fresnel lens and Al scrap PCM combination were selected to enhance the performance of the prototype after comparing the experimental models in the three experiments discussed in Subsection 4.3.2. A cost analysis was done for the experimental models in Subsection 4.3.2 to analyse the cost per litre, it was further discussed in Section 4.5. Experiment 17 only consist of one actual scale prototype using 30 000 ppm saline water and was carried on 12th September 2023, a fairly sunny day. According to Figure 4.28, the solar irradiance was above 700 W/m^2 from 9 am to 1 pm, which was the high solar intensity period. The highest solar irradiance received was at 11 am, which was 1076 W/m^2. At 4 pm, the solar irradiance measured dropped drastically from 584 W/m^2, which was measured at 3 pm, to 266 W/m^2. However, the solar irradiance measured at 5 pm increased to 653 W/m^2 despite the sun is at the lower altitude, this is because of the scattered clouds in the sky causing the solar radiation received to be unpredictable.

Besides that, the water temperature and PCM temperature line plots were similar, with the PCM temperature slightly higher than the water temperature after 11 am. The average water temperature was 53.2 °C, while the average PCM temperature is 54.0 °C, which is slightly higher. Hence, the PCM in this experiment was able to sufficiently provide heat energy to the saline water above with the heat stored. Moreover, the average cover temperature was 46.7 °C, which had a temperature difference of 6.5 °C compared to the average water temperature. Additionally, according to Figure 4.29, the cumulative water yield increased rapidly after 11 am, where the highest irradiance was measured. The freshwater collected increases slower after 2 pm, where the irradiance measured was lower than 600 W/m^2. Even though the solar radiation decreases after 2 pm, the freshwater collected continues to increase quite uniformly (increases around 0.3 kg/m^2 per hour) due to the aid of PCM. No extra saline water was added to the prototype.

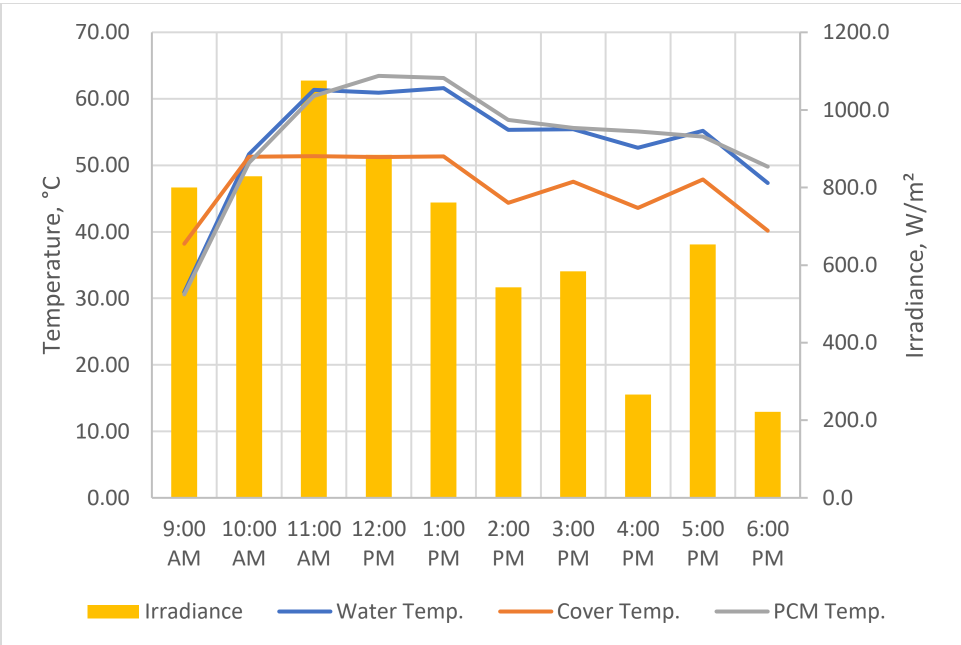

Figure 4.28: Temperature and irradiance result for prototype using Al scrap PCM and FL 33 cm Fresnel lens

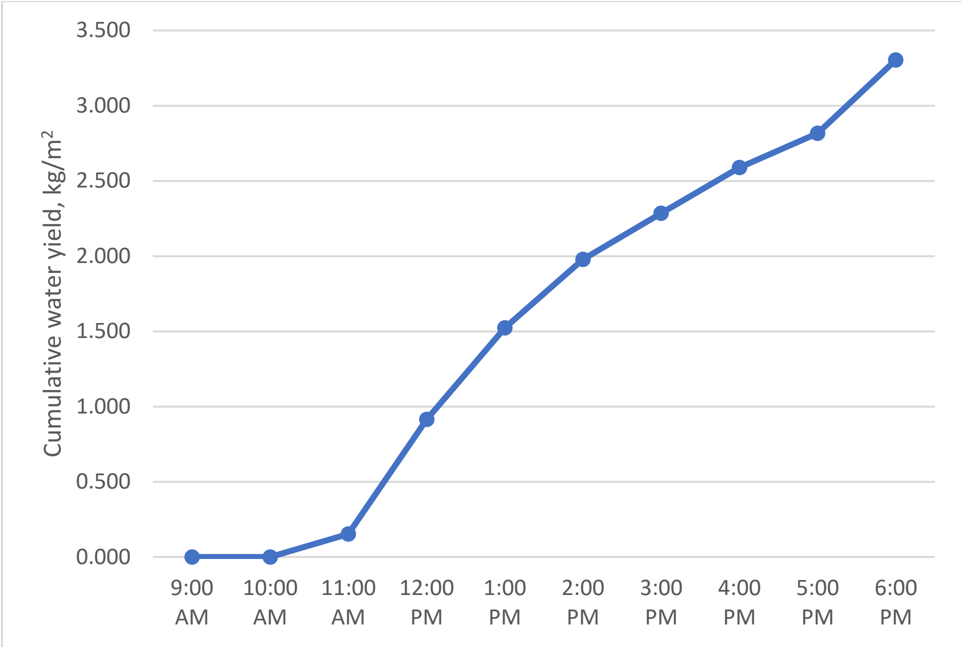

Figure 4.29: Cumulative water yield for prototype using Al scrap PCM and FL 33 cm Fresnel lens

Throughout the experiment, the total water yield collected from 9 am to 6pm was 3.3030 kg/m^2. Furthermore, the energy received from the sun to the receiver (water basin) is 1408.7175 kJ; hence, the productivity obtained was 2.34 g/kJ.m^2 while the efficiency was 35.34 %. The results were further compared in Section 4.5 with other existing works for the economic analysis. The TDS level of the freshwater collected is 16 ppm.

4.4 Uncertainty Analysis

The uncertainties in the experiment were calculated using the type B standard uncertainty, where the uncertainty occurred in the measurand (Rahbar and Esfahani, 2012; Tan et al., 2025). It was calculated using the Equation (4.1) below for the Type B standard uncertainty (u) of the instruments involved in the experiment and was organized in Table 4.21.

$$u = \frac{Accuracy}{\sqrt{3}} \tag{4.1}$$

Table 4.21: Accuracy, range and standard uncertainty of measuring instruments

Instruments	Accuracy	Range	Standard uncertainty
Solar power meter	0.1 W/m^2	0.1 – 3999 W/m^2	0.06 W/m^2
Thermometer (Type K thermocouple)	0.1 °C	-50 – 350 °C	0.06 °C
Electronic scale weight	0.001 kg	0.001 – 3 kg	0.0006 kg

The parameters in Table 4.21 were used to calculate the local uncertainty (y), which were the heat energy (E) and latent heat (h), and X is the measurement.

Local uncertainty

$$\delta y = \sqrt{\sum_{i=1}^{N} \left(\frac{\partial y}{\partial X_i} \delta X_i \right)^2} \tag{4.2}$$

The uncertainty of productivity (R_P) and efficiency (R_η) were calculated with the Equations (4.3) and (4.4) using the local uncertainty obtained.

Uncertainty of productivity and efficiency

$$\frac{\delta R_P}{R_P} = \sqrt{\left(a\frac{\partial m_{yield}}{m_{yield}}\right)^2 + \left(b\frac{\partial E}{E}\right)^2} \tag{4.3}$$

$$\frac{\delta R_\eta}{R_\eta} = \sqrt{\left(a\frac{\partial m_{yield}}{m_{yield}}\right)^2 + \left(b\frac{\partial h}{h}\right)^2 + \left(c\frac{\partial E}{E}\right)^2} \tag{4.4}$$

The uncertainty of productivity and efficiency for all the experiments were arranged in Table 4.22, Table 4.23, Table 4.24, Table 4.25, and Table 4.26.

Table 4.22: Experimental uncertainties for the indoor experiments

Indoor experiment number	Productivity (%)	Efficiency (%)
4.2.1 – Al	0.73	2.31
4.2.1 – Al_2O_3	0.85	2.67
4.2.1 – Cu	0.85	2.67
4.2.1 – Al_2O_3+Cu	0.73	2.32
4.2.2 – Al	0.73	2.32
4.2.2 – Al_2O_3	0.73	2.32
4.2.2 – Cu	0.73	2.32
4.2.2 – Al_2O_3+Cu	0.73	2.32
4.2.3 – Al	1.20	3.79
4.2.3 – Al_2O_3	1.47	4.64
4.2.3 – Cu	1.47	4.63
4.2.3 – Al_2O_3+Cu	1.47	4.64
4.2.4 – Al	1.47	4.64
4.2.4 – Al_2O_3	1.47	4.64
4.2.4 - Cu	1.47	4.64
4.2.4 – Al_2O_3+Cu	1.47	4.64
4.2.5 – Al	1.34	4.26
4.2.5 – Al_2O_3	1.90	6.02
4.2.5 – Cu	1.34	4.25
4.2.5 – Al_2O_3+Cu	1.90	6.02

Table 4.23: Experimental uncertainties for the outdoor experiments comparing different Fresnel lenses

Outdoor experiment number	Productivity (%)	Efficiency (%)
4.3.1.1 – FL 12.7	0.48	1.48
4.3.1.1 – FL 9.9	0.48	1.48
4.3.1.1 – FL 20	0.48	1.48
4.3.1.1 – FL 33	0.55	1.69
4.3.1.2 – FL 12.7	0.66	2.04
4.3.1.2 – FL 9.9	0.65	2.03
4.3.1.2 – FL 20	0.65	2.02
4.3.1.2 – FL 33	0.71	2.16
4.3.1.3 – FL 12.7	1.26	3.92
4.3.1.3 – FL 9.9	1.28	3.98
4.3.1.3 – FL 20	1.20	3.72
4.3.1.3 – FL 33	1.34	4.14
4.3.1.4 – FL 12.7	0.86	2.66
4.3.1.4 – FL 9.9	0.83	2.57
4.3.1.4 – FL 20	0.78	2.43
4.3.1.4 – FL 33	0.80	2.46

Table 4.24: Experimental uncertainties for the outdoor experiments comparing different PCMs

Outdoor experiment number	Productivity (%)	Efficiency (%)
4.3.2.1 – Al_2O_3+Cu	0.62	1.89
4.3.2.1 – Al_2O_3	0.60	1.85
4.3.2.1 – Al	0.60	1.84
4.3.2.1 – Cu	0.60	1.82
4.3.2.2 – Al_2O_3+Cu	0.91	2.80
4.3.2.2 – Al_2O_3	0.91	2.79
4.3.2.2 – Al	0.89	2.73
4.3.2.2 – Cu	0.91	2.77
4.3.2.3 – Al_2O_3+Cu	0.74	2.19
4.3.2.3 – Al_2O_3	0.74	2.21
4.3.2.3 – Al	0.74	2.21
4.3.2.3 – Cu	0.73	2.18

Table 4.25: Experimental uncertainties for the outdoor experiments comparing different Fresnel lenses

Outdoor experiment number	Productivity (%)	Efficiency (%)
4.3.3.1 – 10k	0.86	2.61
4.3.3.1 – 20k	0.84	2.51
4.3.3.1 – 30k	0.83	2.47
4.3.3.2 – 10k	1.08	3.32
4.3.3.2 – 20k	1.03	3.13
4.3.3.2 – 30k	1.02	3.06
4.3.3.3 – 10k	0.77	2.35
4.3.3.3 – 20k	0.78	2.36
4.3.3.3 – 30k	0.77	2.32
4.3.3.4 – 10k	1.03	3.16
4.3.3.4 – 20k	1.00	3.05
4.3.3.4 – 30k	1.01	3.05

Table 4.26: Experimental uncertainties for the prototype

Outdoor experiment number	Productivity (%)	Efficiency (%)
4.3.4 – Prototype	0.12	1.84

4.5 Economic Analysis

An economic analysis was performed on the solar stills done in the experiments of Subsubsection 4.3.2.1, Subsubsection 4.3.2.2 and Subsubsection 4.3.2.3 to decide the best combination of Fresnel lens and PCM in terms of the cost per litre. The calculations were based on the study done by Shafii et al. (2016) and Ho (2021), and were organized in Table 4.27, Table 4.28 and Table 4.29. After the calculations, it was found that regardless of the different weather conditions and salinity of the basin water, the combinations of FL 33 cm Fresnel lens and Al scrap PCM had the lowest cost per litre per unit area. Also considering the productivity and efficiency for the FL 33 and Al combination was slightly lower or at times could be similar with the FL 33 and nanoparticle embedded PCMs combinations, it was decided that the prototype will proceed with the low-cost Al scrap PCM with FL 33 cm Fresnel lens.

Table 4.27: Cost per litre per unit area of the solar stills in Subsubsection 4.3.2.1 (Experiment 10)

Parameters	**Unit**	**4.3.2.1 - Al_2O_3 + Cu**	**4.3.2.1 - Al_2O_3**	**4.3.2.1 - Al**	**4.3.2.1 - Cu**
Principal cost (P)	$	69.44	24.06	21.90	28.34
Salvage Value (S, 10% of P)	$	6.9437	2.4058	2.1898	2.8336
Life (n)	years	10	10	10	10
interest rate (i)	%	-	-	-	-
Capital recovery factor (CRF)	0.117	0.117	0.117	0.117	0.117

Sink fund factor (SFF)	0.017	0.017	0.017	0.017	0.017
Annual First Cost (CRF * P)	$	8.12	2.81	2.56	3.32
Annual salvage value (SFF * S)	$	0.12	0.04	0.04	0.05
Annual Maintenance Cost (0.15 * annual first cost)	$	1.22	0.42	0.38	0.50
Annual Cost (Annual first cost + annual maintenance cost - annual salvage value)	$	9.22	3.20	2.91	3.76
Average Daily Yield	kg/m^2	10.030	8.836	9.018	10.205
Annual Yield of the Still (average daily yield *365)	kg/m^2	3661.11	3225.00	3291.67	3725.00
Cost per Litre per unit area of still (CPL = Annual cost/ Annual Yield of Still)	$\$/(kg/m^2)$	0.0025	0.0010	0.0009	0.0010

Table 4.28: Cost per litre per unit area of the solar stills in Subsubsection 4.3.2.2 (Experiment 11)

Parameters	Unit	4.3.2.2 - Al_2O_3 + Cu	4.3.2.2 - Al_2O_3	4.3.2.2 - Al	4.3.2.2 - Cu
Principal cost (P)	$	69.44	24.06	21.90	28.34
Salvage Value (S, 10% of P)	$	6.9437	2.4058	2.1898	2.8336
Life (n)	years	10	10	10	10
interest rate (i)	%	-	-	-	-
Capital recovery factor (CRF)	0.117	0.117	0.117	0.117	0.117
Sink fund factor (SFF)	0.017	0.017	0.017	0.017	0.017
Annual First Cost (CRF * P)	$	8.12	2.81	2.56	3.32
Annual salvage value (SFF * S)	$	0.12	0.04	0.04	0.05
Annual Maintenance Cost (0.15 * annual first cost)	$	1.22	0.42	0.38	0.50
Annual Cost (Annual first cost + annual maintenance cost - annual salvage value)	$	9.22	3.20	2.91	3.76
Average Daily Yield	kg/m^2	2.930	2.359	2.892	2.968

Annual Yield of the Still (average daily yield *365)	kg/m^2	1069.44	861.11	1055.56	1083.33
Cost per Litre per unit area of still (CPL = Annual cost/ Annual Yield of Still)	$\$/(kg/m^2)$	0.0086	0.0037	0.0028	0.0035

Table 4.29: Cost per litre per unit area of the solar stills in Subsubsection 4.3.2.3 (Experiment 12)

Parameters	**Unit**	**4.3.2.3 - Al_2O_3 + Cu**	**4.3.2.3 - Al_2O_3**	**4.3.2.3 - Al**	**4.3.2.3 - Cu**
Principal cost (P)	$	69.44	24.06	21.90	28.34
Salvage Value (S, 10% of P)	$	6.9437	2.4058	2.1898	2.8336
Life (n)	years	10	10	10	10
interest rate (i)	%	-	-	-	-
Capital recovery factor (CRF)	0.117	0.117	0.117	0.117	0.117
Sink fund factor (SFF)	0.017	0.017	0.017	0.017	0.017
Annual First Cost (CRF * P)	$	8.12	2.81	2.56	3.32

Annual salvage value (SFF * S)	$	0.12	0.04	0.04	0.05
Annual Maintenance Cost (0.15 * annual first cost)	$	1.22	0.42	0.38	0.50
Annual Cost (Annual first cost + annual maintenance cost - annual salvage value)	$	9.22	3.20	2.91	3.76
Average Daily Yield	kg/m^2	10.046	9.932	10.122	10.122
Annual Yield of the Still (average daily yield *365)	kg/m^2	3666.67	3625.00	3694.44	3694.44
Cost per Litre per unit area of still (CPL = Annual cost/ Annual Yield of Still)	$\$/(kg/m^2)$	0.0025	0.0009	0.0008	0.0010

After it was decided that the prototype would proceed with the FL 33 and Al combination, an actual size prototype was fabricated to carry the experiment. Therefore, with the different cost, the calculation of the cost per litre per unit of the prototype was calculated and tabulated in Table 4.30. Then, the current study was compared with various existing works in Table 4.31. Despite that the productivity and efficiency was lower than most of the existing works, the cost per litre per unit area is abundantly lower than all of the existing works compared to. Therefore, the performance of the prototype is relatively high considering the low-cost materials used to fabricate.

Table 4.30: Cost per litre per unit area of the prototype in Subsection 4.3.4 (Experiment 17)

Parameters	Unit	Prototype
Principal cost (P)	$	36.07
Salvage Value (S, 10% of P)	$	3.6072
Life (n)	years	10
interest rate (i)	%	-
Capital recovery factor (CRF)	0.117	0.117
Sink fund factor (SFF)	0.017	0.017
Annual First Cost (CRF * P)	$	4.22
Annual salvage value (SFF * S)	$	0.06
Annual Maintenance Cost (0.15 * annual first cost)	$	0.63
Annual Cost (Annual first cost + annual maintenance cost - annual salvage value)	$	4.79
Average Daily Yield	kg/m^2	3.303
Annual Yield of the Still (average daily yield *365)	kg/m^2	1205.59
Cost per Litre per unit area of still (CPL = Annual cost/ Annual Yield of Still)	$\$/(kg/m^2)$	0.0040

Table 4.31: Comparison of current work with existing solar stills of other studies

References	Modification	Daily water production, kg/m^2	Daily efficiency, %	Cost per litre per unit area, $\$/(kg/m^2)$	Efficiency/CPL, $\%/(\$.kg^{-1}m^{-2})$
Current work	Single slope solar still integrated with Al scrap enhanced PCM and Fresnel lens	3.30	35.34	0.004	8835.00
(Kandeal et al., 2021)	Modified double slope still with copper chips immersed in nanofluid and nano-based PCM	6.52	68.00	0.011	6181.82
(Mevada et al., 2023)	Solar still with zig-zag shape air cooled condenser and CuO nanomaterial	2.66	37.59	0.013	2891.54

(Parsa et al., 2022)	Pyramid-shaped solar still with black painted silver nanoparticle embedded PCM with thermoelectric heating modules	8.88	44.00	0.013	3384.62
	Pyramid-shaped solar still with black painted silver nanoparticle embedded PCM with thermoelectric cooling modules	4.96	23.80	0.023	1034.78
(Rahbar and Esfahani, 2012)	Single slope solar still with heatpipe and thermoelectric module	0.49	7.00	0.180	38.89

(Selimefendigil, Sirin and Oztop, 2022)	Single slope solar still with black paint added into CuO nanoparticle embedded PCM	4.83	19.30	-	-
(Shoeibi et al., 2023)	Single slope solar still with iron scraps submerged in water, thermoelectric modules and reflectors	0.80	13.41	0.071	188.87
(Sonker, Chakraborty and Sarkar, 2022)	Single slope solar still with copper cylinder filled with CuO nanoparticle embedded PCM	2.49	-	3.06	-
(Thamarai Kannan et al., 2022)	Hemispherical solar still with paraffin wax encapsulated in	5.63	61.55	0.11	559.55

	waste
	aluminium cans

4.6 Summary

Several experiments have been conducted and discussed in this chapter, where it was categorised in different sections and subsections. The first section is regarding the indoor experiment, where it was to find the optimum PCM. It was found that among the four PCMs, the Al_2O_3 + Cu combination has the overall best result with or without the implementation of Fresnel lens. Furthermore, another important finding in the indoor experiment is that the result of Cu and Al were similar in four out of five of the experiments. Therefore, it was further investigated in outdoor conditions with longer period of time as the indoor experiment was only carried for three hours and also an addition of a FL 33 cm Fresnel lens, which was unable to use under the solar simulator due to its size.

In the outdoor experiment, it was divided into four subsections where firstly it was to decide the best Fresnel lens under the condition of same PCMs. It was discovered that no matter which PCM used, the Fresnel lens that provides the best performance is FL 33. This was due to the size of the Fresnel lens, which is significantly larger than the solar still; and according to the formula of concentration ratio, which is the ratio of the area of Fresnel lens over the area of the receiver, the FL 33 has the largest concentration ratio as calculated in Section 3.5, Table 3.5. The experimental results of Subsection 4.3.1 were summarized in Figure 4.30, where FL 33 with the highest concentration ratio had the highest productivity.

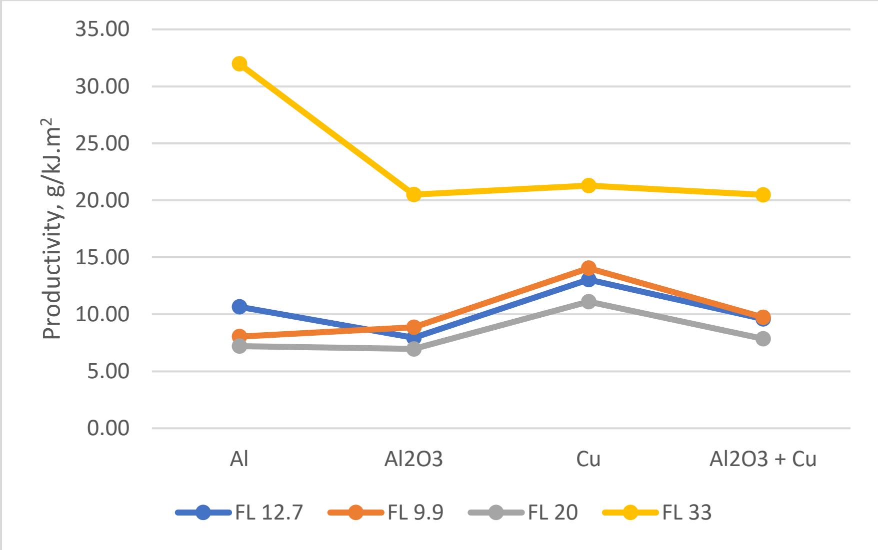

Figure 4.30: Comparison of the productivity with different Fresnel lenses involved (summary of Subsection 4.3.1)

After deciding FL 33 is the optimal Fresnel lens among the four, it was proceeded with the next subsection involving the comparison of PCM with different salinity of basin water in each experiment. The overall best performing PCM is Al_2O_3 + Cu among the four PCMs, and Cu as the runner-up, which is slightly lower than Al_2O_3 + Cu. Thus, the line plot of Al_2O_3 + Cu could not be seen in Figure 4.31 as it overlaps with the line plot of Cu. Furthermore, it was noteworthy that Al had similar or slightly higher result compared with Al_2O_3 + Cu and Cu in the experiments of 20k and 30k, given the usage of the low-cost conductive particle, Al scrap, compared to the costly nanoparticles.

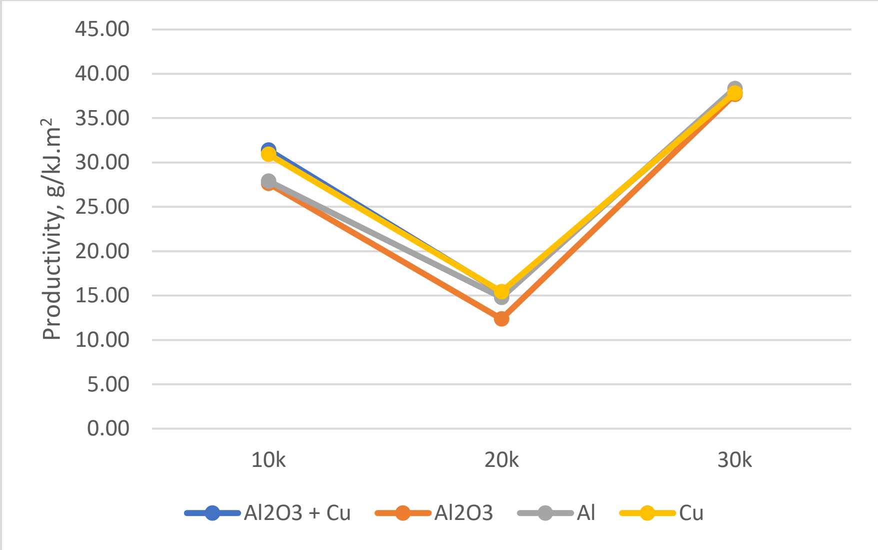

Figure 4.31: Comparison of the productivity with different PCMs involved (summary of Subsection 4.3.2)

Additionally, experiments in Subsection 4.3.3 were to determine the effect of salinity to the performance of the solar stills. According to Figure 4.32, the productivity of the solar stills decreases as the salinity of the basin water increases, except for the plot line of Cu. Moreover, it was observed that the performance gap between 10k and 20k is higher than 20k and 30k; therefore, the relationship between the productivity of the solar still and salinity of basin water is inversely instead of linearly.

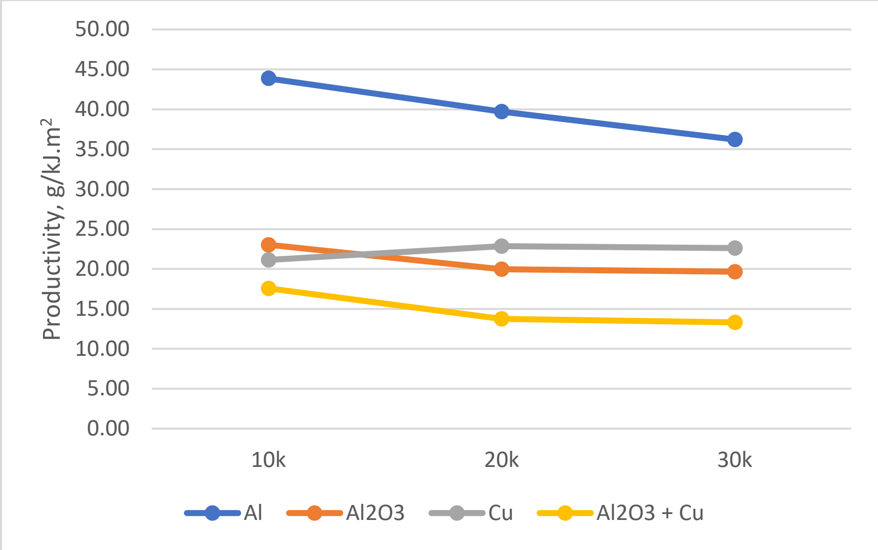

Figure 4.32: Comparison of the productivity with different salinity of basin water (summary of Subsection 4.3.3)

Lastly, the final experiment, which is discussed in Subsection 4.3.4 is the prototype, where it was selected after conducting an economic analysis (Section 4.5) on the experiments in Subsection 4.3.2. By implementing FL 33 cm Fresnel lens and Al scrap PCM on the prototype, it was able to produce 3.3030 kg/m^2 of water yield with a productivity and efficiency of 2.34 g/kJ.m^2 and 35.34 % respectively. The cost per litre per unit area of the prototype is 0.004 \$/(kg/m^2), which is the lowest among the comparison with existing works in Table 4.31. Furthermore, the quality of water for all the experiments measured were below 50 ppm, and was measured to be below 20 ppm for majority of the experiments, whereas the recommended palatable water by WHO (Herschy, 2012) is less than 600 ppm. Besides the literature review, the quality of water is further justified by the study done by Kim et al. (2014), where the distillate was reduced from 40 000 ppm seawater to less than 10 ppm. Therefore, the freshwater produced from the experiments conducted are safe to use for drinking purposes.

CHAPTER 5

CONCLUSION AND RECOMMENDATIONS

5.1 Conclusion

In conclusion, it was found that the 33 cm FL Fresnel lens provides the best performance for the solar still compared to the other three Fresnel lenses. The 33 cm FL Fresnel lens had the largest concentration ratio, which is 25; meanwhile the other Fresnel lenses have a concentration ratio of slightly higher than 10. Besides that, it was observed that the overall best PCM is the combination of Al_2O_3 and Cu NPCM, regardless of indoor or outdoor experiment. Whereas in the outdoor experiment, there were mixed results, where the Cu NPCM is in-par with the Al_2O_3+Cu NPCM combination. Moreover, in Subsubsection 4.3.2.3 where the 30 000 ppm saline water is used, the best PCM combination was the Al scrap PCM.

To further investigate which PCM combination is the optimal, a cost analysis based on the results of Subsection 4.3.2 was done. It was discovered that the solar still with Al_2O_3+Cu NPCM has the highest cost per litre per unit area while the Al scrap PCM has the lowest cost per litre per area. Consequently, Al scrap is a good alternative for the nanomaterials to be implemented as conductive particles in PCMs. Finally, with the combination of the FL 33 cm Fresnel lens and the Al scrap PCM, an effective desalination device in terms of performance and cost was procured and obtained a water yield of 3.3030 kg/m^2, productivity of 2.34 g/kJ.m^2 and efficiency of 35.34 %. The cost per litre per unit area of the prototype is 0.004 \$/(kg/m^2).

Additionally, the study had conducted experiments on comparing different salinity of the basin water while the setup and contents of the solar still remains constant in Subsection 4.3.3. Three out of four of the experiments have similar results, where the relationship of the water yield and the salinity of basin water is inverse; the higher the salinity, the higher the water yield received. The inverse relationship is due to the smaller difference of water yield between 20k and 30k, while the difference of water yield between 10k and 20k is larger. Lastly, the water quality measured in all experiments was consistently below 50 ppm, while the World Health Organization (WHO) recommends palatable water to be under 600 ppm. Therefore, the freshwater produced in these experiments is safe for drinking.

5.2 Recommendation for future works

During the outdoor experiment, there were various failed experiment due to out of focus of the 33 cm FL Fresnel lens, causing the glass cover to break as the sunlight was focused on the glass instead of the water basin. Therefore, the experiment requires frequent observation (around 15 minutes) to adjust the Fresnel lenses during sunlight peak hours, which is around 10 am to 2 pm. Further effective and costly recommendation is to change the typical flat Fresnel lens into curved Fresnel lens. Besides that, a collaboration between solar tracking systems is also an option to develop a more efficient solar desalination system that could effectively focus the sunlight in the correct location of the solar still, which is the receiver.

Besides that, by comparing the design of the scaled down solar still models and solar still prototype, the compact design of the scaled down model is far more efficient than the prototype. Hence, in future works, a more compact design of the solar still can be put into consideration. For example, decreasing the height of the solar still or reduce the inclination angle of the top cover. However, the smaller inclination angle of the top cover increases the chance of condensate to fall back into the water basin, which was observed during the experiments carried in this study. The condensate on the 15 ° glass cover has higher fall-back rate than the 30 ° glass cover. Therefore, an optimum angle could be further investigated in the tropical climate to increase the evaporation of the solar distiller but at the same time reduces the condensate from falling back into the saline water basin.

REFERENCE

Abu-Arabi, M., Al-harahsheh, M., Mousa, H. and Alzghoul, Z., 2018. Theoretical investigation of solar desalination with solar still having phase change material and connected to a solar collector. *Desalination*, 448(August), pp.60–68. https://doi.org/10.1016/j.desal.2018.09.020.

Afolabi, L.O., Enweremadu, C.C., Kareem, M.W., Arogundade, A.I., Irshad, K., Islam, S., Oladosu, K.O., Elfaghi, A.M. and Didane, D.H., 2023. Experimental investigation of double slope solar still integrated with PCM nanoadditives microencapsulated thermal energy storage. *Desalination*, [online] 553(January), p.116477. https://doi.org/10.1016/j.desal.2023.116477.

Agrawal, A., Rana, R.S. and Srivastava, P.K., 2017. Heat transfer coefficients and productivity of a single slope single basin solar still in Indian climatic condition: Experimental and theoretical comparison. *Resource-Efficient Technologies*, 3(4), pp.466–482. https://doi.org/10.1016/j.reffit.2017.05.003.

Ahmed, F., Abdul Aziz, M.S., Shaik, F. and Khor, C.Y., 2024. Salinity impacts on a unique desalination system embedded with concentrated solar energy for cleaner production. *Journal of Cleaner Production*, 434. https://doi.org/10.1016/j.jclepro.2023.140223.

Ai, C., Zhao, L., Song, D., Han, M., Shan, Q. and Liu, S., 2023. Identifying greenhouse gas emission reduction potentials through large-scale photovoltaic-driven seawater desalination. *Science of the Total Environment*, 857. https://doi.org/10.1016/j.scitotenv.2022.159402.

Akshay, C., Soni, P., Dhiman, S.K., Bhowmick, S. and Gaba, V.K., 2021. Thermal modelling of single and double slope passive solar stills for different climatic zones in India. *International Journal of Ambient Energy*. https://doi.org/10.1080/01430750.2021.1946147.

Alam, M.Z., Carpenter-Boggs, L., Mitra, S., Haque, M.M., Halsey, J., Rokonuzzaman, M., Saha, B. and Moniruzzaman, M., 2017. Effect of salinity intrusion on food crops, livestock, and fish species at kalapara coastal belt in Bangladesh. *Journal of Food Quality*, 2017. https://doi.org/10.1155/2017/2045157.

Al-Hamzawi, H.A.H. and Sailawi, A.S.A. Al, 2025. Optimized multi-generation system for sustainable desalination and power production using solar-driven Multi-Effect Distillation (MED) in Basra, Iraq. *Energy for Sustainable Development*, 85. https://doi.org/10.1016/j.esd.2025.101684.

Al-Harahsheh, M., Abu-Arabi, M., Ahmad, M. and Mousa, H., 2022. Self-powered solar desalination using solar still enhanced by external solar collector and phase change material. *Applied Thermal Engineering*, 206(January), p.118118. https://doi.org/10.1016/j.applthermaleng.2022.118118.

Al-harahsheh, M., Abu-Arabi, M., Mousa, H. and Alzghoul, Z., 2018. Solar desalination using solar still enhanced by external solar collector and PCM. *Applied Thermal Engineering*, 128, pp.1030–1040. https://doi.org/10.1016/j.applthermaleng.2017.09.073.

Altarawneh, I., Rawadieh, S., Batiha, M., Al-Makhadmeh, L., Alrowwad, S. and Tarawneh, M., 2017. Experimental and numerical performance analysis and optimization of single slope, double slope and pyramidal shaped solar stills. *Desalination*, 423(September), pp.124–134. https://doi.org/10.1016/j.desal.2017.09.023.

Anon. 2024. *Online Materials Information Resource - MatWeb*. [online] Available at: <https://www.matweb.com/index.aspx> [Accessed 7 October 2024].

Ansari, O., Asbik, M., Bah, A., Arbaoui, A. and Khmou, A., 2013. Desalination of the brackish water using a passive solar still with a heat energy storage system. *Desalination*, 324, pp.10–20. https://doi.org/10.1016/j.desal.2013.05.017.

Arun, C.A. and Sreekumar, P.C., 2018. Modeling and performance evaluation of parabolic trough solar collector desalination system. *Materials Today: Proceedings*, [online] 5(1), pp.780–788. https://doi.org/10.1016/j.matpr.2017.11.147.

Askari, I.B. and Ameri, M., 2020. Thermodynamic analysis of multi effect desalination unit with thermal vapor compression feed by different motive steam pressures. *Desalination and Water Treatment*, 184, pp.57–71. https://doi.org/10.5004/dwt.2020.25387.

Belessiotis, V., Kalogirou, S. and Delyannis, E., 2016. *Thermal Solar Desalination*. *Thermal Solar Desalination*. Joe Hayton at Elsevier Ltd. https://doi.org/10.1016/c2015-0-05735-5.

Bhambare, P.S., Kaithari, D.K. and AI Hosni, S.A.R., 2021. Performance enhancement of a single slope solar still with single basin using Fresnel lens. *Journal of Mechanical Engineering and Sciences*, 15(1), pp.7781–7791. https://doi.org/10.15282/jmes.15.1.2021.14.0614.

Cheng, W.L., Huo, Y.K. and Nian, Y. Le, 2019. Performance of solar still using shape-stabilized PCM: Experimental and theoretical investigation. *Desalination*, [online] 455(January), pp.89–99. https://doi.org/10.1016/j.desal.2019.01.007.

Chiromawa, N.L. and Ibrahim, K., 2015. Concept of Bee-Eyes Array of Fresnel Lenses as a Solar Photovoltaic Concentrator System. *Journal of Photonics*, 2015(March), pp.1–6. https://doi.org/10.1155/2015/327342.

Choong, W.S., Ho, Z.Y. and Bahar, R., 2020. Solar Desalination Using Fresnel Lens as Concentrated Solar Power Device: An Experimental Study in Tropical Climate. *Frontiers in Energy Research*, 8(October), pp.1–8. https://doi.org/10.3389/fenrg.2020.565542.

Dasgupta, S., Huq, M. and Wheeler, D., 2016. Drinking Water Salinity and Infant Mortality in Coastal Bangladesh. *Water Economics and Policy*, 2(1). https://doi.org/10.1142/S2382624X1650003X.

Dsilva Winfred Rufuss, D., Iniyan, S., Suganthi, L. and Davies, P.A., 2016. Solar stills: A comprehensive review of designs, performance and material advances. *Renewable and Sustainable Energy Reviews*, [online] 63, pp.464–496. https://doi.org/10.1016/j.rser.2016.05.068.

Dubey, A. and Arora, A., 2024. *Effect of various energy storage phase change materials (PCMs) and nano-enhanced PCMs on the performance of solar stills: A review*. *Journal of Energy Storage*, https://doi.org/10.1016/j.est.2024.112938.

Dunkle, R. V., 1961. Solar water distillation: The roof type still and a multiple effect diffusion still. *International Developments in Heat Transfer*, pp.895–902.

Dwivedi, V.K. and Tiwari, G.N., 2008. *Annual Energy and Exergy Analysis of Single and Double Slope Passive Solar Stills*. *Trends in Applied Sciences Research*, .

Elashmawy, M., 2019. Effect of surface cooling and tube thickness on the performance of a high temperature standalone tubular solar still. *Applied Thermal Engineering*, 156, pp.276–286. https://doi.org/10.1016/j.applthermaleng.2019.04.068.

El-Sebaii, A.A., Al-Ghamdi, A.A., Al-Hazmi, F.S. and Faidah, A.S., 2009. Thermal performance of a single basin solar still with PCM as a storage medium.

Applied Energy, 86(7–8), pp.1187–1195. https://doi.org/10.1016/j.apenergy.2008.10.014.

Ghaffour, N., Reddy, V.K. and Abu-Arabi, M., 2011. Technology development and application of solar energy in desalination: MEDRC contribution. *Renewable and Sustainable Energy Reviews*, [online] 15(9), pp.4410–4415. https://doi.org/10.1016/j.rser.2011.06.017.

Guo, Z.H., Wang, P.L., Jiang, Y.T. and Ma, M.G., 2025. 3D dual-network structure poly (vinyl alcohol)/cellulose nanofibers/MXene hydrogel evaporator with high-efficiency desalination for solar-driven water purification. *International Journal of Biological Macromolecules*, 307. https://doi.org/10.1016/j.ijbiomac.2025.142176.

Henderson-Sellers, B., 1984. A new formula for latent heat of vaporization of water as a function of temperature. *Quarterly Journal of the Royal Meteorological Society*, 110(466), pp.1186–1190. https://doi.org/https://doi.org/10.1002/qj.49711046626.

Herrera-León, S., Cruz, C., Negrete, M., Chacana, J., Cisternas, L.A. and Kraslawski, A., 2022. Impact of seawater desalination and wastewater treatment on water stress levels and greenhouse gas emissions: The case of Chile. *Science of the Total Environment*, 818. https://doi.org/10.1016/j.scitotenv.2021.151853.

Herschy, R.W., 2012. Water quality for drinking: WHO guidelines. *Encyclopedia of Earth Sciences Series*, pp.876–883. https://doi.org/10.1007/978-1-4020-4410-6_184.

Ho, Z.Y., 2021. *DEVELOPMENT AND PERFORMANCE EVALUATION OF FRESNEL LENS AND PHASE CHANGE MATERIAL ASSISTED PORTABLE SOLAR DESALINATION SYSTEM FOR FRESH WATER PRODUCTION*.

Ho, Z.Y., Bahar, R. and Koo, C.H., 2022. Passive solar stills coupled with Fresnel lens and phase change material for sustainable solar desalination in the tropics. *Journal of Cleaner Production*, 334(November 2021), p.130279. https://doi.org/10.1016/j.jclepro.2021.130279.

Johnson, A., Mu, L., Park, Y.H., Valles, D.J., Wang, H., Xu, P., Kota, K. and Kuravi, S., 2019. A thermal model for predicting the performance of a solar still with fresnel lens. *Water (Switzerland)*, 11(9). https://doi.org/10.3390/w11091860.

Kandeal, A.W., El-Shafai, N.M., Abdo, M.R., Thakur, A.K., El-Mehasseb, I.M., Maher, I., Rashad, M., Kabeel, A.E., Yang, N. and Sharshir, S.W., 2021. Improved thermo-economic performance of solar desalination via copper chips, nanofluid, and nano-based phase change material. *Solar Energy*, [online] 224(February), pp.1313–1325. https://doi.org/10.1016/j.solener.2021.06.085.

Khalil, A., Amjad, M., Noor, F., Hussain, A., Nawaz, S., Filho, E.P.B. and Du, X., 2020. Performance analysis of direct absorption-based parabolic trough solar collector using hybrid nanofluids. *Journal of the Brazilian Society of Mechanical Sciences and Engineering*, 42(11). https://doi.org/10.1007/s40430-020-02654-2.

Kim, Y.D., Thu, K., Masry, M.E. and Ng, K.C., 2014. Water quality assessment of solar-assisted adsorption desalination cycle. *Desalination*, 344, pp.144–151. https://doi.org/10.1016/j.desal.2014.03.021.

Kumar, S. and Tiwari, G.N., 1996. *Performance evaluation of an active solar distillation system.* https://doi.org/https://doi.org/10.1016/0360-5442(96)00015-1.

Kumar, V., Shrivastava, R.L. and Untawale, S.P., 2015. Fresnel lens: A promising alternative of reflectors in concentrated solar power. *Renewable and*

Sustainable Energy Reviews, 44, pp.376–390. https://doi.org/10.1016/j.rser.2014.12.006.

Lin, S.C. and Al-Kayiem, H.H., 2016. Evaluation of copper nanoparticles - Paraffin wax compositions for solar thermal energy storage. *Solar Energy*, 132, pp.267–278. https://doi.org/10.1016/j.solener.2016.03.004.

Linstrom, P.J. and Mallard, W.G., 2023. NIST Standard Reference Database Number 69. In: *NIST Chemistry WebBook*. National Institute of Standards and Technology.

Maghrabie, H.M., Elsaid, K., Sayed, E.T., Radwan, A., Abo-Khalil, A.G., Rezk, H., Abdelkareem, M.A. and Olabi, A.G., 2022. Phase change materials based on nanoparticles for enhancing the performance of solar photovoltaic panels: A review. *Journal of Energy Storage*, 48(November 2021), p.103937. https://doi.org/10.1016/j.est.2021.103937.

Mahmoud, M. and Mohamed, A., 2011. Utilization of Fresnel Lens Solar Collector in Water Heating for Desalination By Humidification-Dehumidification Process. *Iwtc.Info*, pp.1–12.

Mahyan, N.R. and Selaman, O.S., 2016. Water Supply Resources and Management Practices in Sarawak and Other Countries. *Journal of Civil Engineering, Science and Technology*, 7(2), pp.50–57. https://doi.org/10.33736/jcest.304.2016.

Manoj Kumar, P., Sudarvizhi, D., Stalin, P.M.J., Aarif, A., Abhinandhana, R., Renuprasanth, A., Sathya, V. and Ezhilan, N.T., 2021. Thermal characteristics analysis of a phase change material under the influence of nanoparticles. *Materials Today: Proceedings*, 45, pp.7876–7880. https://doi.org/10.1016/j.matpr.2020.12.505.

Mevada, D., Panchal, H., Nayyar, A., Sharma, K., Manokar, A.M., El-Sebaey, M.S. and Hussien, A.G., 2023. Experimental performance evaluation of solar still with zig-zag shape air cooled condenser: An energy–exergy analysis approach. *Energy Reports*, [online] 10, pp.1198–1210. https://doi.org/10.1016/j.egyr.2023.07.053.

Mohamed Tawfik, M.S., Metwally Aly, A.I. and Sirag, N.M., 2025. A study proposal to mitigate carbon dioxide emissions from coastal thermal power plant by using a multistage flash distillation unit followed by alkaline water electrolysis unit. *International Journal of Hydrogen Energy*, 145, pp.851–861. https://doi.org/10.1016/j.ijhydene.2025.06.096.

Molinos-Senante, M. and González, D., 2019. Evaluation of the economics of desalination by integrating greenhouse gas emission costs: An empirical application for Chile. *Renewable Energy*, 133, pp.1327–1337. https://doi.org/10.1016/j.renene.2018.09.019.

Mu, L., Xu, X., Williams, T., Debroux, C., Gomez, R.C., Park, Y.H., Wang, H., Kota, K., Xu, P. and Kuravi, S., 2019. Enhancing the performance of a single-basin single-slope solar still by using Fresnel lens: Experimental study. *Journal of Cleaner Production*, 239, p.118094. https://doi.org/10.1016/j.jclepro.2019.118094.

Nitsas, M. and Koronaki, I.P., 2021. Performance analysis of nanoparticles-enhanced PCM: An experimental approach. *Thermal Science and Engineering Progress*, 25. https://doi.org/10.1016/j.tsep.2021.100963.

Ouikhalfan, M., Sari, A., Chehouani, H., Benhamou, B. and Biçer, A., 2019. Preparation and characterization of nano-enhanced myristic acid using metal oxide nanoparticles for thermal energy storage. *International Journal of Energy Research*, 43(14), pp.8592–8607. https://doi.org/10.1002/er.4856.

Panchal, H., 2016. Performance Investigation on Variations of Glass Cover Thickness on Solar Still: Experimental and Theoretical Analysis. *Technology and Economics of Smart Grids and Sustainable Energy*, 1(1). https://doi.org/10.1007/s40866-016-0007-0.

Panchal, H., Boka, P., Sharma, K., Siddiqui, M.I.H. and Dobrotă, D., 2024. A case study on distillate output of solar still using toner waste powder coated absorber plate. *Case Studies in Thermal Engineering*, 53(December 2023). https://doi.org/10.1016/j.csite.2023.103903.

Parsa, S.M., Yazdani, A., Javadi, D., Afrand, M., Karimi, N. and Ali, H.M., 2022. Selecting efficient side of thermoelectric in pyramid-shape solar desalination units incorporated phase change material (PCM), nanoparticle, turbulator with battery storage powered by photovoltaic. *Journal of Energy Storage*, [online] 51(January), p.104448. https://doi.org/10.1016/j.est.2022.104448.

Poonia, S., Singh, A.K. and Jain, D., 2022. Performance evaluation of PCM based solar concentrator type desalination device. *Materials Today: Proceedings*, [online] 62, pp.5194–5200. https://doi.org/10.1016/j.matpr.2022.02.637.

Prado, G.O., Vieira, L.G.M. and Damasceno, J.J.R., 2016. Solar dish concentrator for desalting water. *Solar Energy*, 136, pp.659–667. https://doi.org/10.1016/j.solener.2016.07.039.

Rahbar, N. and Esfahani, J.A., 2012. Experimental study of a novel portable solar still by utilizing the heatpipe and thermoelectric module. *Desalination*, [online] 284, pp.55–61. https://doi.org/10.1016/j.desal.2011.08.036.

Rajendran, V., Aruldoss, W.J., Athavale, P.A., Pichandi, R. and Gopinath, N.P., 2026. Synergistic enhancement of thermal energy conversion in twin wedge solar stills using graphene nano-coated absorber and nano-composite PCM. *Solar Energy Materials and Solar Cells*, 295. https://doi.org/10.1016/j.solmat.2025.113982.

Rajesh, V.R., Harikrishnan, K., Chaithanya, K.K. and Salim, S., 2016. Performance evaluation of a solar desalination system integrated with a Fresnel lens concentrator. *International Journal of Renewable Energy Research*, 6(1), pp.250–253.

Rosa, L., Gabrielli, P. and Sangiorgio, M., 2026. Global energy, costs, and emissions from reverse osmosis desalination under future water scarcity. *Water Research*, 289. https://doi.org/10.1016/j.watres.2025.124825.

Saadat, A.H.M., Islam, M.S., Sultana, A., Islam, M.S., Shammi, M. and Uddin, M.K., 2018. Desalination Technologies for Developing Countries: A Review. *Journal of Scientific Research*, 10(1), pp.77–97. https://doi.org/10.3329/jsr.v10i1.33179.

Sales, M.T.B.F., 2016. Solar powered desalination system using Fresnel lens. *IOP Conference Series: Materials Science and Engineering*, 162(1). https://doi.org/10.1088/1757-899X/162/1/012002.

Sansom, C., Tonnellier, X., King, P. and Almond, H., 2019. Concentrating Fresnel lens technology for thermal desalination. *AIP Conference Proceedings*, 2126(July). https://doi.org/10.1063/1.5117767.

Sarkar, Md.N.I., Sifat, A.I., Reza, S.M.S. and Sadique, Md.S., 2017. A review of optimum parameter values of a passive solar still and a design for southern

Bangladesh. *Renewables: Wind, Water, and Solar*, 4(1), pp.1–13. https://doi.org/10.1186/s40807-017-0038-8.

Sathyamurthy, R. and El-Agouz, E., 2019. Experimental analysis and exergy efficiency of a conventional solar still with Fresnel lens and energy storage material. *Heat Transfer - Asian Research*, 48(3), pp.885–895. https://doi.org/10.1002/htj.21412.

Sedighi, M., Behvand Usefi, M.M., Ismail, A.F. and Ghasemi, M., 2023. *Environmental sustainability and ions removal through electrodialysis desalination: Operating conditions and process parameters*. *Desalination*, https://doi.org/10.1016/j.desal.2022.116319.

Selimefendigil, F., Sirin, C. and Oztop, H. f., 2022. Experimental analysis of combined utilization of CuO nanoparticles in latent heat storage unit and absorber coating in a single-slope solar desalination system. 233(January), pp.278–286. https://doi.org/10.1016/j.solener.2022.01.039.

Shaaban, S.M., Basem, A., Mohammed, S.A., Alawee, W.H., Aldabesh, A., Majdi, H.S., Omara, Z.M. and Essa, F.A., 2025. Synergistic thermal enhancement in hybrid solar desalination: A vertical wick-spherical still integration with nano-enhanced PCM. *Case Studies in Thermal Engineering*, [online] 75, p.107221. https://doi.org/10.1016/j.csite.2025.107221.

Shafii, M.B., Shahmohamadi, M., Faegh, M. and Sadrhosseini, H., 2016. Examination of a novel solar still equipped with evacuated tube collectors and thermoelectric modules. *Desalination*, 382, pp.21–27. https://doi.org/10.1016/j.desal.2015.12.019.

Sharon, H. and Reddy, K.S., 2015. A review of solar energy driven desalination technologies. *Renewable and Sustainable Energy Reviews*, 41, pp.1080–1118. https://doi.org/10.1016/j.rser.2014.09.002.

Sharqawy, M.H., Lienhard V, J.H. and Zubair, S.M., 2010. Thermophysical properties of seawater: A review of existing correlations and data. *Desalination and Water Treatment*, 16(1–3), pp.354–380. https://doi.org/10.5004/dwt.2010.1079.

Shoeibi, S., Kargarsharifabad, H. and Rahbar, N., 2021. Effects of nano-enhanced phase change material and nano-coated on the performance of solar stills. *Journal of Energy Storage*, [online] 42(August), p.103061. https://doi.org/10.1016/j.est.2021.103061.

Shoeibi, S., Saemian, M., Parsa, S.M., Khiadani, M., Mirjalily, S.A.A. and Kargarsharifabad, H., 2023. A novel solar desalination system equipped with thermoelectric generator, reflectors and low-cost sensible energy-storage for co-production of power and drinking water. *Desalination*, [online] 567(September), p.116955. https://doi.org/10.1016/j.desal.2023.116955.

Singh, P., Rai, A.K. and Sachan, V., 2014. Study of effect of condensing cover materials on the performance of a solar still. *International Journal of Mechanical Engineering and Technology (IJMET)*, 5(5), pp.99–107.

Sivakumar, V., Sundaram, E.G. and Sakthivel, M., 2016. Investigation on the effects of heat capacity on the theoretical analysis of single slope passive solar still. *Desalination and Water Treatment*, 57(20), pp.9190–9202. https://doi.org/10.1080/19443994.2015.1026284.

Sonker, V.K., Chakraborty, J.P. and Sarkar, A., 2022. Development of a frugal solar still using phase change material and nanoparticles integrated with commercialization through a novel economic model. *Journal of Energy Storage*, [online] 51(April), p.104569. https://doi.org/10.1016/j.est.2022.104569.

Tan, J.H., Bahar, R., Jun, H.K. and Low, J., 2023. Effect of conductive particles embedded phase change material on the productivity of a solar still in a controlled environment. In: *IOP Conference Series: Earth and Environmental Science*. Institute of Physics. https://doi.org/10.1088/1755-1315/1281/1/012021.

Tan, J.H., Liew, Y.Y., Bahar, R., Jun, H.K. and Low, J., 2025. Enhancing solar still productivity in tropical climate with conductive particle-assisted phase change material. *Solar Energy Materials and Solar Cells*, 279. https://doi.org/10.1016/j.solmat.2024.113227.

Thamarai Kannan, B., Madhu, B., Kabeel, A.E., Thakur, A.K., Velraj, R., Lynch, I., Saidur, R. and Sathyamurthy, R., 2022. Improved freshwater generation via hemispherical solar desalination unit using paraffin wax as phase change material encapsulated in waste aluminium cans. *Desalination*, [online] 538(May), p.115907. https://doi.org/10.1016/j.desal.2022.115907.

Thimmaraju, M., Sreepada, D., Babu, G.S., Dasari, B.K., Velpula, S.K. and Vallepu, N., 2018. Desalination of Water. In: *Desalination and Water Treatment*. InTech. https://doi.org/10.5772/intechopen.78659.

Tiwari, G.N. and Sahota, L., 2017. *Green Energy and Technology Advanced Solar-Distillation Systems Basic Principles, Thermal Modeling, and Its Application*. [online] Available at: <http://www.springer.com/series/8059>.

Tiwari, G.N., Tiwari, A. and Shyam, 2016. *Handbook of Solar Energy Theory, Analysis and Applications*. Springer.

Tiwari, S. and Rathore, P.K.S., 2022. Performance enhancement of solar still for water desalination integrated with thermal energy storage. *Materials Today: Proceedings*, [online] (xxxx). https://doi.org/10.1016/j.matpr.2022.08.048.

Tofani, K. and Tiari, S., 2021. Nano-enhanced phase change materials in latent heat thermal energy storage systems: A review. *Energies*, 14(13). https://doi.org/10.3390/en14133821.

Too, Y.N., 2021. *STUDY OF NANO-PARTICLES ASSISTED SOLAR DISTILLATION*.

Venkatesh, R., Hossain, I., Mohanavel, V., Elahi M. Soudagar, M., Ali Alharbi, S. and Al Obaid, S., 2024. Flat plate solar collector activated with alumina-silicon dioxide-copper oxide hybrid nanofluid: Thermal performance study. *Applied Thermal Engineering*, 257. https://doi.org/10.1016/j.applthermaleng.2024.124496.

APPENDICES

Appendix A: Experimental Data

Table A-1: Experimental data for Al in Subsection 4.2.1

Time (mins)	Temp. of water, °C	Temp. of PCM, °C	Temp. of cover, °C	Irradiance, W/m²	Cumulative water yield, kg/m^2	Water Yield per basin area per hour, kg/m^2
0	35.25	28.84	30.35	1000.0	0.0000	0.0000
30	38.05	34.85	36.39	1000.0	0.0000	0.0000
60	39.79	37.07	37.84	1000.0	0.0000	0.0000
90	41.07	38.52	37.81	1000.0	0.0000	0.0000
120	41.43	39.42	38.65	1000.0	0.0304	0.0304
150	41.88	39.89	38.59	1000.0	0.0913	0.0609
180	41.83	40.02	38.10	1000.0	0.1522	0.0609
Overnight					0.2740	0.1218

Table A-2: Experimental data for Al_2O_3 in Subsection 4.2.1

Time (mins)	Temp. of water, °C	Temp. of PCM, °C	Temp. of cover, °C	Irradiance, W/m²	Cumulative water yield, kg/m^2	Water Yield per basin area per hour, kg/m^2
0	36.93	31.73	33.84	1000.0	0.0000	0.0000
30	38.63	36.18	34.93	1000.0	0.0000	0.0000
60	40.27	38.38	36.26	1000.0	0.0000	0.0000
90	40.82	39.31	37.24	1000.0	0.0152	0.0152
120	41.67	40.13	37.88	1000.0	0.0609	0.0457
150	41.55	40.32	37.93	1000.0	0.1142	0.0533
180	41.10	40.87	37.23	1000.0	0.1674	0.0533
Overnight					0.3044	0.1370

Table A-3: Experimental data for Cu in Subsection 4.2.1

Time (mins)	Temp. of water, °C	Temp. of PCM, °C	Temp. of cover, °C	Irradiance, W/m²	Cumulative water yield, kg/m^2	Water Yield per basin area per hour, kg/m^2
0	36.52	28.26	32.28	1000.0	0.0000	0.0000
30	37.41	35.09	36.15	1000.0	0.0000	0.0000
60	38.86	37.44	37.29	1000.0	0.0000	0.0000
90	39.67	39.20	37.95	1000.0	0.0152	0.0152
120	40.34	39.82	38.31	1000.0	0.0609	0.0457
150	41.04	40.17	39.04	1000.0	0.1218	0.0609
180	41.31	40.26	38.63	1000.0	0.2207	0.0989
Overnight					0.2740	0.0533

Table A-4: Experimental data for Al_2O_3 + Cu in Subsection 4.2.1

Time (mins)	Temp. of water, °C	Temp. of PCM, °C	Temp. of cover, °C	Irradiance, W/m²	Cumulative water yield, kg/m²	Water Yield per basin area per hour, kg/m²
0	35.27	27.89	29.33	1000.0	0.0000	0.0000
30	37.62	34.93	35.30	1000.0	0.0000	0.0000
60	39.01	37.50	36.05	1000.0	0.0000	0.0000
90	40.10	38.94	37.16	1000.0	0.0000	0.0000
120	40.11	39.68	37.41	1000.0	0.0457	0.0457
150	40.86	40.27	37.29	1000.0	0.1218	0.0761
180	41.28	40.40	37.62	1000.0	0.1826	0.0609
Overnight					0.3120	0.1294

Table A-5: Experimental data for Al in Subsection 4.2.2

Time (mins)	Temp. of water, °C	Temp. of PCM, °C	Temp. of cover, °C	Irradiance, W/m^2	Cumulative water yield, kg/m^2	Water Yield per basin area per hour, kg/m^2
0	37.66	33.02	28.17	1000.0	0.0000	0.0000
30	36.75	33.55	33.26	1000.0	0.0000	0.0000
60	37.43	34.27	34.19	1000.0	0.0000	0.0000
90	37.88	34.54	34.70	1000.0	0.0000	0.0000
120	38.04	34.81	34.96	1000.0	0.0152	0.0152
150	37.47	34.51	35.30	1000.0	0.0761	0.0609
180	37.56	34.58	35.36	1000.0	0.1522	0.0761
Overnight					0.2435	0.0913

Table A-6: Experimental data for Al_2O_3 in Subsection 4.2.2

Time (mins)	Temp. of water, °C	Temp. of PCM, °C	Temp. of cover, °C	Irradiance, W/m²	Cumulative water yield, kg/m^2	Water Yield per basin area per hour, kg/m^2
0	38.67	29.75	29.63	1000.0	0.0000	0.0000
30	36.22	32.29	36.11	1000.0	0.0000	0.0000
60	37.19	32.68	37.56	1000.0	0.0000	0.0000
90	37.68	33.04	38.23	1000.0	0.0000	0.0000
120	37.86	33.02	38.43	1000.0	0.0304	0.0304
150	38.01	33.03	38.53	1000.0	0.1218	0.0913
180	38.13	33.09	38.28	1000.0	0.1979	0.0761
Overnight					0.2588	0.0609

Table A-7: Experimental data for Cu in Subsection 4.2.2

Time (mins)	Temp. of water, °C	Temp. of PCM, °C	Temp. of cover, °C	Irradiance, W/m²	Cumulative water yield, kg/m²	Water Yield per basin area per hour, kg/m²
0	35.79	33.25	30.15	1000.0	0.0000	0.0000
30	34.55	35.76	34.48	1000.0	0.0000	0.0000
60	37.82	36.64	36.06	1000.0	0.0000	0.0000
90	38.45	36.56	36.92	1000.0	0.0000	0.0000
120	38.99	37.04	37.52	1000.0	0.0304	0.0304
150	38.95	37.49	37.74	1000.0	0.0913	0.0609
180	39.01	37.83	37.89	1000.0	0.1522	0.0609
Overnight					0.2359	0.0837

Table A-8: Experimental data for Al_2O_3 + Cu in Subsection 4.2.2

Time (mins)	Temp. of water, °C	Temp. of PCM, °C	Temp. of cover, °C	Irradiance, W/m²	Cumulative water yield, kg/m^2	Water Yield per basin area per hour, kg/m^2
0	39.06	33.07	32.90	1000.0	0.0000	0.0000
30	37.30	34.56	36.52	1000.0	0.0000	0.0000
60	37.94	34.88	37.39	1000.0	0.0000	0.0000
90	38.28	35.08	37.85	1000.0	0.0000	0.0000
120	38.44	35.20	38.09	1000.0	0.0381	0.0381
150	38.61	35.25	38.29	1000.0	0.1294	0.0913
180	38.58	35.09	38.48	1000.0	0.1826	0.0533
Overnight					0.2968	0.1142

Table A-9: Experimental data for Al in Subsection 4.2.3

Time (mins)	Temp. of water, °C	Temp. of PCM, °C	Temp. of cover, °C	Irradiance, W/m²	Cumulative water yield, kg/m^2	Water Yield per basin area per hour, kg/m^2
0	37.93	30.74	27.77	500.0	0.0000	0.0000
30	37.30	33.38	33.14	500.0	0.0000	0.0000
60	38.24	34.07	34.44	500.0	0.0000	0.0000
90	38.82	34.59	35.18	500.0	0.0000	0.0000
120	39.22	34.93	35.65	500.0	0.0000	0.0000
150	39.08	34.53	35.90	500.0	0.0913	0.0913
180	39.26	34.57	35.92	500.0	0.1674	0.0761
Overnight					0.2435	0.0761

Table A-10: Experimental data for Al_2O_3 in Subsection 4.2.3

Time (mins)	Temp. of water, °C	Temp. of PCM, °C	Temp. of cover, °C	Irradiance, W/m²	Cumulative water yield, kg/m^2	Water Yield per basin area per hour, kg/m^2
0	35.89	29.40	29.62	500.0	0.0000	0.0000
30	35.79	32.15	34.74	500.0	0.0000	0.0000
60	37.07	33.20	36.24	500.0	0.0000	0.0000
90	38.29	34.31	37.28	500.0	0.0000	0.0000
120	38.83	34.61	37.90	500.0	0.0609	0.0609
150	38.85	34.44	38.04	500.0	0.1370	0.0761
180	39.37	35.17	38.03	500.0	0.1826	0.0457
Overnight					0.2664	0.0837

Table A-11: Experimental data for Cu in Subsection 4.2.3

Time (mins)	Temp. of water, °C	Temp. of PCM, °C	Temp. of cover, °C	Irradiance, W/m²	Cumulative water yield, kg/m²	Water Yield per basin area per hour, kg/m²
0	41.65	34.70	30.04	500.0	0.0000	0.0000
30	38.85	35.32	35.72	500.0	0.0000	0.0000
60	39.00	35.06	36.88	500.0	0.0000	0.0000
90	39.25	35.29	37.40	500.0	0.0000	0.0000
120	39.40	35.32	37.65	500.0	0.1065	0.1065
150	39.34	36.77	37.66	500.0	0.1370	0.0304
180	39.33	36.64	37.86	500.0	0.2131	0.0761
Overnight					0.3196	0.1065

Table A-12: Experimental data for Al_2O_3 + Cu in Subsection 4.2.3

Time (mins)	Temp. of water, °C	Temp. of PCM, °C	Temp. of cover, °C	Irradiance, W/m²	Cumulative water yield, kg/m^2	Water Yield per basin area per hour, kg/m^2
0	39.34	32.32	31.59	500.0	0.0000	0.0000
30	36.46	33.42	36.27	500.0	0.0000	0.0000
60	37.01	33.92	36.99	500.0	0.0000	0.0000
90	37.31	34.11	37.41	500.0	0.0000	0.0000
120	37.40	34.06	37.60	500.0	0.1218	0.1218
150	37.44	34.23	37.55	500.0	0.1370	0.0152
180	37.46	34.31	37.64	500.0	0.1826	0.0457
Overnight					0.3425	0.1598

Table A-13: Experimental data for Al in Subsection 4.2.4

Time (mins)	Temp. of water, °C	Temp. of PCM, °C	Temp. of cover, °C	Irradiance, W/m²	Cumulative water yield, kg/m^2	Water Yield per basin area per hour, kg/m^2
0	37.66	33.02	28.17	500.0	0.0000	0.0000
30	36.75	33.55	33.26	500.0	0.0000	0.0000
60	37.43	34.27	34.19	500.0	0.0000	0.0000
90	37.88	34.54	34.70	500.0	0.0000	0.0000
120	38.04	34.81	34.96	500.0	0.0152	0.0152
150	37.47	34.51	35.30	500.0	0.0761	0.0609
180	37.56	34.58	35.36	500.0	0.1522	0.0761
Overnight					0.2435	0.0913

Table A-14: Experimental data for Al_2O_3 in Subsection 4.2.4

Time (mins)	Temp. of water, °C	Temp. of PCM, °C	Temp. of cover, °C	Irradiance, W/m²	Cumulative water yield, kg/m^2	Water Yield per basin area per hour, kg/m^2
0	38.67	29.75	29.63	500.0	0.0000	0.0000
30	36.22	32.29	36.11	500.0	0.0000	0.0000
60	37.19	32.68	37.56	500.0	0.0000	0.0000
90	37.68	33.04	38.23	500.0	0.0000	0.0000
120	37.86	33.02	38.43	500.0	0.0304	0.0304
150	38.01	33.03	38.53	500.0	0.1218	0.0913
180	38.13	33.09	38.28	500.0	0.1979	0.0761
Overnight					0.2588	0.0609

Table A-15: Experimental data for Cu in Subsection 4.2.4

Time (mins)	Temp. of water, °C	Temp. of PCM, °C	Temp. of cover, °C	Irradiance, W/m²	Cumulative water yield, kg/m^2	Water Yield per basin area per hour, kg/m^2
0	35.79	33.25	30.15	500.0	0.0000	0.0000
30	34.55	35.76	34.48	500.0	0.0000	0.0000
60	37.82	36.64	36.06	500.0	0.0000	0.0000
90	38.45	36.56	36.92	500.0	0.0000	0.0000
120	38.99	37.04	37.52	500.0	0.0304	0.0304
150	38.95	37.49	37.74	500.0	0.0913	0.0609
180	39.01	37.83	37.89	500.0	0.1522	0.0609
Overnight					0.2359	0.0837

Table A-16: Experimental data for Al_2O_3 + Cu in Subsection 4.2.4

Time (mins)	Temp. of water, °C	Temp. of PCM, °C	Temp. of cover, °C	Irradiance, W/m²	Cumulative water yield, kg/m²	Water Yield per basin area per hour, kg/m²
0	39.06	33.07	32.90	500.0	0.0000	0.0000
30	37.30	34.56	36.52	500.0	0.0000	0.0000
60	37.94	34.88	37.39	500.0	0.0000	0.0000
90	38.28	35.08	37.85	500.0	0.0000	0.0000
120	38.44	35.20	38.09	500.0	0.0381	0.0381
150	38.61	35.25	38.29	500.0	0.1294	0.0913
180	38.58	35.09	38.48	500.0	0.1826	0.0533
Overnight					0.2968	0.1142

Table A-17: Experimental data for Al in Subsection 4.2.5

Time (mins)	Temp. of water, °C	Temp. of PCM, °C	Temp. of cover, °C	Irradiance, W/m²	Cumulative water yield, kg/m^2	Water Yield per basin area per hour, kg/m^2
0	40.19	32.27	28.34	315.5	0.0000	0.0000
30	35.07	32.07	34.58	315.5	0.0000	0.0000
60	34.89	31.79	34.82	315.5	0.0000	0.0000
90	34.84	31.89	34.88	315.5	0.0000	0.0000
120	34.98	31.98	34.91	315.5	0.0000	0.0000
150	35.05	32.12	35.04	315.5	0.0000	0.0000
180	36.56	33.50	35.55	315.5	0.0609	0.0609
Overnight					0.1826	0.1218

Table A-18: Experimental data for Al_2O_3 in Subsection 4.2.5

Time (mins)	Temp. of water, °C	Temp. of PCM, °C	Temp. of cover, °C	Irradiance, W/m²	Cumulative water yield, kg/m^2	Water Yield per basin area per hour, kg/m^2
0	42.16	31.19	28.43	315.5	0.0000	0.0000
30	35.90	31.24	37.34	315.5	0.0000	0.0000
60	35.16	30.49	36.18	315.5	0.0000	0.0000
90	34.57	29.98	35.53	315.5	0.0000	0.0000
120	34.38	30.01	35.42	315.5	0.0000	0.0000
150	34.07	29.81	35.05	315.5	0.0304	0.0304
180	33.75	28.96	34.75	315.5	0.0913	0.0609
Overnight					0.1903	0.0989

Table A-19: Experimental data for Cu in Subsection 4.2.5

Time (mins)	Temp. of water, °C	Temp. of PCM, °C	Temp. of cover, °C	Irradiance, W/m²	Cumulative water yield, kg/m^2	Water Yield per basin area per hour, kg/m^2
0	42.11	33.17	29.48	315.5	0.0000	0.0000
30	36.82	34.74	35.70	315.5	0.0000	0.0000
60	36.17	34.24	36.21	315.5	0.0000	0.0000
90	35.69	33.25	36.16	315.5	0.0000	0.0000
120	35.57	33.24	36.05	315.5	0.0000	0.0000
150	35.46	33.17	35.95	315.5	0.0000	0.0000
180	35.40	33.10	35.85	315.5	0.0913	0.0913
Overnight					0.1598	0.0685

Table A-20: Experimental data for Al_2O_3 + Cu in Subsection 4.2.5

Time (mins)	Temp. of water, °C	Temp. of PCM, °C	Temp. of cover, °C	Irradiance, W/m²	Cumulative water yield, kg/m²	Water Yield per basin area per hour, kg/m²
0	39.51	33.56	33.70	315.5	0.0000	0.0000
30	35.81	33.54	36.28	315.5	0.0000	0.0000
60	35.46	33.13	36.16	315.5	0.0000	0.0000
90	35.32	33.04	36.08	315.5	0.0000	0.0000
120	35.21	32.88	36.06	315.5	0.0000	0.0000
150	35.23	32.80	36.14	315.5	0.0457	0.0457
180	35.11	32.34	36.15	315.5	0.1065	0.0609
Overnight					0.1826	0.0761

Table A-21: Experimental data for FL 12.7 in Subsubsection 4.3.1.1

Time	Temp. of water, °C	Temp. of PCM, °C	Temp. of cover, °C	Irradiance, W/m²	Cumulative water yield, kg/m^2	Water Yield per basin area per hour, kg/m^2
9:00 AM	29.03	28.90	29.66	279.0	0.000	0.000
10:00 AM	48.49	43.73	45.53	993.0	0.000	0.000
11:00 AM	58.99	52.64	56.18	1020.0	0.457	0.457
12:00 PM	61.88	55.24	55.86	1093.0	0.913	0.457
1:00 PM	60.80	60.12	55.39	1161.0	1.560	0.647
2:00 PM	65.15	59.88	58.36	1088.0	2.237	0.677
3:00 PM	58.21	56.63	53.57	1035.0	2.892	0.654
4:00 PM	53.61	54.53	46.73	936.0	3.196	0.304
5:00 PM	49.36	50.34	44.60	608.0	3.539	0.342
6:00 PM	39.91	40.48	35.84	163.0	3.805	0.266

Table A-22: Experimental data for FL 9.9 in Subsubsection 4.3.1.1

Time	Temp. of water, °C	Temp. of PCM, °C	Temp. of cover, °C	Irradiance, W/m²	Cumulative water yield, kg/m²	Water Yield per basin area per hour, kg/m²
9:00 AM	29.06	28.95	58.48	268.0	0.000	0.000
10:00 AM	39.38	38.54	38.58	945.0	0.000	0.000
11:00 AM	51.37	50.09	47.23	1058.0	0.221	0.221
12:00 PM	55.42	52.94	51.08	1110.0	0.502	0.282
1:00 PM	57.33	58.01	48.30	1192.0	0.951	0.449
2:00 PM	62.36	60.35	55.14	1082.0	1.499	0.548
3:00 PM	59.51	57.89	52.69	1058.0	1.979	0.479
4:00 PM	59.16	57.93	50.47	954.0	2.359	0.381
5:00 PM	53.36	55.75	45.36	591.0	2.626	0.266
6:00 PM	41.99	43.44	37.07	123.0	2.869	0.244

Table A-23: Experimental data for FL 20 in Subsubsection 4.3.1.1

Time	Temp. of water, °C	Temp. of PCM, °C	Temp. of cover, °C	Irradiance, W/m²	Cumulative water yield, kg/m²	Water Yield per basin area per hour, kg/m²
9:00 AM	29.35	28.77	27.97	310.0	0.000	0.000
10:00 AM	38.40	42.00	37.89	952.0	0.000	0.000
11:00 AM	51.12	47.71	44.56	1045.0	0.167	0.167
12:00 PM	55.92	52.10	48.21	1021.0	0.449	0.282
1:00 PM	57.10	54.67	48.75	1158.0	0.837	0.388
2:00 PM	63.59	58.73	55.06	1093.0	1.256	0.419
3:00 PM	65.47	60.10	53.07	1115.0	1.674	0.419
4:00 PM	60.91	58.82	49.72	965.0	2.055	0.381
5:00 PM	51.45	54.26	42.19	529.0	2.321	0.266
6:00 PM	40.54	42.40	35.91	165.0	2.565	0.244

Table A-24: Experimental data for FL 33 in Subsubsection 4.3.1.1

Time	Temp. of water, °C	Temp. of PCM, °C	Temp. of cover, °C	Irradiance, W/m²	Cumulative water yield, kg/m^2	Water Yield per basin area per hour, kg/m^2
9:00 AM	29.77	29.10	30.50	263.0	0.000	0.000
10:00 AM	72.14	60.13	69.66	915.0	0.457	0.457
11:00 AM	77.06	76.50	80.94	1037.0	2.892	2.435
12:00 PM	79.43	76.87	73.60	1074.0	4.642	1.750
1:00 PM	70.58	69.35	64.96	1099.0	5.556	0.913
2:00 PM	84.93	71.39	71.07	1098.0	6.012	0.457
3:00 PM	65.37	62.39	61.55	1062.0	7.344	1.332
4:00 PM	71.24	70.31	64.83	910.0	10.350	3.006
5:00 PM	55.88	58.77	47.20	535.0	10.921	0.571
6:00 PM	43.49	50.37	36.12	392.0	11.416	0.495

Table A-25: Experimental data for FL 12.7 in Subsubsection 4.3.1.2

Time	Temp. of water, °C	Temp. of PCM, °C	Temp. of cover, °C	Irradiance, W/m²	Cumulative water yield, kg/m²	Water Yield per basin area per hour, kg/m²
9:00 AM	30.01	28.50	30.99	177.0	0.000	0.000
10:00 AM	46.35	41.68	45.47	835.0	0.000	0.000
11:00 AM	56.76	53.17	54.23	891.0	0.304	0.304
12:00 PM	57.35	56.33	48.89	945.0	0.578	0.274
1:00 PM	55.84	58.79	51.24	957.0	1.050	0.472
2:00 PM	54.53	55.43	48.58	1027.0	1.408	0.358
3:00 PM	51.81	55.17	44.99	1001.0	1.811	0.403
4:00 PM	41.31	44.96	36.96	44.6	1.865	0.053
5:00 PM	29.53	29.81	27.66	95.0	1.979	0.114
6:00 PM	31.38	31.08	29.25	103.8	2.055	0.076

Table A-26: Experimental data for FL 9.9 in Subsubsection 4.3.1.2

Time	Temp. of water, °C	Temp. of PCM, °C	Temp. of cover, °C	Irradiance, W/m²	Cumulative water yield, kg/m^2	Water Yield per basin area per hour, kg/m^2
9:00 AM	31.44	28.60	30.03	151.0	0.000	0.000
10:00 AM	46.09	39.10	42.29	820.0	0.000	0.000
11:00 AM	60.33	51.95	52.55	914.0	0.274	0.274
12:00 PM	59.98	55.04	50.65	993.0	0.479	0.205
1:00 PM	60.06	57.13	51.41	948.0	0.951	0.472
2:00 PM	58.73	53.31	50.10	1047.0	1.317	0.365
3:00 PM	54.44	53.90	46.14	1030.0	1.621	0.304
4:00 PM	40.09	43.21	36.62	42.7	1.865	0.244
5:00 PM	29.05	29.90	26.85	102.3	2.245	0.381
6:00 PM	31.89	31.05	29.86	100.7	2.321	0.076

Table A-27: Experimental data for FL 20 in Subsubsection 4.3.1.2

Time	Temp. of water, °C	Temp. of PCM, °C	Temp. of cover, °C	Irradiance, W/m²	Cumulative water yield, kg/m²	Water Yield per basin area per hour, kg/m²
9:00 AM	30.39	29.03	30.13	172.0	0.000	0.000
10:00 AM	41.72	39.95	38.52	863.0	0.000	0.000
11:00 AM	52.58	49.78	45.94	845.0	0.221	0.221
12:00 PM	53.09	52.74	45.54	997.0	0.426	0.205
1:00 PM	54.21	54.40	46.36	988.0	0.776	0.350
2:00 PM	56.23	50.92	47.10	1031.0	1.065	0.289
3:00 PM	55.60	52.92	46.72	1024.0	1.370	0.304
4:00 PM	42.36	44.75	35.04	46.9	1.636	0.266
5:00 PM	29.36	29.62	27.07	95.8	1.735	0.099
6:00 PM	31.69	31.51	28.47	96.4	1.826	0.091

Table A-28: Experimental data for FL 33 in Subsubsection 4.3.1.2

Time	Temp. of water, °C	Temp. of PCM, °C	Temp. of cover, °C	Irradiance, W/m²	Cumulative water yield, kg/m²	Water Yield per basin area per hour, kg/m²
9:00 AM	29.29	28.00	30.84	182.0	0.000	0.000
10:00 AM	59.50	53.88	55.48	851.0	0.190	0.190
11:00 AM	74.74	73.15	72.48	948.0	1.750	1.560
12:00 PM	72.59	62.59	56.06	981.0	2.473	0.723
1:00 PM	61.89	57.51	52.44	989.0	3.562	1.088
2:00 PM	63.77	53.28	51.05	1034.0	4.163	0.601
3:00 PM	63.11	54.77	50.88	1022.0	4.718	0.556
4:00 PM	39.22	41.70	32.57	43.1	5.061	0.342
5:00 PM	29.53	29.29	26.96	80.9	5.289	0.228
6:00 PM	31.43	30.80	30.03	99.9	5.441	0.152

Table A-29: Experimental data for FL 12.7 in Subsubsection 4.3.1.3

Time	Temp. of water, °C	Temp. of PCM, °C	Temp. of cover, °C	Irradiance, W/m²	Cumulative water yield, kg/m^2	Water Yield per basin area per hour, kg/m^2
9:00 AM	30.57	29.23	29.88	188.0	0.000	0.000
10:00 AM	41.24	38.97	38.93	346.0	0.000	0.000
11:00 AM	56.85	51.55	54.42	687.0	0.152	0.152
12:00 PM	56.03	55.19	51.72	520.0	0.419	0.266
1:00 PM	54.26	53.88	48.55	554.0	0.761	0.342
2:00 PM	56.55	57.42	50.96	497.0	1.104	0.342
3:00 PM	47.13	52.02	41.91	98.1	1.370	0.266
4:00 PM	29.91	30.69	27.01	62.4	1.484	0.114
5:00 PM	27.37	32.36	29.56	178.0	1.659	0.175
6:00 PM	32.09	27.34	30.03	90.3	1.788	0.129

Table A-30: Experimental data for FL 9.9 in Subsubsection 4.3.1.3

Time	Temp. of water, °C	Temp. of PCM, °C	Temp. of cover, °C	Irradiance, W/m²	Cumulative water yield, kg/m²	Water Yield per basin area per hour, kg/m²
9:00 AM	30.28	29.15	29.05	184.0	0.000	0.000
10:00 AM	38.88	38.56	38.41	371.0	0.000	0.000
11:00 AM	52.76	50.49	53.04	625.0	0.213	0.213
12:00 PM	53.40	54.03	52.33	506.0	0.495	0.282
1:00 PM	53.29	53.46	52.22	582.0	0.791	0.297
2:00 PM	55.74	56.52	51.43	480.0	1.218	0.426
3:00 PM	48.33	53.31	44.19	100.4	1.484	0.266
4:00 PM	30.00	30.42	26.83	64.8	1.522	0.038
5:00 PM	31.35	31.53	32.08	177.0	1.773	0.251
6:00 PM	31.93	32.37	29.86	91.9	1.903	0.129

Table A-31: Experimental data for FL 20 in Subsubsection 4.3.1.3

Time	Temp. of water, °C	Temp. of PCM, °C	Temp. of cover, °C	Irradiance, W/m²	Cumulative water yield, kg/m^2	Water Yield per basin area per hour, kg/m^2
9:00 AM	30.39	29.76	30.05	198.0	0.000	0.000
10:00 AM	39.01	38.49	37.61	400.0	0.000	0.000
11:00 AM	51.87	50.52	48.56	653.0	0.228	0.228
12:00 PM	52.83	53.25	49.93	519.0	0.502	0.274
1:00 PM	52.41	53.35	49.65	623.0	0.799	0.297
2:00 PM	53.58	56.57	49.46	508.0	0.951	0.152
3:00 PM	45.28	52.76	40.47	134.3	1.225	0.274
4:00 PM	29.67	30.30	28.31	78.6	1.301	0.076
5:00 PM	31.05	30.88	29.23	181.0	1.514	0.213
6:00 PM	31.42	31.55	29.11	83.7	1.598	0.084

Table A-32: Experimental data for FL 33 in Subsubsection 4.3.1.3

Time	Temp. of water, °C	Temp. of PCM, °C	Temp. of cover, °C	Irradiance, W/m²	Cumulative water yield, kg/m^2	Water Yield per basin area per hour, kg/m^2
9:00 AM	30.19	29.76	29.50	179.0	0.000	0.000
10:00 AM	47.83	47.65	40.64	374.0	0.122	0.122
11:00 AM	70.80	71.64	63.22	643.0	0.715	0.594
12:00 PM	56.60	57.71	49.03	536.0	1.332	0.616
1:00 PM	53.01	55.50	45.80	567.0	1.979	0.647
2:00 PM	57.83	60.77	51.23	524.0	2.131	0.152
3:00 PM	48.70	54.39	41.75	97.5	2.397	0.266
4:00 PM	29.94	30.83	26.36	110.0	2.626	0.228
5:00 PM	32.81	31.75	28.26	182.0	2.778	0.152
6:00 PM	31.37	32.58	27.97	85.0	2.991	0.213

Table A-33: Experimental data for FL 12.7 in Subsubsection 4.3.1.4

Time	Temp. of water, °C	Temp. of PCM, °C	Temp. of cover, °C	Irradiance, W/m²	Cumulative water yield, kg/m²	Water Yield per basin area per hour, kg/m²
9:00 AM	31.05	28.70	31.49	246.0	0.000	0.000
10:00 AM	37.44	34.82	37.22	521.0	0.000	0.000
11:00 AM	51.86	46.14	44.99	283.0	0.091	0.091
12:00 PM	56.93	51.67	51.32	1023.0	0.449	0.358
1:00 PM	51.75	52.29	45.48	1140.0	0.837	0.388
2:00 PM	53.63	55.64	45.50	260.0	1.218	0.381
3:00 PM	51.54	54.04	43.07	475.0	1.553	0.335
4:00 PM	41.27	43.53	35.98	190.0	1.712	0.160
5:00 PM	38.57	38.85	34.58	167.2	1.781	0.068
6:00 PM	37.52	37.83	34.06	388.0	1.918	0.137

Table A-34: Experimental data for FL 9.9 in Subsubsection 4.3.1.4

Time	Temp. of water, °C	Temp. of PCM, °C	Temp. of cover, °C	Irradiance, W/m²	Cumulative water yield, kg/m^2	Water Yield per basin area per hour, kg/m^2
9:00 AM	30.04	29.23	29.49	250.0	0.000	0.000
10:00 AM	36.09	35.16	33.68	547.0	0.000	0.000
11:00 AM	49.09	47.38	43.01	260.0	0.099	0.099
12:00 PM	55.82	54.32	50.32	1064.0	0.396	0.297
1:00 PM	53.54	53.73	47.46	1161.0	0.746	0.350
2:00 PM	58.74	57.58	46.59	276.0	1.180	0.434
3:00 PM	55.89	54.36	43.06	500.0	1.553	0.373
4:00 PM	44.89	43.11	34.93	203.0	1.728	0.175
5:00 PM	38.67	38.93	35.22	158.9	1.819	0.091
6:00 PM	39.62	38.04	33.25	427.0	2.009	0.190

Table A-35: Experimental data for FL 20 in Subsubsection 4.3.1.4

Time	Temp. of water, °C	Temp. of PCM, °C	Temp. of cover, °C	Irradiance, W/m²	Cumulative water yield, kg/m²	Water Yield per basin area per hour, kg/m²
9:00 AM	30.88	30.15	30.35	259.0	0.000	0.000
10:00 AM	36.34	35.44	36.02	632.0	0.000	0.000
11:00 AM	47.24	46.12	40.10	299.0	0.076	0.076
12:00 PM	54.62	52.73	46.95	1125.0	0.358	0.282
1:00 PM	51.85	52.75	44.60	1181.0	0.677	0.320
2:00 PM	53.77	55.98	43.68	267.0	1.126	0.449
3:00 PM	52.70	54.03	45.02	538.0	1.317	0.190
4:00 PM	43.11	42.52	37.03	202.0	1.431	0.114
5:00 PM	38.23	38.75	34.49	151.7	1.553	0.122
6:00 PM	39.14	37.81	33.97	477.0	1.712	0.160

Table A-36: Experimental data for FL 33 in Subsubsection 4.3.1.4

Time	Temp. of water, °C	Temp. of PCM, °C	Temp. of cover, °C	Irradiance, W/m²	Cumulative water yield, kg/m²	Water Yield per basin area per hour, kg/m²
9:00 AM	32.27	31.18	31.81	244.0	0.000	0.000
10:00 AM	41.10	36.93	38.62	678.0	0.000	0.000
11:00 AM	63.07	54.14	52.39	282.0	0.426	0.426
12:00 PM	81.01	67.46	67.66	1101.0	1.256	0.830
1:00 PM	70.49	60.55	53.52	1217.0	2.321	1.065
2:00 PM	68.68	65.81	52.26	283.0	3.257	0.936
3:00 PM	62.30	63.05	49.02	559.0	3.881	0.624
4:00 PM	42.68	48.71	37.94	209.0	4.209	0.327
5:00 PM	38.10	40.07	35.70	138.6	4.429	0.221
6:00 PM	39.15	37.69	34.55	472.0	4.521	0.091

Table A-37: Experimental data for Al_2O_3 + Cu in Subsubsection 4.3.2.1

Time	Temp. of water, °C	Temp. of PCM, °C	Temp. of cover, °C	Irradiance, W/m²	Cumulative water yield, kg/m²	Water Yield per basin area per hour, kg/m²
9:00 AM	30.43	29.94	31.00	354.0	0.000	0.000
10:00 AM	60.02	52.70	51.80	930.0	0.381	0.381
11:00 AM	64.03	66.36	59.43	1173.0	1.522	1.142
12:00 PM	66.85	75.67	61.98	348.0	3.326	1.804
1:00 PM	63.57	66.88	61.04	989.0	4.703	1.377
2:00 PM	66.34	72.34	61.12	967.0	6.301	1.598
3:00 PM	69.05	69.64	62.08	594.0	7.443	1.142
4:00 PM	68.04	72.51	63.08	763.0	8.699	1.256
5:00 PM	54.80	56.38	46.50	801.0	9.231	0.533
6:00 PM	51.68	57.03	41.22	587.0	10.030	0.799

Table A-38: Experimental data for Al_2O_3 in Subsubsection 4.3.2.1

Time	Temp. of water, °C	Temp. of PCM, °C	Temp. of cover, °C	Irradiance, W/m²	Cumulative water yield, kg/m^2	Water Yield per basin area per hour, kg/m^2
9:00 AM	30.60	29.50	29.91	352.0	0.000	0.000
10:00 AM	60.80	51.94	48.49	911.0	0.304	0.304
11:00 AM	67.20	66.54	56.50	1138.0	1.446	1.142
12:00 PM	62.81	66.65	47.84	328.0	3.021	1.575
1:00 PM	59.75	58.75	53.23	982.0	4.033	1.012
2:00 PM	71.67	72.07	59.14	1009.0	5.365	1.332
3:00 PM	81.28	71.49	63.26	705.0	6.659	1.294
4:00 PM	63.68	65.53	57.38	725.0	7.565	0.906
5:00 PM	54.10	54.98	48.88	802.0	8.120	0.556
6:00 PM	50.94	52.86	41.83	558.0	8.836	0.715

Table A-39: Experimental data for Al in Subsubsection 4.3.2.1

Time	Temp. of water, °C	Temp. of PCM, °C	Temp. of cover, °C	Irradiance, W/m²	Cumulative water yield, kg/m^2	Water Yield per basin area per hour, kg/m^2
9:00 AM	61.52	53.61	53.99	950.0	0.000	0.000
10:00 AM	61.07	60.63	51.59	1116.0	0.381	0.381
11:00 AM	59.40	62.62	52.20	326.0	1.446	1.065
12:00 PM	63.34	59.96	57.53	1015.0	3.143	1.697
1:00 PM	64.21	64.97	54.23	1057.0	4.224	1.081
2:00 PM	74.10	79.03	70.68	722.0	5.670	1.446
3:00 PM	64.78	68.19	63.37	714.0	6.545	0.875
4:00 PM	53.78	56.23	47.23	792.0	7.686	1.142
5:00 PM	52.81	54.73	43.01	545.0	8.219	0.533
6:00 PM	61.52	53.61	53.99	950.0	9.018	0.799

Table A-40: Experimental data for Cu in Subsubsection 4.3.2.1

Time	Temp. of water, °C	Temp. of PCM, °C	Temp. of cover, °C	Irradiance, W/m²	Cumulative water yield, kg/m^2	Water Yield per basin area per hour, kg/m^2
9:00 AM	33.33	30.59	39.20	350.0	0.000	0.000
10:00 AM	72.03	63.15	62.19	939.0	0.457	0.457
11:00 AM	75.27	71.48	70.72	1100.0	1.788	1.332
12:00 PM	60.17	62.32	55.13	341.0	3.615	1.826
1:00 PM	69.11	66.79	63.09	1024.0	4.604	0.989
2:00 PM	70.51	69.73	58.90	1132.0	6.400	1.796
3:00 PM	96.68	72.63	74.52	731.0	7.846	1.446
4:00 PM	74.29	72.06	70.45	761.0	8.912	1.065
5:00 PM	57.16	57.87	52.83	812.0	9.521	0.609
6:00 PM	53.65	56.06	48.74	556.0	10.205	0.685

Table A-41: Experimental data for Al_2O_3 + Cu in Subsubsection 4.3.2.2

Time	Temp. of water, °C	Temp. of PCM, °C	Temp. of cover, °C	Irradiance, W/m²	Cumulative water yield, kg/m^2	Water Yield per basin area per hour, kg/m^2
9:00 AM	30.18	30.36	30.77	397.0	0.000	0.000
10:00 AM	46.29	43.66	44.61	779.0	0.000	0.000
11:00 AM	47.42	49.85	41.79	214.0	0.381	0.381
12:00 PM	54.36	50.03	47.18	512.0	0.799	0.419
1:00 PM	46.08	48.49	39.44	269.0	1.142	0.342
2:00 PM	35.94	34.71	33.19	218.0	1.332	0.190
3:00 PM	54.28	45.40	49.70	463.0	1.484	0.152
4:00 PM	48.10	47.53	40.44	999.0	2.055	0.571
5:00 PM	47.09	53.92	41.16	198.0	2.511	0.457
6:00 PM	48.13	49.55	42.47	436.0	2.930	0.419

Table A-42: Experimental data for Al_2O_3 in Subsubsection 4.3.2.2

Time	Temp. of water, °C	Temp. of PCM, °C	Temp. of cover, °C	Irradiance, W/m²	Cumulative water yield, kg/m^2	Water Yield per basin area per hour, kg/m^2
9:00 AM	30.75	30.27	30.53	383.0	0.000	0.000
10:00 AM	46.29	45.49	39.46	778.0	0.000	0.000
11:00 AM	46.08	47.16	38.43	204.0	0.190	0.190
12:00 PM	51.05	49.76	42.96	515.0	0.563	0.373
1:00 PM	43.16	44.19	35.67	269.0	0.791	0.228
2:00 PM	34.97	35.92	30.05	234.0	0.967	0.175
3:00 PM	53.43	50.26	45.85	447.0	1.119	0.152
4:00 PM	48.25	47.70	40.40	985.0	1.522	0.403
5:00 PM	45.95	46.58	39.11	203.0	1.941	0.419
6:00 PM	46.03	45.95	39.25	462.0	2.359	0.419

Table A-43: Experimental data for Al in Subsubsection 4.3.2.2

Time	Temp. of water, °C	Temp. of PCM, °C	Temp. of cover, °C	Irradiance, W/m²	Cumulative water yield, kg/m²	Water Yield per basin area per hour, kg/m²
9:00 AM	30.54	30.49	30.39	383.0	0.000	0.000
10:00 AM	46.55	45.72	38.78	776.0	0.000	0.000
11:00 AM	47.04	48.53	39.06	208.0	0.304	0.304
12:00 PM	59.30	51.13	47.51	532.0	0.799	0.495
1:00 PM	46.00	47.14	36.79	269.0	1.142	0.342
2:00 PM	35.52	36.11	30.05	255.0	1.294	0.152
3:00 PM	54.30	49.76	46.40	453.0	1.446	0.152
4:00 PM	53.56	52.69	44.65	1006.0	1.865	0.419
5:00 PM	48.01	50.16	41.58	208.0	2.390	0.525
6:00 PM	47.79	49.72	42.85	502.0	2.892	0.502

Table A-44: Experimental data for Cu in Subsubsection 4.3.2.2

Time	Temp. of water, °C	Temp. of PCM, °C	Temp. of cover, °C	Irradiance, W/m²	Cumulative water yield, kg/m^2	Water Yield per basin area per hour, kg/m^2
9:00 AM	30.61	30.10	32.59	368.0	0.000	0.000
10:00 AM	51.17	49.05	44.68	819.0	0.000	0.000
11:00 AM	49.97	51.28	44.85	197.0	0.304	0.304
12:00 PM	63.05	57.61	53.85	550.0	0.875	0.571
1:00 PM	48.76	49.41	41.48	253.0	1.218	0.342
2:00 PM	36.90	35.38	34.39	245.0	1.446	0.228
3:00 PM	50.85	49.03	46.78	459.0	1.598	0.152
4:00 PM	51.83	48.89	53.97	971.0	2.093	0.495
5:00 PM	51.57	52.74	46.66	211.0	2.534	0.441
6:00 PM	50.68	51.05	49.24	445.0	2.968	0.434

Table A-45: Experimental data for Al_2O_3 + Cu in Subsubsection 4.3.2.3

Time	Temp. of water, °C	Temp. of PCM, °C	Temp. of cover, °C	Irradiance, W/m²	Cumulative water yield, kg/m^2	Water Yield per basin area per hour, kg/m^2
9:00 AM	29.20	28.24	30.65	498.0	0.000	0.000
10:00 AM	43.72	41.61	39.48	478.0	0.000	0.000
11:00 AM	81.87	75.56	66.93	1246.0	1.104	1.104
12:00 PM	82.87	75.99	69.15	470.0	2.816	1.712
1:00 PM	74.73	69.85	67.12	1233.0	4.414	1.598
2:00 PM	68.43	64.52	51.60	261.0	6.164	1.750
3:00 PM	77.78	66.76	59.16	1065.0	8.105	1.941
4:00 PM	72.90	67.21	60.84	809.0	9.247	1.142
5:00 PM	54.42	56.73	42.66	129.0	9.703	0.457
6:00 PM	46.09	50.61	36.35	39.2	10.046	0.342

Table A-46: Experimental data for Al_2O_3 in Subsubsection 4.3.2.3

Time	Temp. of water, °C	Temp. of PCM, °C	Temp. of cover, °C	Irradiance, W/m²	Cumulative water yield, kg/m²	Water Yield per basin area per hour, kg/m²
9:00 AM	29.09	28.29	30.19	527.0	0.000	0.000
10:00 AM	44.87	42.14	40.65	466.0	0.000	0.000
11:00 AM	84.93	79.20	74.12	1240.0	1.484	1.484
12:00 PM	75.08	77.26	71.00	470.0	2.854	1.370
1:00 PM	66.94	74.50	66.34	1216.0	4.300	1.446
2:00 PM	63.64	60.85	49.47	261.0	6.126	1.826
3:00 PM	73.48	66.35	57.58	1025.0	7.877	1.750
4:00 PM	80.25	66.35	58.20	818.0	9.056	1.180
5:00 PM	54.85	57.16	43.05	129.0	9.551	0.495
6:00 PM	44.99	46.48	36.13	40.3	9.932	0.381

Table A-47: Experimental data for Al in Subsubsection 4.3.2.3

Time	Temp. of water, °C	Temp. of PCM, °C	Temp. of cover, °C	Irradiance, W/m²	Cumulative water yield, kg/m^2	Water Yield per basin area per hour, kg/m^2
9:00 AM	27.04	28.34	30.05	514.0	0.000	0.000
10:00 AM	42.38	43.32	39.19	492.0	0.000	0.000
11:00 AM	81.16	79.88	77.94	1258.0	1.522	1.522
12:00 PM	85.21	75.19	72.31	463.0	2.892	1.370
1:00 PM	88.11	80.28	76.33	1206.0	4.718	1.826
2:00 PM	60.40	63.54	50.72	265.0	6.545	1.826
3:00 PM	65.75	70.07	62.87	966.0	8.333	1.788
4:00 PM	63.23	68.59	55.76	870.0	9.399	1.065
5:00 PM	54.06	56.45	43.34	127.0	9.779	0.381
6:00 PM	45.29	46.93	37.28	40.3	10.122	0.342

Table A-48: Experimental data for Cu in Subsubsection 4.3.2.3

Time	Temp. of water, °C	Temp. of PCM, °C	Temp. of cover, °C	Irradiance, W/m²	Cumulative water yield, kg/m^2	Water Yield per basin area per hour, kg/m^2
9:00 AM	28.75	28.77	30.62	497.0	0.000	0.000
10:00 AM	45.67	44.52	39.88	495.0	0.000	0.000
11:00 AM	86.11	86.46	80.71	1258.0	1.484	1.484
12:00 PM	79.53	88.25	74.25	473.0	2.892	1.408
1:00 PM	75.87	90.00	68.07	1215.0	4.566	1.674
2:00 PM	61.46	64.53	55.02	274.0	6.317	1.750
3:00 PM	74.67	88.14	69.31	1010.0	8.219	1.903
4:00 PM	66.34	80.79	59.10	896.0	9.513	1.294
5:00 PM	50.86	55.62	42.90	121.0	9.893	0.381
6:00 PM	43.00	45.47	36.58	43.3	10.122	0.228

Table A-49: Experimental data for 10k in Subsubsection 4.3.3.1

Time	Temp. of water, °C	Temp. of PCM, °C	Temp. of cover, °C	Irradiance, W/m²	Cumulative water yield, kg/m^2	Water Yield per basin area per hour, kg/m^2
9:00 AM	34.05	31.25	37.55	757.0	0.000	0.000
10:00 AM	78.27	74.62	74.65	956.0	0.799	0.799
11:00 AM	81.04	73.20	71.36	1056.0	2.397	1.598
12:00 PM	77.72	75.48	70.02	1111.0	5.289	2.892
1:00 PM	80.96	68.96	65.30	1189.0	7.344	2.055
2:00 PM	70.96	69.72	62.04	251.0	9.041	1.697
3:00 PM	54.54	56.76	46.15	189.0	10.320	1.279
4:00 PM	49.12	51.57	39.98	76.7	10.525	0.205
5:00 PM	37.28	37.03	34.58	83.8	10.738	0.213
6:00 PM	35.98	35.43	33.26	129.9	10.830	0.091

Table A-50: Experimental data for 20k in Subsubsection 4.3.3.1

Time	Temp. of water, °C	Temp. of PCM, °C	Temp. of cover, °C	Irradiance, W/m²	Cumulative water yield, kg/m^2	Water Yield per basin area per hour, kg/m^2
9:00 AM	31.44	30.87	32.74	725.0	0.000	0.000
10:00 AM	77.11	75.71	68.34	975.0	0.403	0.403
11:00 AM	93.52	92.38	89.68	1070.0	2.207	1.804
12:00 PM	79.67	88.72	76.19	1128.0	4.300	2.093
1:00 PM	70.29	74.90	63.79	1190.0	6.469	2.169
2:00 PM	66.49	71.86	56.42	244.0	8.181	1.712
3:00 PM	53.91	57.54	42.85	189.0	9.361	1.180
4:00 PM	48.27	52.09	39.34	78.9	9.551	0.190
5:00 PM	37.18	37.56	37.22	79.1	9.680	0.129
6:00 PM	35.85	35.90	32.02	126.4	9.817	0.137

Table A-51: Experimental data for 30k in Subsubsection 4.3.3.1

Time	Temp. of water, °C	Temp. of PCM, °C	Temp. of cover, °C	Irradiance, W/m²	Cumulative water yield, kg/m^2	Water Yield per basin area per hour, kg/m^2
9:00 AM	31.91	32.10	31.76	700.0	0.000	0.000
10:00 AM	76.83	74.15	66.76	973.0	0.723	0.723
11:00 AM	75.48	73.04	66.61	1055.0	2.055	1.332
12:00 PM	79.57	79.36	67.58	1094.0	4.338	2.283
1:00 PM	76.47	70.47	61.12	1184.0	6.164	1.826
2:00 PM	72.52	72.16	58.77	253.0	7.496	1.332
3:00 PM	56.86	57.75	44.13	193.0	8.546	1.050
4:00 PM	53.52	53.65	40.36	76.4	8.600	0.053
5:00 PM	41.01	41.20	35.39	80.4	8.737	0.137
6:00 PM	37.69	37.79	34.43	127.4	8.843	0.107

Table A-52: Experimental data for 10k in Subsubsection 4.3.3.2

Time	Temp. of water, °C	Temp. of PCM, °C	Temp. of cover, °C	Irradiance, W/m²	Cumulative water yield, kg/m^2	Water Yield per basin area per hour, kg/m^2
9:00 AM	29.91	29.76	29.88	135.4	0.000	0.000
10:00 AM	49.93	50.56	41.50	325.0	0.129	0.129
11:00 AM	44.13	44.63	37.87	262.0	0.419	0.289
12:00 PM	59.30	55.79	48.84	1090.0	0.875	0.457
1:00 PM	74.85	73.39	62.30	911.0	2.588	1.712
2:00 PM	52.01	53.05	40.14	368.0	3.349	0.761
3:00 PM	43.53	42.34	36.03	337.0	3.501	0.152
4:00 PM	42.55	42.02	37.47	385.0	3.729	0.228
5:00 PM	36.77	37.48	33.35	117.8	3.881	0.152
6:00 PM	35.23	35.79	32.61	182.4	4.033	0.152

Table A-53: Experimental data for 20k in Subsubsection 4.3.3.2

Time	Temp. of water, °C	Temp. of PCM, °C	Temp. of cover, °C	Irradiance, W/m²	Cumulative water yield, kg/m^2	Water Yield per basin area per hour, kg/m^2
9:00 AM	30.57	29.71	30.04	140.6	0.000	0.000
10:00 AM	51.58	51.95	42.46	332.0	0.114	0.114
11:00 AM	47.39	47.38	39.38	279.0	0.495	0.381
12:00 PM	53.88	53.67	45.58	1138.0	0.723	0.228
1:00 PM	76.67	80.21	65.44	1006.0	2.359	1.636
2:00 PM	54.24	54.75	39.07	364.0	2.930	0.571
3:00 PM	44.74	44.52	36.02	344.0	3.196	0.266
4:00 PM	43.60	43.74	36.47	355.0	3.349	0.152
5:00 PM	37.65	38.64	33.49	113.5	3.501	0.152
6:00 PM	36.48	36.10	31.98	183.0	3.615	0.114

Table A-54: Experimental data for 30k in Subsubsection 4.3.3.2

Time	Temp. of water, °C	Temp. of PCM, °C	Temp. of cover, °C	Irradiance, W/m²	Cumulative water yield, kg/m^2	Water Yield per basin area per hour, kg/m^2
9:00 AM	30.51	29.50	30.06	137.2	0.000	0.000
10:00 AM	53.72	50.26	45.07	331.0	0.129	0.129
11:00 AM	45.86	45.69	40.15	267.0	0.457	0.327
12:00 PM	65.07	52.27	50.36	1144.0	0.989	0.533
1:00 PM	68.90	69.58	61.37	1041.0	2.511	1.522
2:00 PM	47.47	53.23	37.82	391.0	2.892	0.381
3:00 PM	44.39	43.65	36.86	341.0	3.158	0.266
4:00 PM	44.21	44.22	37.35	370.0	3.387	0.228
5:00 PM	37.31	38.72	32.99	114.6	3.463	0.076
6:00 PM	36.47	36.66	33.66	182.4	3.615	0.152

Table A-55: Experimental data for 10k in Subsubsection 4.3.3.3

Time	Temp. of water, °C	Temp. of PCM, °C	Temp. of cover, °C	Irradiance, W/m²	Cumulative water yield, kg/m^2	Water Yield per basin area per hour, kg/m^2
9:00 AM	29.44	27.52	32.11	536.0	0.000	0.000
10:00 AM	60.38	55.22	57.61	407.0	0.000	0.000
11:00 AM	80.90	76.38	73.63	1069.0	1.240	1.240
12:00 PM	60.49	63.79	52.21	501.0	2.154	0.913
1:00 PM	66.63	66.83	55.51	1216.0	2.839	0.685
2:00 PM	61.13	59.42	51.15	535.0	3.295	0.457
3:00 PM	53.62	54.68	44.55	526.0	3.904	0.609
4:00 PM	50.62	55.55	44.24	320.0	4.285	0.381
5:00 PM	48.64	54.65	41.79	203.0	4.665	0.381
6:00 PM	38.60	39.54	34.14	126.0	4.893	0.228

Table A-56: Experimental data for 20k in Subsubsection 4.3.3.3

Time	Temp. of water, °C	Temp. of PCM, °C	Temp. of cover, °C	Irradiance, W/m²	Cumulative water yield, kg/m^2	Water Yield per basin area per hour, kg/m^2
9:00 AM	29.60	26.56	33.48	538.0	0.000	0.000
10:00 AM	56.89	48.02	47.18	415.0	0.000	0.000
11:00 AM	82.71	69.54	68.19	1093.0	1.294	1.294
12:00 PM	62.35	63.55	53.31	565.0	2.283	0.989
1:00 PM	70.11	66.53	60.27	1159.0	3.120	0.837
2:00 PM	61.91	60.46	49.41	442.0	3.615	0.495
3:00 PM	53.48	54.70	44.34	553.0	4.262	0.647
4:00 PM	59.86	53.28	44.83	348.0	4.566	0.304
5:00 PM	50.50	54.65	40.51	181.0	5.023	0.457
6:00 PM	40.89	41.40	33.76	103.0	5.251	0.228

Table A-57: Experimental data for 30k in Subsubsection 4.3.3.3

Time	Temp. of water, °C	Temp. of PCM, °C	Temp. of cover, °C	Irradiance, W/m²	Cumulative water yield, kg/m²	Water Yield per basin area per hour, kg/m²
9:00 AM	29.50	27.38	37.06	597.0	0.000	0.000
10:00 AM	58.40	52.52	52.66	415.0	0.000	0.000
11:00 AM	77.19	64.76	74.76	1091.0	1.180	1.180
12:00 PM	59.69	62.63	59.09	435.0	2.321	1.142
1:00 PM	69.56	65.93	61.26	1182.0	3.272	0.951
2:00 PM	57.87	57.90	49.19	494.0	3.767	0.495
3:00 PM	50.46	53.60	42.73	576.0	4.376	0.609
4:00 PM	50.57	50.39	47.49	345.0	4.604	0.228
5:00 PM	45.64	49.13	39.65	203.0	4.985	0.381
6:00 PM	38.03	39.00	33.09	119.0	5.251	0.266

Table A-58: Experimental data for 10k in Subsubsection 4.3.3.4

Time	Temp. of water, °C	Temp. of PCM, °C	Temp. of cover, °C	Irradiance, W/m²	Cumulative water yield, kg/m^2	Water Yield per basin area per hour, kg/m^2
9:00 AM	29.34	28.39	28.92	294.0	0.000	0.000
10:00 AM	36.41	36.96	31.73	178.0	0.000	0.000
11:00 AM	33.37	34.33	29.65	162.0	0.000	0.000
12:00 PM	32.08	26.85	27.51	191.0	0.000	0.000
1:00 PM	32.60	28.76	30.27	201.0	0.282	0.282
2:00 PM	39.13	36.76	34.90	330.0	0.282	0.000
3:00 PM	52.68	51.85	43.61	1184.0	0.381	0.099
4:00 PM	73.13	71.56	64.61	356.0	1.712	1.332
5:00 PM	42.39	44.89	36.54	177.0	2.169	0.457
6:00 PM	43.77	44.33	37.03	152.0	2.412	0.244

Table A-59: Experimental data for 20k in Subsubsection 4.3.3.4

Time	Temp. of water, °C	Temp. of PCM, °C	Temp. of cover, °C	Irradiance, W/m²	Cumulative water yield, kg/m^2	Water Yield per basin area per hour, kg/m^2
9:00 AM	29.29	28.35	29.19	309.0	0.000	0.000
10:00 AM	35.93	36.21	32.56	184.0	0.000	0.000
11:00 AM	32.86	33.67	29.63	162.0	0.000	0.000
12:00 PM	30.72	31.27	28.91	186.0	0.000	0.000
1:00 PM	30.97	32.21	29.50	204.0	0.259	0.259
2:00 PM	37.44	37.15	35.30	332.0	0.259	0.000
3:00 PM	50.59	50.16	43.17	1180.0	0.350	0.091
4:00 PM	69.74	69.89	61.55	356.0	1.370	1.020
5:00 PM	45.13	49.21	35.99	181.0	1.674	0.304
6:00 PM	44.88	45.89	37.34	161.0	1.903	0.228

Table A-60: Experimental data for 30k in Subsubsection 4.3.3.4

Time	Temp. of water, °C	Temp. of PCM, °C	Temp. of cover, °C	Irradiance, W/m²	Cumulative water yield, kg/m²	Water Yield per basin area per hour, kg/m²
9:00 AM	29.25	28.02	28.82	312.0	0.000	0.000
10:00 AM	36.35	36.85	32.75	184.0	0.000	0.000
11:00 AM	32.99	34.12	29.62	154.0	0.000	0.000
12:00 PM	31.65	34.91	28.50	186.0	0.000	0.000
1:00 PM	32.14	34.46	29.76	200.0	0.251	0.251
2:00 PM	38.49	38.54	35.53	327.0	0.251	0.000
3:00 PM	50.48	51.87	45.85	1171.0	0.342	0.091
4:00 PM	64.43	66.95	58.71	354.0	1.332	0.989
5:00 PM	45.16	50.70	38.67	177.0	1.636	0.304
6:00 PM	42.69	44.00	36.98	158.0	1.826	0.190

Table A-61: Experimental data for prototype in Subsection 4.3.4

Time	Temp. of water, °C	Temp. of PCM, °C	Temp. of cover, °C	Irradiance, W/m²	Cumulative water yield, kg/m^2	Water Yield per basin area per hour, kg/m^2
9:00 AM	30.90	30.59	38.21	800.0	0.000	0.000
10:00 AM	51.68	50.38	51.30	829.0	0.000	0.000
11:00 AM	61.35	60.43	51.38	1076.0	0.152	0.152
12:00 PM	60.90	63.45	51.23	884.0	0.913	0.761
1:00 PM	61.61	63.13	51.32	761.0	1.522	0.609
2:00 PM	55.34	56.81	44.35	543.0	1.979	0.457
3:00 PM	55.41	55.63	47.55	584.0	2.283	0.304
4:00 PM	52.66	55.08	43.57	266.0	2.588	0.304
5:00 PM	55.21	54.34	47.88	653.0	2.816	0.228
6:00 PM	47.34	49.78	40.16	222.0	3.303	0.487

Appendix B: Publications

1. Tan, J.H., Bahar, R., Jun, H.K. and Low, J., 2023. Effect of conductive particles embedded phase change material on the productivity of a solar still in a controlled environment. In: *IOP Conference Series: Earth and Environmental Science*. Institute of Physics. https://doi.org/10.1088/1755-1315/1281/1/012021.

2. Tan, J.H., Liew, Y.Y., Bahar, R., Jun, H.K. and Low, J., 2025. Enhancing solar still productivity in tropical climate with conductive particle-assisted phase change material. *Solar Energy Materials and Solar Cells*, 279. https://doi.org/10.1016/j.solmat.2024.113227.